

Spring 5-31-2002

Experiments with a Galton board

Christopher Oshman
New Jersey Institute of Technology

Follow this and additional works at: <https://digitalcommons.njit.edu/theses>



Part of the [Mechanical Engineering Commons](#)

Recommended Citation

Oshman, Christopher, "Experiments with a Galton board" (2002). *Theses*. 705.
<https://digitalcommons.njit.edu/theses/705>

This Thesis is brought to you for free and open access by the Electronic Theses and Dissertations at Digital Commons @ NJIT. It has been accepted for inclusion in Theses by an authorized administrator of Digital Commons @ NJIT. For more information, please contact digitalcommons@njit.edu.

Copyright Warning & Restrictions

The copyright law of the United States (Title 17, United States Code) governs the making of photocopies or other reproductions of copyrighted material.

Under certain conditions specified in the law, libraries and archives are authorized to furnish a photocopy or other reproduction. One of these specified conditions is that the photocopy or reproduction is not to be “used for any purpose other than private study, scholarship, or research.” If a user makes a request for, or later uses, a photocopy or reproduction for purposes in excess of “fair use” that user may be liable for copyright infringement,

This institution reserves the right to refuse to accept a copying order if, in its judgment, fulfillment of the order would involve violation of copyright law.

Please Note: The author retains the copyright while the New Jersey Institute of Technology reserves the right to distribute this thesis or dissertation

Printing note: If you do not wish to print this page, then select “Pages from: first page # to: last page #” on the print dialog screen

The Van Houten library has removed some of the personal information and all signatures from the approval page and biographical sketches of theses and dissertations in order to protect the identity of NJIT graduates and faculty.

ABSTRACT

EXPERIMENTS WITH A GALTON BOARD

by

Christopher Oshman

Galton boards have been used for over a half-century as a tool to illustrate the formation of Gaussian shaped distributions as well as the Central Limit Theorem. Here, the Galton board was used to study the spontaneous percolation of a particle through an ordered array of rigid scatterers. The apparatus that was designed and fabricated provided a means to release 1/8" diameter spheres one at a time in a controlled and precise manner at any location on the board. The three experimental variables used in these experiments were the particle material, the release height, and the board tilt angle. The data, consisting of residence time and exit location, were analyzed and the relationship between statistical values and parameter settings was found to be as follows: (1) standard deviation of the radial displacement increased with release height and was unaffected by board angle, (2) average residence time increased with release height and decreased with board angle, (3) standard deviation of the residence time increased with release height, (4) average axial velocity was unaffected by release height and increased with board angle, and (5) standard deviation of the axial velocity increased with a decrease of release height and increased with an increase in board angle. From an analysis of the data, it can be inferred that the motion of particles on the Galton board is governed by a diffusional mechanism.

EXPERIMENTS WITH A GALTON BOARD

**By
Christopher Oshman**

**A Thesis
Submitted to the Faculty of
New Jersey Institute of Technology
In Partial Fulfillment of the Requirements for the Degree of
Master of Science in Mechanical Engineering**

Department of Mechanical Engineering

May 2002

Blank Page

APPROVAL PAGE

EXPERIMENTS WITH A GALTON BOARD

Christopher Oshman

Dr. Anthony D. Rosato, Thesis Advisor Date
Associate Chairperson for Graduate Studies and
Associate Professor of Mechanical Engineering, NJIT

Dr. Pushpendra Singh, Committee Member Date
Associate Professor of Mechanical Engineering, NJIT

Dr. Denis Blackmore, Committee Member Date
Professor of Mathematical Science, NJIT

BIOGRAPHICAL SKETCH

Author: Christopher Oshman

Degree: Master of Science

Date: May 2002

Undergraduate and Graduate Education:

- Master of Science in Mechanical Engineering
New Jersey Institute of Technology, Newark, NJ, 2002
- Bachelor of Science in Mechanical Engineering Technology
New Jersey Institute of Technology, Newark, NJ, 1999
- Associate of Applied Science in Mechanical Engineering Technology
Middlesex County College, Edison, NJ, 1997

Major: Mechanical Engineering

To my parents.

ACKNOWLEDGEMENT

I would like to thank Dr. Anthony Rosato who served as my academic and research advisor and also inspired me to look with curiosity at the wonders of the universe. Special thanks are given to Dr. Pushpendra Singh and Dr. Denis Blackmore for serving as members of the committee.

I would also like to thank the students of the Granular Science Laboratory including: Ninghua Zhang, Jian Liu, Liam Buckley, and Michael Sweetman. I would like to especially thank my good friend and lab partner Mark Johnson. This project would not have been possible without his dedication and technical wizardry.

TABLE OF CONTENTS

Chapter	Page
1 INTRODUCTION.....	1
2 LITERATURE SURVEY	5
2.1 Historical Background	5
2.2 Technical and Scientific Background	7
3 OBJECTIVE	15
4 EXPERIMENT METHODS	16
4.1 Experimental Apparatus	16
4.1.1 Frame Assembly	16
4.1.2 Galton Board Assembly	17
4.1.3 Releaser Assembly.....	20
4.1.4 Hopper Assembly	24
4.1.5 Timer Assembly.....	25
4.2 Experimental Procedure.....	27
4.2.1 Leveling the Frame Assembly	27
4.2.2 Leveling the Board Assembly.....	28
4.2.3 Set the Release Height and Board Angle.....	29
4.2.4 Filling the Hopper	32
4.2.5 Centering the Release Nozzle	33
4.3 Data Collection Systems	34
4.3.1 Manual Data Collection	35
4.3.2 Automatic Data Collection	36
4.4 Data Analysis	40
5 RESULTS AND DISCUSSION	46
5.1 Design Results	46
5.2 Experimental Results	48
5.2.1 Average Radial Displacement	50
5.2.2 Standard Deviation of the Radial Displacement.....	52

TABLE OF CONTENTS

(Continued)

Chapter	Page
5.2.3 Average Residence Time	53
5.2.4 Standard Deviation of the Residence Time	54
5.2.5 Confidence Interval for the Residence Time	55
5.2.6 Average Axial Velocity	57
5.2.7 Standard Deviation of the Axial Velocity.....	58
5.2.8 Radial Velocity	59
5.3 Radial Dispersion.....	59
6 CONCLUSIONS.....	64
6.1 Conclusion	64
6.2 Ideas for Future Work.....	66
APPENDIX A: TABLES.....	69
APPENDIX B: FIGURES	88
APPENDIX C: TECHNICAL DRAWINGS.....	115
REFERENCES	147

LIST OF TABLES

Table	Page
5.1 Rows of the Galton board and their Corresponding Heights in Centimeters.....	49
A.1 Radial Displacement Distances (R) for Slot Numbers of the Galton Board.	69
A.2 Height (H) Conversion for Row Numbers of the Galton Board	70
A.3 Sample Excel Data for Brass Balls Dropped from a Height of 60 Rows and an Angle of 40 Degrees.	71
A.4 Sample of Data from the Automatic Data Collection System	72
A.5 Values to Find the Radial Dispersion Coefficient..... (1/8" Brass, Release Height 60 rows).	73
A.6 Number of Data Points Collected for Each Parameter Setting	74
A.7 Radial Displacement from the Centerline in Centimeters.....	75
A.8 Standard Deviation of the Radial Displacement from the Center..... in Centimeters.	76
A.9 Average Residence Time in Seconds	77
A.10 Standard Deviation of the Residence Time in Seconds	78
A.11 95% Confidence Interval of the Residence Time	79
A.12 Average Axial Velocity in Centimeter/Second.....	80
A.13 Standard Deviation of the Axial Velocity in Centimeter/Second	81
A.14 Average Radial Velocity in Centimeters/Second.....	82
A.15 Standard Deviation of the Radial Velocity in Centimeters/Second.....	83
A.16 Slope of R^2 vs. $\ln(N/(N-N_0))$ in Units of cm^2	84
A.17 R^2 or Coefficient of Determination of the Linear Regression..... Line of the Radial Dispersion Coefficient.	85

LIST OF TABLES
(Continued)

Table	Page
A.18 Radial Dispersion Coefficient in Units of cm^2/s	86
A.19 Coefficient of Restitution	87

LIST OF FIGURES

Figure	Page
1.1 Diagram of one cell of a typical Galton board used to illustrate the geometry used to find the diameter of the particle required for spontaneous percolation.	2
1.2 A typical distribution of particles at the bottom of a Galton board	3
2.1 A schematic of the experimental apparatus used by Bruno et al in their Galton board experiments.	12
4.1 Diagram of the release mechanism before the release of a particle	22
4.2 Diagram of the release mechanism during the release of a particle	23
4.3 Diagram of the release mechanism after the release of a particle	23
4.4 Diagram of the timer system	26
4.5 Diagram of the Galton board and its leveling system	28
4.6 Diagram of the release mechanism height adjustment	30
4.7 Sketch of the ball being released above the center pin of the Galton board and the probability of the ball going to the left or right of the pin.	34
4.8 End view of the ball detector. This shows how an off-center hole can cause a misreading by the data collection system.	38
4.9 Sketch of the relative positions of the start and stop beams with the pins on the Galton board.	43
4.10 An illustration of the slots and their corresponding radial distance	44
5.1 Typical particle distributions at the bottom of the Galton board	51
5.2 Gaussian distributions with a high and low standard deviations	52

**LIST OF FIGURES
(Continued)**

Figure	Page
B.1 Logic flowchart for the automatic data collection system	88
B.2 Plots of the radial dispersion coefficient.....	90
B.3 Standard deviation of the radial displacement vs. release height of 1/8" diameter aluminum spheres for various board angles.	91
B.4 Standard deviation of the radial displacement vs. board angle..... of 1/8" diameter aluminum spheres for various release heights.	91
B.5 Standard deviation of the radial displacement vs. release height of 1/8" diameter brass spheres for various board angles.	92
B.6 Standard deviation of the radial displacement vs. board angle..... of 1/8" diameter brass spheres for various release heights.	92
B.7 Standard deviation of the radial displacement vs. release height of 1/8" diameter stainless steel spheres for various board angles.	93
B.8 Standard deviation of the radial displacement vs. board angle..... of 1/8" diameter stainless steel spheres for various release heights.	93
B.9 Average residence time vs. release height of 1/8" diameter aluminum spheres for various board angles.	94
B.10 Average residence time vs. board angle of 1/8" diameter aluminum spheres for various release heights.	94
B.11 Average residence time vs. release height of 1/8" diameter brass spheres for various board angles.	95
B.12 Average residence time vs. board angle of 1/8" diameter brass spheres for various release heights.	95
B.13 Average residence time vs. release height of 1/8" diameter stainless steel spheres for various board angles.	96
B.14 Average residence time vs. board angle of 1/8" diameter stainless steel spheres for various release heights.	96

**LIST OF FIGURES
(Continued)**

Figure	Page
B.15 Standard deviation of the residence time vs. release height..... of 1/8" aluminum spheres for various board angles.	97
B.16 Standard deviation of the residence time vs. board angle..... of 1/8" aluminum spheres for various release heights.	97
B.17 Standard deviation of the residence time vs. release height..... of 1/8" brass spheres for various board angles.	98
B.18 Standard deviation of the residence time vs. board angle..... of 1/8" brass spheres for various release heights.	98
B.19 Standard deviation of the residence time vs. release height..... of 1/8" stainless steel spheres for various board angles.	99
B.20 Standard deviation of the residence time vs. board angle..... of 1/8" stainless steel spheres for various release heights.	99
B.21 Average axial velocity vs. release height of 1/8" aluminum spheres for various board angles.	100
B.22 Average axial velocity vs. board angle of 1/8" aluminum..... spheres for various release heights.	100
B.23 Average axial velocity vs. release height of 1/8" brass spheres for various board angles.	101
B.24 Average axial velocity vs. board angle of 1/8" brass..... spheres for various release heights.	101
B.25 Average axial velocity vs. release height of 1/8" stainless steel..... spheres for various board angles.	102
B.26 Average axial velocity vs. board angle of 1/8" stainless steel spheres for various release heights.	102
B.27 Standard deviation of the axial velocity vs. release height..... of 1/8" aluminum spheres for various board angles.	103

LIST OF FIGURES
(Continued)

Figure	Page
B.28 Standard deviation of the axial velocity vs. board angle of 1/8" aluminum spheres for various release heights.	103
B.29 Standard deviation of the axial velocity vs. release height of 1/8" brass spheres for various board angles.	104
B.30 Standard deviation of the axial velocity vs. board angle of 1/8" brass spheres for various release heights.	104
B.31 Standard deviation of the axial velocity vs. release height of 1/8" stainless steel spheres for various board angles.	105
B.32 Standard deviation of the axial velocity vs. board angle of 1/8" stainless steel spheres for various release heights.	105
B.33 Standard deviation of the radial velocity vs. release height..... of 1/8" aluminum spheres for various board angles.	106
B.34 Standard deviation of the radial velocity vs. board angle of 1/8" aluminum spheres for various release heights.	106
B.35 Standard deviation of the radial velocity vs. release height..... of 1/8" brass spheres for various board angles.	107
B.36 Standard deviation of the radial velocity vs. board angle of 1/8" brass spheres for various release heights.	107
B.37 Standard deviation of the radial velocity vs. release height..... of 1/8" stainless steel spheres for various board angles.	108
B.38 Standard deviation of the radial velocity vs. board angle of 1/8" stainless steel spheres for various release heights.	108
B.39 Slope of $[r^2 \text{ vs. } \ln (N_0/(N_0-N))]$ vs. release height of 1/8" aluminum spheres for various board angles.	109
B.40 Slope of $[r^2 \text{ vs. } \ln (N_0/(N_0-N))]$ vs. board angle of 1/8" aluminum spheres for various release heights.	109
B.41 Slope of $[r^2 \text{ vs. } \ln (N_0/(N_0-N))]$ vs. release height of 1/8" brass spheres for various board angles.	110

LIST OF FIGURES
(Continued)

Figure	Page
B.42 Slope of $[r^2 \text{ vs. } \ln (N_0/(N_0-N))]$ vs. board angle of 1/8" brass spheres for various release heights.	110
B.43 Slope of $[r^2 \text{ vs. } \ln (N_0/(N_0-N))]$ vs. release height of 1/8" stainless steel spheres for various board angles.	111
B.44 Slope of $[r^2 \text{ vs. } \ln (N_0/(N_0-N))]$ vs. board angle of 1/8" stainless steel..... spheres for various release heights.	111
B.45 Radial Dispersion Coefficient vs. release height of 1/8" aluminum..... spheres for various board angles.	112
B.46 Radial Dispersion Coefficient vs. board angle of 1/8" aluminum spheres for various release heights.	112
B.47 Radial Dispersion Coefficient vs. release height of 1/8" brass spheres for various board angles.	113
B.48 Radial Dispersion Coefficient vs. board angle of 1/8" brass spheres for various release heights.	113
B.49 Radial Dispersion Coefficient vs. release height of 1/8" stainless steel spheres for various board angles.	114
B.50 Radial Dispersion Coefficient vs. board angle of 1/8" stainless steel spheres for various release heights.	114

LIST OF DRAWINGS

Drawing	Page
C.1 Assembly of Galton board system	115
C.2 Close up of Galton board assembly.....	116
C.3 Axle.....	117
C.4 Brass sensor housing.....	118
C.5 Carriage.....	119
C.6 Bottom of the release housing.....	120
C.7 Top of the release housing	121
C.8 Channel.....	122
C.9 Control Panel.....	123
C.10 Foot.....	124
C.11 Frame.....	125
C.12 Galton board.....	126
C.13 Glider.....	127
C.14 Hopper.....	128
C.15 Level.....	129
C.16 Nozzle.....	130
C.17 Nut.....	131
C.18 Plexiglass platform.....	132
C.19 Release block.....	133
C.20 Screw for the releaser assembly.....	134
C.21 Screw for the timing sensors.....	135

LIST OF DRAWINGS
(Continued)

Drawing	Page
C.22 Timing sensor	136
C.23 Timing sensor bracket	137
C.24 Agitation servo for the hopper	138
C.25 Single axis movement slider	139
C.26 Slots assembly	140
C.27 Bottom release solenoid valve	141
C.28 Top release solenoid valve	142
C.29 Leveling spring.....	143
C.30 Transverse	144
C.31 Transverse riser	145
C.32 Wooden platform.....	146

CHAPTER 1

INTRODUCTION

A Galton board is a flat board, which has an array of convex scatterers or pins mounted on its surface. Particles are dropped from a location on the board and they collide with the scatterers, or obstacles, as they descend under the influence of gravity to the bottom of the board. This device was made popular by Sir Francis Galton [1] to illustrate the Central Limit Theorem and how it can relate to the study of genetics and heredity. This thesis will not be concerned with any direct application of the Galton board or its characteristics. Instead, an investigation will be made of the behaviors that the particles exhibit during the process of spontaneous percolation through the rigid scatterers.

Inter-particle percolation is a mechanism by which the segregation of different sized particles takes place under the influence of gravity [2]. For example, if a vessel were filled with a mixture of very small particles and very large particles, the small particles would tend to fall down between the large gaps formed by the large particles. This phenomenon does not usually happen by itself, or spontaneously. It usually requires some form of vibration of the vessel to start the segregation by inter-particle percolation. If, however, the diameter of the particle is less than or equal to the smallest gap in the packing particles, spontaneous inter-particle percolation will occur. The following figure illustrates the geometry of the pins of a Galton board. D is the diameter of the pins, d is the diameter of the ball, and X is the horizontal spacing of the pins.

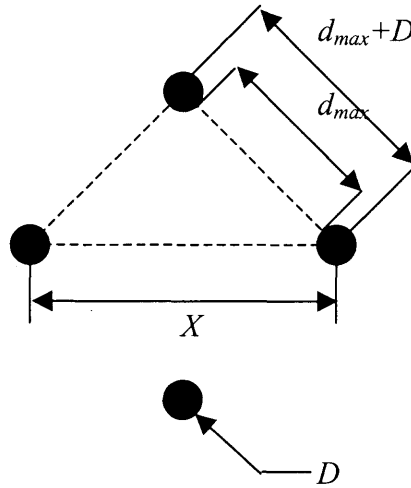


Figure 1.1 Diagram of one cell of a typical Galton board used to illustrate the geometry used to find the diameter of the particle required for spontaneous percolation.

$$X = (d_{\max} + D)\sqrt{2} \quad (1.1)$$

$$\frac{X\sqrt{2}}{2} - D = d_{\max} \quad \text{for a Galton board} \quad (1.2)$$

If equation (1.2) is true, then the small particles will automatically fall to the bottom of the vessel. This is essentially what occurs in a Galton board system. The reason the Galton board particles spontaneously fall to the bottom of the vessel, or in this case the board, is that the interstice, or gap between the pins, is large compared to the size of the percolating particles.

As one would expect, the particles do not usually fall straight down the Galton board. The stationary obstacles or pins block their path of travel. When a particle collides with a pin, it rebounds with a velocity that depends on the coefficient of restitution of the material of pins and ball. Eventually, though, after bouncing and changing its direction of travel many times, the particle reaches the bottom of the board.

The classic use of a Galton board is to illustrate a principal in statistics called the Central Limit Theorem, and also to illustrate the formation of a Gaussian, or bell shaped, distribution [1]. It has been observed that most of the particles that are released from the top center of a Galton board exit from the center or very near the center at the bottom. A few particles will exit from outside the center and a very few particles will exit far from the centerline of the board. This can be spoken about in terms of probability. There is a high probability that a particle will exit at or very near the center of the board and a very small probability that a particle will exit very far from the center of the board. Suppose there are slots at the bottom of the board into which the particles that fall remain. If many particles are released from a height at the center of the Galton board, the resulting distribution of particles will resemble the distribution depicted below.

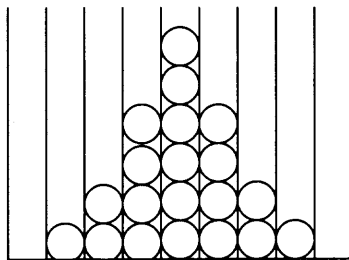


Figure 1.2 A typical distribution of particles at the bottom of a Galton board.

This is a Gaussian, or bell shaped distribution. This distribution occurs very often in measuring natural phenomenon. One of the most widely used examples of a Gaussian distribution is the variation of heights of a large group of randomly selected people. If a histogram is constructed where the horizontal axis is the height range and the vertical axis is the number of people that fall in that range, a Gaussian distribution will result.

In the following experiments, because of a lack of resources of time and money, only one type Galton board was used. Also, only three different types of particles were used. The apparatus that was designed and built allowed control over two parameters, namely the release height and the board angle. The apparatus was also designed to release the particles the same way each time with little or no initial angular or translational velocity. A system was fabricated to automatically release a particle, display the residence time, and identify its exit location. The two pieces of data, residence time and exit location were recorded either manually or automatically. From an analysis of this collected data for different parameter settings, several behaviors were observed, as well as the relationship between the behaviors and the experimental variables. This thesis is a report of the design and fabrication of the experimental apparatus and the study of the mechanics and behavior of the Galton board system.

CHAPTER 2

LITERATURE SURVEY

2.1 Historical Background

Sir Francis Galton was born on February 16, 1822 in Sparkbrook, England. He died on January 17, 1911 at the age of 88 in Haslemere, England. He was the ninth child born into a relatively wealthy family. His father was a banker. One of his grandfathers was Erasmus Darwin, the grandfather of Charles Darwin who originated the theory of evolution. The other grandfather was a Fellow of the Royal Society. At an early age, Francis Galton showed promising mathematics skills, but originally went to study medicine. After getting frustrated with studying medicine at the age of eighteen, Galton went to Cambridge University to read mathematics. He had a nervous breakdown after three years at Cambridge and went back to studying medicine.

When Galton was twenty-two years old, his father died, leaving him and his family with a very large inheritance. This money freed him up so he didn't have to work. For the next six or so years, he traveled extensively around Europe, Asia, and Africa, having adventures and exploring. When he finally returned to England in 1850 at the age of 28, he received a gold medal from the Royal Geographical Society. Also in the same year, he was elected to the Royal Society. It is believed that because of his frustration at not being able to have children with his wife, he began looking into the field of Eugenics. Eugenics is defined as a science that deals with the improvement of hereditary qualities in a series of generations of a race or breed by social control of human mating and reproduction. He believed that certain physical characteristics such as height and weight

and certain psychological characteristics such as sensory functions and mental capacity could be inherited and improved in successive generations by selective breeding. After conducting studies on father and son traits and the size difference in sweet pea pods, Galton concluded that the traits of successive generations regressed to a mean value. In other words, the offspring of tall parents will be slightly shorter and the offspring of short parents will be slightly taller. This is called regression, or returning to the mean. Because of his studies and experiments, Francis Galton proved that the concept of selective breeding in Eugenics was not possible.

During his time studying eugenics, Galton had devised a few instruments to aid in the process of data collection and illustration. A device known today as a Galton bar was invented and used by Galton. The Galton bar is a horizontal bar, which is bisected with an adjustable vertical line and was used to measure the length judgment in humans. Another testing device invented by Galton is the Galton whistle. This instrument was used to test the upper limit of audibility and produced a variable, high-pitched tone. By far, the most famous of his inventions was the Galton board. This, unlike the two previously mentioned devices, was used to illustrate the laws of error and hereditary processes. This Galton board, also known as a “quincunx”, was a box with a glass front and horizontal pins imbedded in the back like nails. These pins were arranged in a regular triangular array. Lead shot was dropped into the board with a funnel and was collected in slots at the bottom. He observed that the distribution of the shot at the bottom formed a normal curve. After doing more sophisticated experiments with the board, he proved that a normal distribution was normally a mixture of normal distributions. This is essentially the Central Limit Theorem used today in the field of statistics. Modern texts state that if

random samples containing a fixed number (n) of measurements are repeatedly drawn from a population with a finite mean μ and a standard deviation σ , then if n is large, the sample means will have a distribution that is approximately normal [7]. The shot forming the normal curve was analogous to the distributions of quantifiable characteristics such as height, weight, etc. For his contributions to the fields of eugenics, statistics, meteorology, and anthropology, Francis Galton was knighted in 1909.

2.2 Technical and Scientific Background

The Galton board apparently first appeared in print in an article published in *Scientific American* in 1964. This article [1] written by Mark Kac gave a brief historical overview of the development of the field of statistics from its early beginnings in the 1600's to what was then modern day advances such as stochastic processes and Markov chains. In his historical development, Kac gave a short description of the significance of Galton's board and even presented a very nice photograph of the board at work and the resulting Gaussian distribution.

In 1969, Bridgwater et al. published a paper [2] on particle mixing by percolation. This work consisted of packing a cylinder with spheres. The packing spheres used were of differing materials and sizes. Mostly glass spheres with a diameter, $D=1.2$ cm, were used. Solid plastic spheres and table tennis balls were also used for the packing. The percolating particles were much smaller than the packing particles and also varied in size and material. The percolating particles, which were dropped into the packed bed through a hole in the center of the top lid, fell through the bed and escaped from the bottom through a screen, and then landed onto a circular plate marked with equally spaced

concentric circles. This resembled a target used in the sport of archery. Five thousand particles were dropped through the bed and stuck to the target that was coated with a thin layer of grease. In what follows, Bridgwater et al.'s model is described. The evolution of n , the number of particles per unit area perpendicular to the percolation direction, was modeled as a diffusive process governed by,

$$\frac{\partial n}{\partial t} = E_r \left(\frac{\partial^2 n}{\partial r^2} + \frac{1}{r} \frac{\partial n}{\partial r} \right) = E_r \nabla^2 n(r, t) \quad (2.1)$$

Here, E_r is the radial dispersion. The boundary conditions are,

$$n \rightarrow 0 \text{ as } r \rightarrow \infty \text{ for } t > 0 \quad (2.2)$$

As the radius increases, the number of particles decreases.

$$n = 0 \text{ for } r > 0 \text{ for } t = 0 \quad (2.3)$$

This condition states that there are no particles occupying the container at the start of the experiment.

$$\int_0^{\infty} 2\pi r n dr = N_0 \text{ for } t > 0 \quad (2.4)$$

This condition states that the number of particles in the container remains fixed for all time. The solution of (2.1) subject to the conditions (2.2-2.4) is given as,

$$n = \frac{N_0}{4\pi E_r t} \exp\left(-\frac{r^2}{4E_r t}\right) \quad (2.5)$$

Thus, the number of percolating particles N whose centers lie within a radius r at a time t was found to be,

$$N = \int_0^r 2\pi r n dr = N_0 \left[1 - \exp\left(-\frac{r^2}{4E_r t}\right) \right] \quad (2.6)$$

which, upon rearranging, yielded,

$$4E_r t = \frac{r^2}{\ln\left(\frac{N_0}{N_0 - N}\right)} \quad (2.7)$$

Bridgwater et al. analyzed the experimental data by plotting r^2 values against $\ln(N_0/(N_0 - N))$ for the various materials used. The graphs indicated a straight-line relationship between r^2 and $\ln(N_0/(N_0 - N))$, from which it was concluded that the process was essentially diffusional in the radial direction. The second part of Bridgwater's analysis began with a discussion of the variables that may determine the radial dispersion coefficient, E_r . After some dimensional analysis, it was shown that,

$$\frac{vD}{E_r} = h(e) \quad (2.8)$$

where $\frac{vD}{E_r}$ is the radial Peclet number, v is the mean velocity, D is the diameter of the packing spheres, and e is the coefficient of restitution. Since the mean velocity is $v \approx l/t$, where l is the height of the packed bed and t is the mean residence time, the radial Peclet number, Pe_r becomes,

$$Pe_r = \frac{lD}{E_r t} \quad (2.9)$$

It was found that Pe_r generally decreased as e increased.

Two years after publishing the previously reviewed paper, Bridgwater et al. [3] published a paper that dealt not with the radial behavior of a percolating particle in a packed bed, but with its axial behavior. The experimental setup was essentially the same as the previous experiments, but with an improvement in the timing precision and accuracy. The residence time for this experiment was found using a light beam detector at the entrance of the packed bed. When the particle broke this light beam, a digital timer

was triggered to start. After the percolating particle exited the bottom of the packed bed, it struck a thin metal plate with an attached microphone that was “acoustically sealed”. The signal from the particle striking the plate would stop the timer. Since there was a distance of free flight of the particle above and below the bed, a correction factor was subtracted from the time given by the digital reading. Seven different experiments were done for the four hundred particles dropped in each experiment. Each experiment differed in particle material, particle size, and/ or entry location.

In 1988, seventeen years after Bridgwater’s packed bed experiments, Sergeev et al. [4] published their work on the flow of a medium in a model of a granular bed. This paper compares the Galton board experimental results to predictions of a model derived from principals of statistical physics. The experiments were carried out using two types of Galton boards. The first of these was the larger one and had pins that were uniformly spaced with almost equal horizontal and vertical spacing. The parameter N was used here to describe the “density of the boards”, defined as the number of pins divided by the area of the board. The values of N used in this board were 2780 and 5000 pins/m². The second type of board was smaller and had a linearly changing horizontal step. Both boards were attached to a frame, which could be pivoted about a horizontal axis in the plane of the board. Small, round shot of some material (not specified in the paper) was dropped from points at the top of the board and the time of descent and location of landing were recorded. The horizontal distribution at the bottom was also recorded.

A paper by Hoover and Moran [5], published in 1992, looked at the theory and numerical simulations of the Galton Board using isokinetic equations of motion. The introduction of this paper gave a very brief look at previous works related to the board.

The model of the Galton board was the typical triangular lattice of pins. The density of the pins was chosen to be $4/5$ of the maximum packing density. A numerical simulation was conducted using a periodic half-cell. It was shown that the phase-space distribution of the isokinetic dynamical system showed a complex structure, or strange attractor.

In 1993, a paper by Lue and Brenner [6] took a look at many different aspects of Galton's board. These included the phase-flow dynamics of the system, Poincaré map dynamics, numerical computation of the dynamical system, and statistical results. It was hypothesized that although for many years, the Galton board had been used to demonstrate randomness and the laws of probability, that in fact, the board is deterministic and obeys Newton's laws of motion. The Galton board has been formally defined here as "a spatially periodic array of rigid convex scatterers". The work done by these authors gives possible insights into the important parameters that effect the particle distributions and residence times.

A 1997 paper published by Ippolito et al. [8] represented the preliminary results of experiments of particle diffusion in a cylindrical packed bed. The setup was essentially the same as Bridgwater et al. [2] and [3]. It consisted of a cylinder filled with a random packing of glass spheres of two possible diameters, D . Steel shot of diameter d were released from the top of the bed. An optical sensor started a timer and a microphone stopped the timer. The bottom plate was coated with an adhesive to catch the steel shot. The steel shot were dropped from different heights H . From a plot of residence time t vs. H , it was found that the particles reached a steady state velocity very quickly, about 3-4 sphere layers. These plots showed a linear relationship. It is also noted that a histogram of residence times was very well fitted by a Gaussian curve.

In 2000, Bruno et al. [9] reported experimental results on mixing processes in a Galton Board. A 2-D Galton board was made by using discs that served as obstacles glued to a clear board. These obstacles had a diameter of 0.4 cm and were arranged in a regular, hexagonal pattern with a horizontal spacing of 1.5 cm. The flowing particles were also made from discs but varied in diameter of either, 0.4, 0.6, or 1 cm. It was not stated however, what materials were used or the properties of the materials. The experiment consisted of dropping a large number of two different diameter discs; each from two bins at the top of the board as shown the figure below.

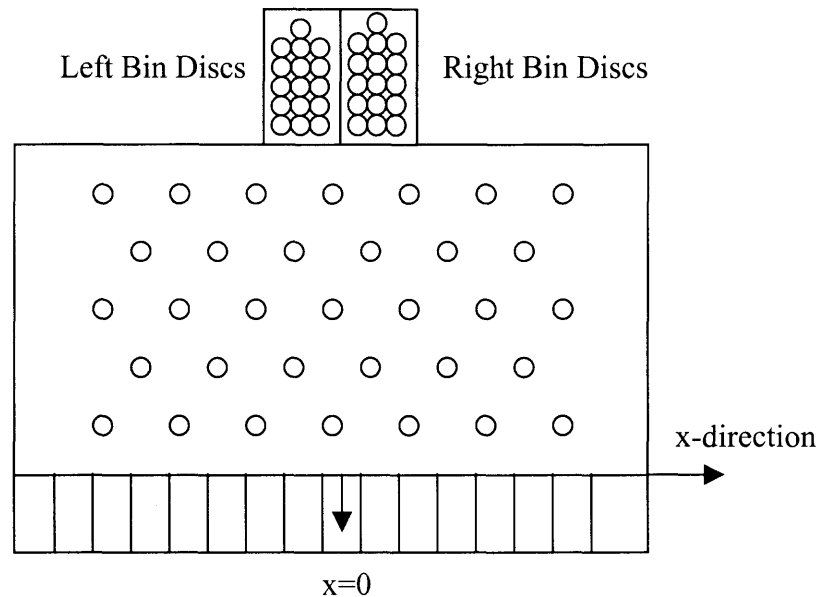


Figure 2.1 A schematic of the experimental apparatus used by Bruno et al. in their Galton board experiments.

As the discs descended the board, they collided inelastically with the obstacles and other flowing particles. When all of the particles landed in the slots in the bottom of the board, a CCD camera and software were used to process and analyze the final positions of the particles. Histograms of the horizontal (x) and vertical (y) distributions were made from

the data. Equations were given which were used to describe the mixing quantitatively. Each slot was assigned a number x , such that $x=0$ is the center slot. For each slot x , let the probability of the discs from the left side bin falling in that slot $P_L(x)$, equal to the number of discs from the left bin $N_L(x)$ in the slot divided by the total number of discs from the left bin N_{0L} .

$$P_L(x) = \frac{N_L(x)}{N_{0L}} \quad (2.10)$$

Conversely, the “spatial distribution” of the right bin discs is given by,

$$P_R(x) = \frac{N_R(x)}{N_{0R}} \quad (2.11)$$

The term “spatial distribution” refers to either $P_L(x)$ or $P_R(x)$. The mixing parameter along the x -direction, $M(x)$, is defined as the ratio of the spatial distributions. In other words,

$$M(x) = \frac{P_R(x)}{P_L(x)} \quad \text{if } x < 0 \quad (2.12)$$

$$M(x) = \frac{P_L(x)}{P_R(x)} \quad \text{if } x > 0 \quad (2.13)$$

This is rewritten in terms of the number of particles in the slot,

$$M(x) = \frac{N_R(x)}{N_L(x)} a \quad \text{if } x < 0 \quad (2.14)$$

$$M(x) = \frac{N_L(x)}{N_R(x)} \frac{1}{a} \quad \text{if } x > 0 \quad (2.15)$$

where,

$$a = \frac{N_{0L}}{N_{0R}} \quad (2.16)$$

With these definitions, the mixture parameter equals unity when the ratio of left bin particles to right bin particles in a slot is equal to the inverse of the ratio of the total

number of left bin particles to the total number of right bin particles. From their experimental data, Bruno et al. found that the Galton Board as configured could indeed be used as an effective mixing device for discrete particles. It was also found that the size ratio of the particles didn't significantly affect the quality of the mixing. What did affect the mixing greatly was the presence of obstacles in the particle path in that there was a strong correlation between obstacle spacing and quality of mixing. A useful idea from this work is the equations used to quantify the spatial distribution of the particles in a slot. Also of interest is the histograms shown for different ratios of disc diameter (d) to the pin diameter (D). The histograms demonstrated that as the diameter ratio d/D increased, the spread σ (standard deviation) of the normal distribution also increased.

CHAPTER 3

OBJECTIVE

There are two objectives that are accomplished in this thesis. One is the design and construction of an experimental apparatus that will allow the precise collection of data from a Galton board. This data consists of two pieces of information on each experimental trial: the residence time and the exit location of the particle. The second objective is to perform the experiments and collect enough data to allow an investigation into the mechanics and behavior of the Galton board system for the experimental parameters chosen.

CHAPTER 4

EXPERIMENTAL METHODS

4.1 Experimental Apparatus

This section gives a detailed description of the experimental apparatus used in the Galton board experiments. The apparatus has been divided into five different assemblies including the frame assembly, Galton board assembly, releaser assembly, hopper assembly, and the timer assembly.

4.1.1 Frame Assembly

The whole Galton board system was mounted on a frame. The frame was a triangular structure made from wooden 2x4s, as can be seen in Drawing 11 in Appendix C (C.11). The 2x4s were held together with wood screws and the whole frame was painted white. There were four adjustable leveling feet (Drawing C.10) supporting the frame. The leveling feet were used to roughly level the Galton board. A 5/8" thru hole was drilled into the top of the frame about 50" off the ground. A threaded rod (Drawing C.3) was inserted into the holes in the frame and served as an axle on which the Galton board could pivot.

The Galton board itself was mounted indirectly onto a wooden platform (Drawing C.32). This platform was made with 3/4" plywood, and 2x4 pieces on the sides for support. The platform was painted the same as the frame. Holes were drilled into the sides of the platform to insert the threaded rod. This allowed the platform to pivot to any angle for

experimentation. When the desired angle was achieved, the platform was locked into place by tightening nuts (Drawing C.17) at the ends of the axle.

As stated above, the Galton board was not mounted directly on the wooden platform because there would be no way to fine-tune the level of the board. Instead, all of the hardware was mounted on a 7/16" thick clear acrylic platform (Drawing C.18), which was 34" wide and 36" long. It was suspended above the wood platform with four 1" springs (Drawing C.29), and was held in place with four 1/4" bolt going through the springs. These bolts were also used to adjust the leveling of the Galton board.

An "Angle Finder Plus Level" (manufactured by DascoPro Inc., Rockford IL) (Drawing C.15) was mounted onto the upper left portion of the acrylic platform in order to measure the tilt angle of the board. This angle finder gave angle readings with a precision of $\pm 1/2^\circ$. Since the angle finder could only provide the board's vertical angle and not its horizontal angle, a 9" torpedo level was used to check the Galton board for levelness. It was very important that the board be level because any slight deviation from being level would cause an unwanted bias in the direction of particle travel.

An extruded aluminum channel (Drawing C.8) was mounted onto the acrylic platform to allow adjustments of the height of the "release device" and the optical timing sensors. These were held on the channel by using steel gliders (Drawing C.13) that allowed the position of the channel to be quickly adjusted with a screwdriver.

4.1.2 Galton Board Assembly

The Galton board (Drawings C.12 and C.2) used in the following experiments was made from a 16" x 16 1/2" x 5/16" aluminum plate. Holes were drilled through the plate using a

CNC milling machine equipped with a $1/16$ " drill bit. The horizontal spacing of the holes was $5/16$ " and the vertical spacing was $5/32$ ". The holes in each consecutive row were offset by $5/32$ " from the previous row, thereby creating a triangular (or hexagonal) lattice. There were 100 rows and 100 columns of holes. A $1/16$ " diameter alloy steel pin with a length of $5/8$ " was inserted into each hole. In order to make the pins enter the holes easier, a pin holder was machined to guide and support the pin into the hole without damage to either the pin or the board. The pins were also lubricated with machine oil to aid in the insertion. Using the pin insertion tool, each pin was hammered into place. Once all of the pins were in place, the board was scrubbed with a clean toothbrush and liquid soap to remove any leftover oils and contaminants. After washing, the board was dried quickly using an air nozzle.

An array of forty-nine slots was used to collect the balls exiting the Galton board and to determine the position of the ball's exit. The slots (Drawing C.26) were constructed from a base of $5/16$ " thick aluminum plate and vertical slats of $1/16$ " aluminum plate. The base plate was $19 \frac{1}{4}$ " x 3" and the fifty slats were $2 \frac{1}{2}$ " long and protruded $3/8$ " above the base plate. Originally, the balls would fall into a slot and stay there until released by removing a thin nylon strip from the end of the slots. The position of a ball's exit was recorded visually and written down in a data collection book. After collecting the preliminary experimental data, it was noted that the original method of data collection was too time consuming. An automatic position detection system was then developed for the board. This will be discussed in further detail in Section 4.3.2.

There was initially a problem in finding a way to detect the passing of such small particles. After considering many different possible mechanical and electrical systems of

ball detection, it was decided that an optical system would be the easiest to develop. The optical system, developed by Mark Johnson, was simply a series of 49 LEDs and optical sensors mounted into a brass housing (Drawing C.4). This was a custom made piece that consists of a 3" length of 3/16" square brass tube with a 3/4" length of 5/32" round brass tube soldered onto it 1/4" from the end. A 1/16" hole was drilled coaxial with the round tube through the square tube. The LED was then inserted into the free end of the round tube and held in place with heat shrunk tubing. On the opposite side of the square tubing, the optical sensor was glued in place with a fast setting cyanoacrylate glue so that the eye of the sensor was lined up directly with the through hole. Each of the forty-nine brass sensors was set up in the following way. The wires of each of the sensors ran to a microprocessor system. This system created a data file that recorded the residence time and final position of each particle in an experimental run. Of course, the data for the position came from the signal it received from the brass sensor unit.

The entire array of brass sensors was held in place by a series of screws mounted on a thick plate of acrylic. There was one screw to hold down each of the brass sensors. A piece of aluminum angle was needed to reinforce the acrylic plate because the force of the screws on the brass sensors would bend the plate and make it difficult to tighten all of the screws.

A small collector was fabricated in order to catch the balls descending along the acrylic platform. This collector was made from two 15" long pieces of 1" PVC angle. They were taped together with masking tape to form a channel, which was then mounted to the acrylic platform with a screw.

4.1.3 Releaser Assembly

The purpose of the releaser assembly was to release one ball at a time onto the Galton board in a controlled and precise manner. The actual release device was mounted onto a precision, single-axis movement stage (Drawings C.5 and C.25). The manufacturer of the stage was unknown but the specifications are as follows:

Total Travel:	7"
Travel/ Revolution:	0.050"
Base Size:	11"L x 1 3/4"W x 3/4"H
Stage Size:	3"L x 2 3/4"W x 3/4"H
Precision:	± 0.001"

This stage was mounted (bolted) onto a piece of 2"x 2" PVC angle called the transverse (Drawing C.30). This transverse was then attached to the two channels on the frame assembly. In order to increase, and if needed, adjust the height of the release assembly, small PVC shims called transverse risers (Drawing C.31) were placed under the transverse at both ends.

As stated before, the release device was attached to a single-axis movement stage. This allowed very precise horizontal positioning of the point of ball release. This was very important because any slight deviation off center would introduce an unwanted bias in the experiment. The release device was designed and built to release one ball at a time. The housing of the releaser was constructed from a 2" PVC angle with a length of 6". The two housing angles (Drawings C.6 and C.7) were screwed together to form a case. This served as a place to mount the release mechanism.

The release mechanism itself consisted of a releaser block, two solenoids, and a nozzle. The release block (Drawing C.19) was a $\frac{3}{4}$ " x $\frac{3}{4}$ " x $2\frac{1}{8}$ " block of nylon with a $\frac{1}{8}$ " diameter hole through the center in the longitudinal direction. This was the path the balls followed from the feed tube. There were also two $\frac{1}{16}$ " diameter holes drilled transversely into the center of the block. They were drilled halfway through the block, opposite to each other, and were offset, thereby producing a $\frac{1}{8}$ " gap between them. These holes served as guides for the releaser pins. The two releaser pins were connected to their respective solenoid valves. The two solenoid valves (Drawings C.27 and C.28) were activated by 24VDC. In their unactivated positions, the bottom solenoid pin blocked the flow of balls, and the top solenoid pin was retracted into the block away from the path of the balls. The bottom solenoid pulled when activated and the top solenoid pushed when activated. Both solenoids were attached to light springs (mounted on the case) to return each to their unactivated positions.

At the bottom surface of the release block, a nozzle (Drawing C.16) was inserted into a counter bored hole coaxial with the through hole for the ball travel. The nozzle was simply a $\frac{7}{8}$ " long brass tube having a $\frac{1}{8}$ " OD and $\frac{3}{16}$ " ID. The bottom end of the nozzle was trimmed at a 45° angle to allow the balls to exit onto the board when released by the mechanism. In order to have a precise ball exit, the tip of the nozzle rested on the top surface of the board and the height of the nozzle exit was close to the ball diameter. In this study, the ball diameter was $\frac{1}{8}$ ". Another important aspect of the ball release was the direction of the nozzle exit. The ball was to be directed downward when released from the nozzle. If not, this would have given the ball an unwanted initial velocity in the transverse direction, thereby biasing the experiment. It should be noted here that this

method of releasing the ball does, in fact, introduce some randomness in the initial conditions.

The steps involved in releasing a single ball from the release mechanism are as follows:

1. Set: This is the initial starting position of release. Both solenoids are in their unactivated positions. The upper solenoid pin is retracted as to not be in the ball's pathway. The lower solenoid pin is extended in order to block the path of the balls. The weight of the balls in the feed tube is resting on the lower pin at this point and one ball is in position to be released.

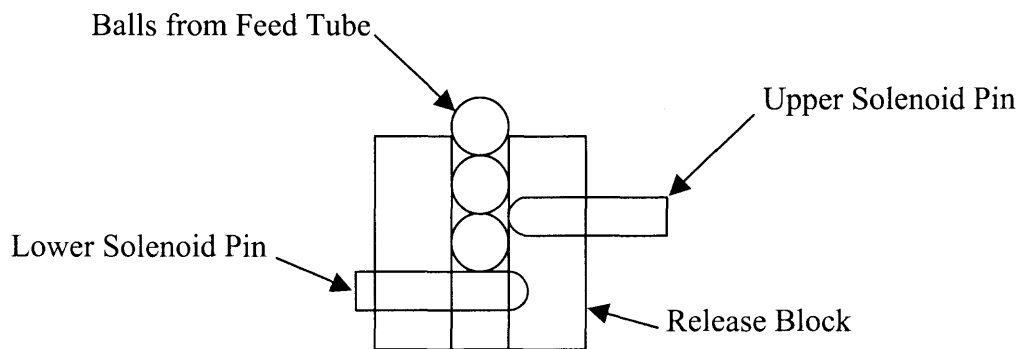


Figure 4.1 Diagram of the release mechanism before the release of a particle.

2. Release: This is the action part of the releasing procedure. A signal is given to the microprocessor by either a human activated switch or another microprocessor. Once the signal is received by the microprocessor, the release procedure is activated. First, a signal is sent to activate the upper solenoid. The upper solenoid pin is extended into the path of the balls thereby stopping any movement of the balls in the feed tube. A half second later, another signal is sent to the lower

solenoid to activate it. This causes the lower solenoid pin to retract into the releaser block allowing the one ball to fall past it on its way to the release nozzle and eventually down the Galton board.

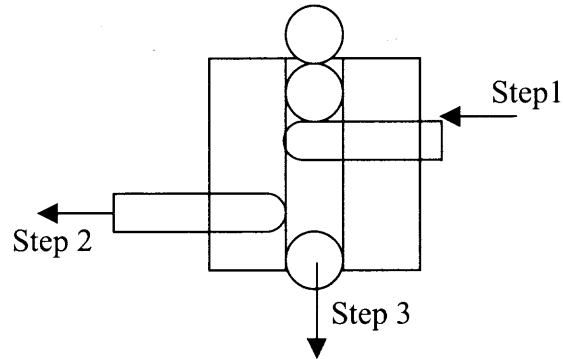


Figure 4.2 Diagram of the release mechanism during the release of a particle.

3. Reset: Another half second later, the signal to the lower solenoid is turned off. This extends the lower solenoid pin into the path of the balls. Yet another half second passes and the signal going to the upper solenoid is turned off. This retracts the upper solenoid pin into the releaser block allowing the next ball to drop into position. The system is now ready to release another ball beginning the cycle again.

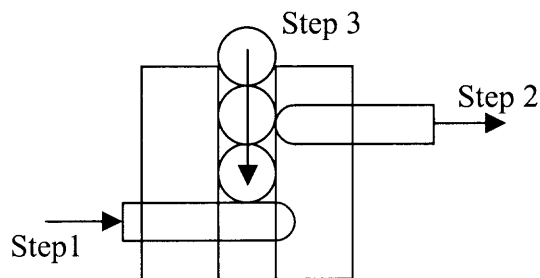


Figure 4.3 Diagram of the release mechanism after the release of a particle.

4.1.4 Hopper Assembly

The purpose of the hopper assembly was to provide a continuous supply of balls to the release mechanism. The hopper assembly consisted of a few parts, which all worked together to accomplish this goal. The main part of the assembly was the hopper itself (Drawing C.14). This was formed from a 1/8" thick piece of clear acrylic. The acrylic was bent into a box shape with dimensions 4"H x 4 1/4" W x 4 1/4" D. The hopper had no top and was formed using a 500-watt heater/bender (Model EMX-1, Kidder Manufacturing Company: Thornhill, Ontario, Canada). An aluminum angle was glued to each of the four vertical corners of the hopper to seal it and to increase rigidity and strength. Holes were drilled into the bottom of the hopper to accept a servo, feed tube, and the servo mounting screws.

The servo (Drawing C.24) was used to agitate the particles in the hopper. This agitation assisted the balls flowing into the feed tube. The servo used was a Parallax Standard Servo (Parallax Inc: Rocklin, CA 95765 www.parallaxinc.com) with dimensions 1 1/2"H x 1 1/2" W x 3/4" D. At 4.8 VDC, the servo operated at a speed of 260°/sec (4.54 rad/sec) with a torque of 3.4 kg*cm (0.608 in*lb). It was mounted on the bottom of the hopper with two screws.

The feed tube was a flexible nylon tube with a 1/4" OD and 3/16" ID. The tube was about 20" long. One end of it was glued to a hole in the bottom of the hopper and the other end was inserted into the counter bore at the top of the release block. There was a small detector installed on the feed tube about 4" from the bottom of the hopper. This detector was actually a small 3/4" wood cube which acts as a tube coupler. A 3/16" longitudinal hole and a 1/8" transverse hole were drilled through the block. At one end of

the transverse hole was an LED and at the other end was an optical sensor. The wires for the servo, LED, and optical sensor fed into a 9 pin D-Sub connector mounted on the front of the hopper. The entire assembly was seated on a shelf above the Galton board. Velcro was used to hold it in place.

The mechanism for the hopper was quite simple. If the optical sensor “saw” that the feed tube was empty, the microprocessor sent a signal to the servo to start turning. The servo was programmed to turn in one direction for one second, and then reverse direction in order to agitate the mass of balls in the hopper. For each turn of the servo, a number of balls (usually 1-5) fell into the feed tube. When the height of the balls in the feed tube reached the sensor location, the optical beam was broken and the microprocessor stopped the servo movement. As the balls were released into the Galton board, the level of the balls in the tube decreased. When it decreased past the optical sensor, the servo was again activated and the feed tube was filled once again.

4.1.5 Timer Assembly

The purpose of the timer assembly was to give a precise and accurate residence time reading for the balls descending the Galton board. The system used here was able to measure the residence time with a precision of a thousandth of a second.

At first, during the development of the experiment, there were problems associated with finding a suitable method for measuring the times of such small particles ($\phi 1/8''$). By searching through electronics catalogs, a product was found that had the ability to detect the position of a very small particle. In order to start and stop the timer, Amplified Mini Optical Sensors with a Pin Point Beam (Drawing C.22) were used. These

sensors were manufactured by Omron (www.omron.com) and have part number E3T-ST12. Two sets of sensors were needed, one to start the timer and one set to stop the timer. Each of the four sensors was mounted onto custom-made sensor brackets (Drawing C.23) made from a PVC angle. The sensor brackets were mounted onto the frame channels. This allowed the sensor's placement to be infinitely adjustable to any height or angle. The beam of the start sensor was placed directly above the top row of pins. The beam of the stop sensor was placed directly below the bottom row of pins.

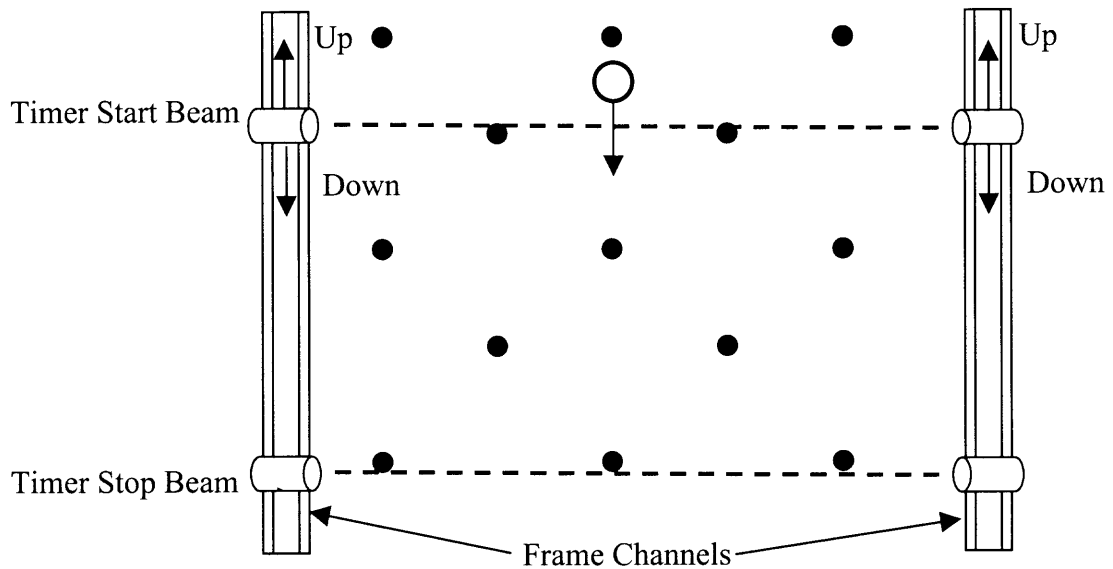


Figure 4.4 Diagram of the timer system.

The signals from the start/stop sensors ran to a MDMU Miniature Electronic 6-Digit Counter/ Timer/ Tachometer manufactured by Red Lion (www.Redlion-controls.com York, PA 17402) with a part number MDMU0000. The timer was configured to give a precision of a thousandth of a second. Once the timer was wired correctly, it was mounted in a plastic enclosure (Drawing C.9), which served as the main

controller for the experiment. Also mounted on the control enclosure were the main on/off power switch, auto/manual control switch, feed tube indicator LED, and start/stop optics indicator LEDs.

4.2 Experimental Procedure

The procedure used in the Galton board experiment to collect data is described below. Although every detail of the procedure may not be represented in the following paragraphs, there is sufficient information to successfully reproduce the experiments performed.

4.2.1 Leveling the Frame Assembly

It was very important to have a level frame for the Galton board experiment. If the frame was not leveled, then every other part of the experiment could not be level, since every other part rests on the frame structure. The frame was composed of a triangular structure of 2x4 lumber, which was supported above the floor by four carriage bolts. These bolts serve as adjustable leveling feet. A wooden platform was fixed to the frame structure by a threaded rod, which served as an axle. The platform, which is considered here as part of the frame structure, was able to rotate about a horizontal axis through its center. The procedure to level this frame assembly is as follows.

1. Adjust all four leveling feet to their central positions.
2. Set the swinging wooden platform to 0° (horizontal). This should be set using a torpedo bubble level for greatest accuracy. The level is positioned longitudinally on the platform.

3. The platform is now set to be level in the transverse direction. Place a bubble level on the wooden platform in the transverse direction. Note which side is too high, the left or the right. Lower the two feet on the side that is too high by one complete turn.
4. Check for levelness again. Repeat step #3 until the bubble level indicates that the wooden platform is level in the transverse direction.
5. The frame is now level.

4.2.2 Leveling the Board Assembly

Of all the components involved in this experiment, the leveling of the Galton board was the most important. Now that the frame has been leveled, the experimental procedure can continue by making the Galton board assembly level. The entire experiment and almost all the apparatus were fixed in some way to a thick acrylic sheet. This sheet, which was suspended above the wooden platform of the frame assembly by four steel compression springs, was held in place by four bolts running through the acrylic platform, the springs, and the wooden platform.

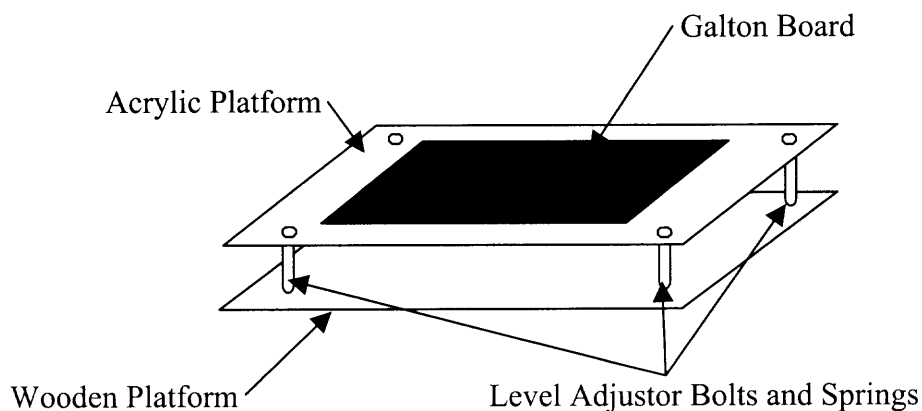


Figure 4.5 Diagram of the Galton board and its leveling system.

The height of the Galton board above the wooden platform was adjusted by turning one or more of those four bolts. The following describes the procedure used to level the Galton board.

1. With the wooden platform still set to its perfectly horizontal position, set all four bolts to a gap of one inch between the two platforms.
2. Place the bubble level on the top surface of the left side of the acrylic platform.
3. Note which side of the platform is too high.
4. Using a straight blade screwdriver, turn the screw on the high side of the platform one turn clockwise, thereby lowering the high end of the platform.
5. Recheck for levelness. If it is still not level, go back to step #3.
6. This side of the platform is level. Going in a clockwise direction, check the levelness of the top, right, the bottom sides of the platform. Essentially, repeat steps #3-#5 for the other three sides.
7. The Galton board assembly is now level.

4.2.3 Set the Release Height and Board Angle

The ball release height and angle of tilt of the Galton board were two of the three variable experimental parameters. The third was the particle material. In the experiments, which were conducted with this Galton board, specific values were chosen for each parameter. There were five different angle settings used. They ranged from 30° - 70° with 10° intervals. This range of angle settings was chosen for a reason. It was observed that for

any angle settings larger than around 70° , the percolating particles would have a large tendency to jump off of the surface of the board. It was also observed that at any angles smaller than 30° , the balls would tend to get stuck on the tops of the pins. This happened because they lacked the energy needed to rebound off of the pins and continue down the board. There were also five different release height settings that were used in the experiments. The release heights ranged from 20-100 rows in 20 row increments. In order to easily set the release height, the entire release mechanism was moved as one unit. It was held in place by four bolts, which were attached to steel glider pieces (Drawing C.13) in an extruded aluminum channel. The aluminum channel was mounted onto the acrylic platform.

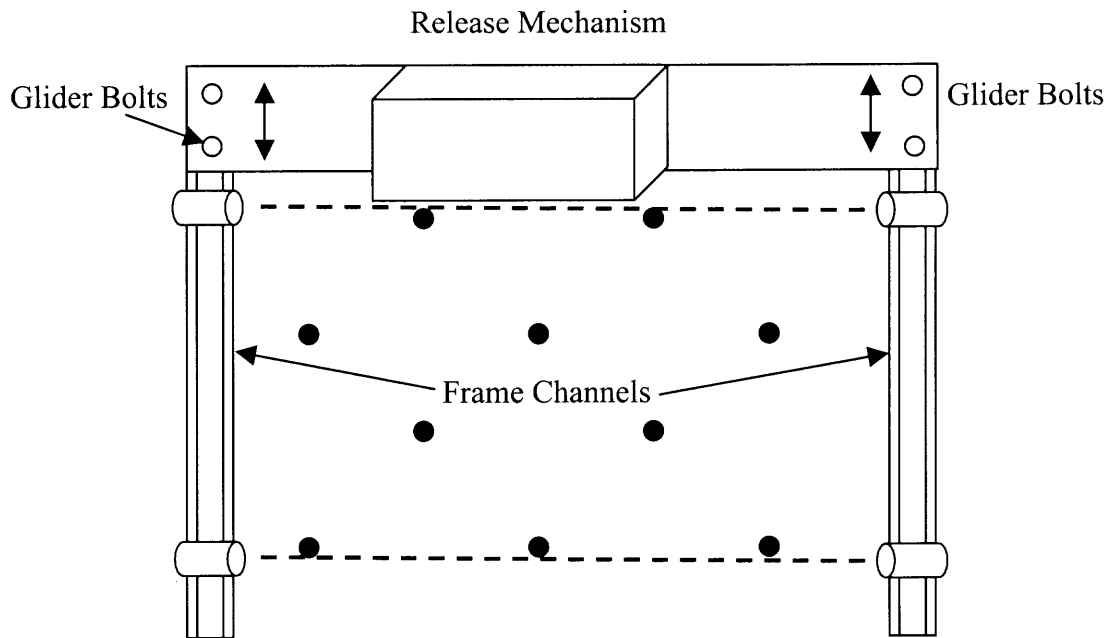


Figure 4.6 Diagram of the release mechanism height adjustment.

The following describes the procedure used to set the release height of the particles and the angle of the Galton board.

1. Loosen and remove the four screws holding the release assembly to the aluminum channel.
2. Holding the releaser assembly approximately horizontal, position the release nozzle in the gap between the pins (interstice) at the desired release height.
3. Slide the four gliders in the aluminum channel to be nearly under the four screws at the ends of the release mechanism.
4. Using a straight blade screwdriver, lightly tighten the screws at the ends of the release mechanism into the glider pieces in the aluminum channel.
5. Position the release nozzle to be just barely touching the pin directly above it. Also, assure that the release assembly is parallel with the transverse direction of the board.
6. Tighten all four release assembly screws completely. Check that the release assembly is secure.
7. Position the two components of the upper (start timer) optical beam to be directly above the top row of pins. Using the LED indicator located on the main control box, adjust the beam emitter to focus on the beam sensor.
8. Rotate the platform to the desired angle of experimentation. The angle is set using the angle finder unit attached to the surface of the acrylic platform.
9. Lightly tap the angle finder in order to eliminate the effects of sticking (hysteresis) that may be present in the device. Recheck the angle setting and continue tapping the instrument until it is very certain that the proper angle is set.

4.2.4 Filling the Hopper

The hopper is a small acrylic box located on a wall-mounted shelf above the Galton board. This was where the particles used in the experiment were stored. The particles were delivered from the hopper to the release mechanism via a flexible feed tube. It was very important that only one type of particle be in the hopper. Therefore, when changing the type of experimental particle, all other particles (balls) were removed first (the hopper should be empty), and then only the current experimental particles were put in the hopper. Enough particles were placed in the hopper to do at least one complete experiment at a given parameter setting. This was not as important in manual mode as it was in the automatic mode. Under manual mode, the trials were supervised. In the automatic mode, the trials were triggered and data was collected by a microprocessor without human observation. Here is the procedure used to fill the hopper.

1. Turn the power off the control unit.
2. Empty the hopper of all particles that are not to be used for the experiments.
3. Fill the hopper with more than the number of trials to be performed.
4. Turn on the power for the control unit.
5. Observe the balls falling down and filling the feed tube.
6. When the balls reach the feed tube sensor, the agitator servo should stop rotating. If it does not stop rotating, turn off the power to find the problem. If the servo does stop spinning, proceed with the experimental trials.

4.2.5 Centering the Release Nozzle

It was imperative that the release nozzle be centered exactly above the center pin. If this were not done, an unwanted bias would have been introduced into the experiment. The horizontal position of the releaser assembly was finely adjusted with a one-axis movement stage. This allowed for movements as precise as one thousandth of an inch in either direction. This was done by rotating a hand wheel at the end of the stage the appropriate distance as read on the graduations marked on the edge of the wheel. One complete rotation of the hand wheel translated to 0.050" in linear movement. It was observed that if the release nozzle was moved even one thousandth of an inch to the left or the right after being centered, the ball would fall to that side with a probability greater than 50%. Because of this fact, the probability of the ball going to the left or the right of the center pin of the Galton board was used. The following is the procedure that was used to align the releaser nozzle with the center pin.

1. Make sure that the system mode is switched to manual, the power is on, and the hopper and feed tube are full of balls.
2. Position the releaser nozzle to be directly above the top center pin by turning the hand wheel in the appropriate direction.
3. Release about ten balls separately from the release chamber observing if they fall to the left or right of the pin (as shown in the figure below).

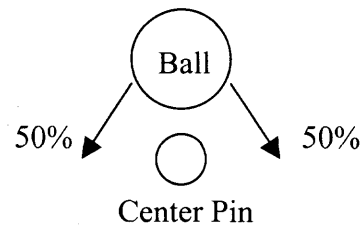


Figure 4.7 Sketch of the ball being released above the center pin of the Galton board and the probability of the ball going to the left or right of the pin.

4. If most (7-10) of the balls fell to the left of the pin, move the releaser assembly to the right one thousandth of an inch, then repeat step #3. If most (7-10) of the balls fell to the right of the pin, move the releaser assembly to the left one thousandth of an inch, then repeat step #3. If the balls fell equally in both directions, go to the next step.
5. The releaser nozzle is now centered to within the accuracy allowed by the experimental apparatus.

4.3 Data Collection Systems

The purpose of the Galton board data collection system was to automatically sense and record the residence time of the particles percolating down the board and the radial exit location of the particle. Upon completion of the steps below for each experiment, data collection was done in either manual or automatic mode.

- A. Frame and Galton board leveled.
- B. Release height and board angle set to desired values.
- C. Hopper and feed tube filled with particles.
- D. Release nozzle is centered.

4.3.1 Manual Data Collection System

In the manual data collection system, a manual momentary pushbutton switch triggered the experimental trials. When the switch was depressed, a ball was released from the release device. As soon as the ball exited the release nozzle and hit the surface of the Galton board, an optical sensor beam was broken. A microprocessor sensed that the optical sensor beam had been broken and then sent an electric signal to a digital timer equipped with an LED readout. The timer had been configured to give a residence time in thousandths of a second. The timer began the timing when it received the signal from the microprocessor. The ball continued to move down the Galton board. Immediately after it passed the last row of pins, another optical sensor beam was broken. The microprocessor detected this broken beam as a difference in voltage coming from the optical sensor. Once the microprocessor “saw” this, it then sent another electronic signal to the timer unit instructing it to stop the timing and display the total time. This was the residence time of the ball in seconds. After breaking this last optical beam, the ball continued on its way and fell into a slot. The slot location into which it fell depended on where in the bottom row the ball exited the last row of pins. The slot numbers ranged from 1-49 with 25 being the exact center slot. The experimenter carefully observed the slot number into which the ball exited the board, and recorded it in a data collection book. After the slot number was recorded, the experimenter observed the time on the LED display and then recorded that as well along side the slot number. When both pieces of data were recorded in the data collection book, that trial was then finished and the next trial began. When the momentary pushbutton switch was pressed for the next trial, the microprocessor sensed this and then sent a signal to the timer unit to reset it and also sent a signal to the

solenoids in the release system to release a ball. The cycle begins again. The following is a step-by-step procedure for collecting data manually.

Manual Mode

1. Activate the main power on the control box.
2. Depress the button to release one ball from the release chamber.
3. Observe the ball's descent and the slot number into which it falls.
4. If the ball gets stuck on a pin, tap it with a piece of wire and disregard that data point. If the ball leaps from the Galton board and does not fall into a slot, disregard that data point.
5. Record the slot number and residence time for that trial in a data collection log. The residence time is displayed above the board on an LED display mounted on the control unit.
6. Repeat steps #2-#5 until the desired number of trials have been performed.
7. Go home and sleep.

4.3.2 Automatic Data Collection System

Physically, the automatic data collection system functioned in the same manner as the manual one. The first step was selecting the automatic mode on the main controller box (Drawing C.9) by flipping the mode selector switch to "Auto". This action switched the main controls from the pushbutton release switch and the main controller box to another microprocessor, which controlled the automatic data collection. Once the mode switch was set, the experimenter started the data collection program on the PC. This began the automatic data collection process. The main microprocessor then sent signals to the two solenoids of the releaser assembly. This released one ball down the release nozzle and

onto the surface of the Galton board. As in the manual mode, when the ball began its descent along the board, an optical sensor beam was broken. The main microprocessor detected the resulting change in voltage output from the first optical sensor and then sent a signal to it in order to begin an internal timer. The ball continued its trajectory down the board and when it passed the last row of pins, it broke a second optical sensor beam. The microprocessor then detected the change in the output voltage from this optical sensor and as a result, stopped its internal timing circuit. This time was stored on the microprocessor until after the cycle was nearly complete. The ball continued even further down the board and fell through one of a series of forty-nine brass detectors.

Each of the brass detectors was equipped with an LED and an optical sensor. As the ball went through a brass detector, it blocked the light coming from the LED going to the optical sensor. The output voltage of the sensor changed and the microprocessor detected this change of voltage. Because there was a separate detector for each slot, the microprocessor could “tell” which of the 49 detectors the ball fell through by which pin on the chip was activated. This information of slot number and residence time was then sent to the serial port of the PC. The PC received this information and displayed it in the microprocessor interfacing software package. Once this information was sent to the PC, all registers of the microprocessor were reset and the cycle began again and continued to a preset number of trials. In the following experiments, 1000 trials were carried out.

Occasionally, during an experiment, a trial would fail. That is, a ball may have gotten stuck on a pin on its descent along the Galton board. In this case, neither the timer stop optical beam was broken, nor was the slot detector triggered. When this happened, the main microprocessor waited approximately 15 seconds before it sent a signal to the

PC that displayed, “The ball has gotten stuck on the board!” While this was displayed for that trial on the PC screen, the system was then reset and the next trial began. If this happened more than ten times in a row, the experiment would be stopped automatically by the microprocessor until the experimenter began a new experiment.

Sometimes the ball makes its way down the board successfully and goes through the brass detector, but the slot number is not detected by the microprocessor. This can happen for one of two reasons. First, the 1/16” hole in the brass detector may have been drilled a little off center and the ball made its way through the far end of the detector as seen in the next figure.

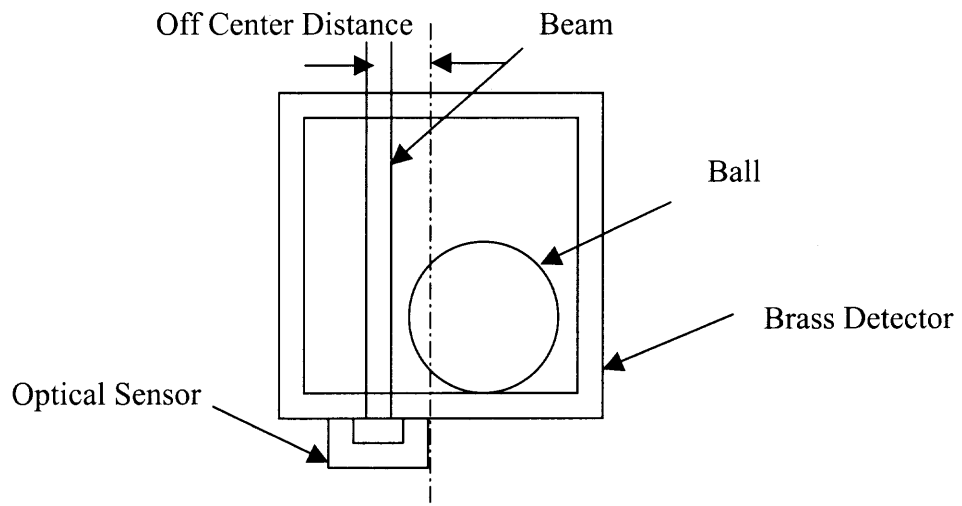


Figure 4.8 End view of the ball detector. This shows how an off-center hole can cause a misreading by the data collection system.

In this case, the ball does not break the beam and of course is not sensed by the microprocessor. The other reason that the slot is not detected is because the frequency of the microprocessor is too slow to sense a very short duration of change in voltage output from the detectors. This can also happen because of an off center hole in the detector unit, or it can happen from simply “bad timing”. The microprocessor speed is 400 MHz. This

means that it takes 2.5×10^{-9} sec (2.5 nanoseconds) for each cycle. It takes one cycle to check the status of one detector. So, the time required to check all 49 detectors for a voltage change is about 123×10^{-9} sec (123 nanoseconds). If the ball breaks the detector beam in less than this time, say for 120×10^{-9} sec (120 nanoseconds), then the microprocessor may potentially miss that signal. In all practicality, the chances of this happening are very slim. If however, this did happen and the microprocessor didn't detect the ball passing through a detector, a message would be sent to the PC for that trial stating, "The ball was not detected!" The microprocessor would then reset the system and continue with the next trial. If the ball was not detected more than ten times in a row, the experiment would stop automatically until it is checked and reset by the experimenter. The logic flowchart for this system can be found in Figure B.1.

Once the system performed 1000 (or the specified amount) of trials, the system stopped. When the experimenter noticed that the preset amount of trials has been reached, the file was then saved on the PC and also on a floppy disk. The data in this file was then imported into a statistical software package for further analysis.

The following is a step-by-step procedure for collecting data from the Galton board using the automatic data collection system.

1. Turn on the power to the system.
2. Turn on the PC and start the data collection program.
3. Using the mouse, click on the "start" icon on the screen.
4. The balls should drop automatically with about ten second intervals.

5. Watch the PC monitor to see the data being collected. If the data is not being displayed on the screen or if there are many errors, turn off the power to the system and fix the problem.
6. If the data is being collected and the system seems to be running smoothly, let the system run and go to lunch for 2-3 hours.
7. When the system stops running or all of the data has been collected, save the data to a floppy disk. The filename depends on the parameter settings and is in the following format: Material_R##_D##
Material is Aluminum, Brass, or SS. The two digits after the R is the release height in rows. The two digits after the D is the board angle in degrees.
8. Repeat steps #3-#7 for each of the parameter settings.

4.4 Data Analysis

The data collected from the Galton board experiment was analyzed with the help of a few different software packages. Each package had its own special feature for organizing the data. The two software packages used most often in this project are Microsoft Excel 2000 and PSI-Plot 6.0 made by Poly Software International. The procedure and tools used in each step of the data analysis will now be discussed.

When the experiments were run manually, the residence times and exit locations of the particles were recorded in a laboratory notebook. Once enough data was collected, it was entered by hand using a keyboard into an Excel spreadsheet as can be seen in Table A.3 (Appendix A, Table 3). When the automatic data collection system was used,

the data was automatically recorded into Microsoft Notepad as a comma separated text file. This is shown in Table A.4.

When all of the data for one experiment was collected, it was imported to a sheet in PSI-Plot. The automatic data needed quite a bit of “massaging” in order to make any sense of it. The first and second columns (cumulative errors and cumulative trials respectively) were deleted, as they were of no use during the analysis. Two columns remained, the slot number (0-49) and residence time in thousandths of a second. A new column was created to give the residence time in seconds by dividing the time column by one thousand. The old time column was then deleted and two columns were once again left, i.e, the slot number and residence time in seconds. This was also the same data that was recorded in the manual mode. The next task was to sort the slot numbers in ascending order along with their corresponding residence times. At this point, it was possible to determine if all of the slot sensors were working properly. During the initial automatic data collection experiments, it was found that slot sensor #14 was not working. This was noticed because of a lack of data for that slot number when there should have been data. Thus, the defective sensor was replaced so that data for that slot could be collected.

The next step was to find certain statistical information about each of the two columns of data. Numbers of interest were the average and standard deviation of the slot number and the residence time. Also of interest was the 95% confidence interval of the residence time. These statistical values were found very easily using the descriptive statistical report feature of PSI-Plot. As stated in Section 4.2 Experimental Procedure, there were three variable parameters in this experiment. These were the release height of

the particles, the board tilt angle, and the particle material. Five release heights, five board angles, and 3 different particle materials were used and the values of these can be seen in Tables A.6-A.18. This gives a total of seventy-five parameter settings. Once these values were found for each of the seventy-five parameter settings, they were entered into an Excel table for further analysis. These tables can be found in Appendix A. Besides the statistics found using PSI-Plot, other useful quantities were then calculated. One quantity calculated was the radial distance of slots from the center of the board. There are forty-nine slots at the bottom of the Galton board numbered consecutively from left to right. Knowing that the center slot is number twenty-five, the radial slot number (n), where the center slot is zero, can be calculated from,

$$n = \text{Slot} - 25 \quad (4.1)$$

Given the radial slot number, the radial distance can be found. The distance between the slots is $5/16''$ or 0.79375 cm. The radial distance (r) from the center of a Galton board is,

$$r = 0.79375n = 0.79375(\text{Slot} - 25) \text{ cm} \quad (4.2)$$

Slot numbers and their equivalent radial slot number (n) and radial displacement distances (r) can be found on Table A.1. The particle release height in centimeters is found in Table A.2 given the release height in number of rows. Each row is $5/32''$ or 0.396875 cm high. The timer detects the ball after it passes the first row of pins. The timer stops after it passes the last row of pins. The effective release height is the height in pins minus one row times the distance between rows plus the width of one pin,

$$H = 0.15875 + 0.396875(\text{Row} - 1) \text{ cm} \quad (4.3)$$

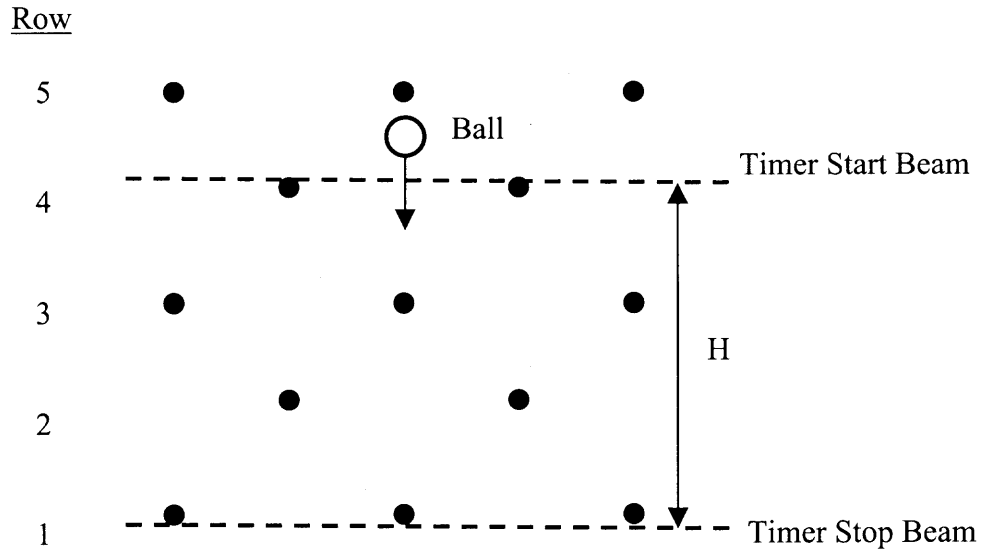


Figure 4.9 Sketch of the relative positions of the start and stop beams with the pins on the Galton board.

The average axial and radial velocities were calculated for each experiment. The equations used to find these quantities were,

$$V_A = H/t_{avg} \quad \text{cm/s} \quad (4.4)$$

$$V_R = r_{avg}/t_{avg} \quad \text{cm/s} \quad (4.5)$$

Where H is the release height (cm), r_{avg} is the average radial displacement (cm), and t_{avg} is the average residence time. Tabulated results are found in Tables A.8-A.18. In these tabulated results, a technique was used to compare the numerical values of different materials for the same board angle and release height. Referring to Table A.9, it can be seen that in order to compare the quantities of average residence time for aluminum, brass, and stainless steel, each cell is shaded in one of three different shades. Very dark shading refers to the highest value, medium shading is the middle value, and the lightest shading refers to the lowest value. Next to each table is a percentage of which shading is contained in the table. For example, in Table A.9, 68% of the 25 cells in the aluminum

table are the lowest residence time and 96% of the cells in the stainless steel table are the highest residence time. It can then be inferred that the aluminum particles generally have a shorter residence time than the stainless steel particles. This shading technique has been used in Tables A.8, A.9, A.10, A.12, A.13, A.15, A.16, and A.18.

In order to plot the data, it was necessary to bring it into PSI-Plot. This allowed plotting of more than one set of data on one graph. For each table of data, two plots were created. One plot has the release height as the independent variable and the other has the board angle as the independent variable. These plots can be seen in Appendix B. The two graphs for each set of data showed how the dependent variable is affected by both the release height and the board angle.

A special technique based on the method developed by Bridgwater et al. [2], was used to find the “radial” dispersion coefficient. The use of the word “radial” in this case refers to the direction perpendicular to the particle movement and is also called the x -direction. It was necessary to determine how many particles fell within a certain radial distance from the center. In the analysis here, eight different radial distances were used, which were three slots away from each other. Thus, this corresponds to: 24-26, 18-32, 15-35, 12-38, 9-41, 6-44, and 3-47, as shown in the figure below.

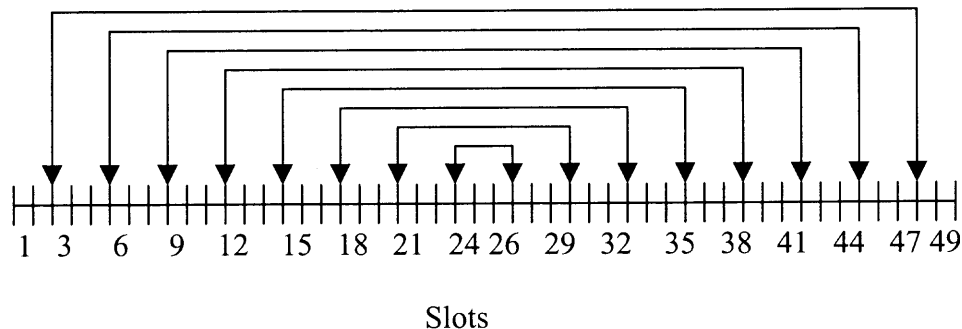


Figure 4.10 An illustration of the slots and their corresponding radial distance.

Using the sorted data in PSI-Plot, the particles falling in each range were tallied for each parameter setting. A sample of this is illustrated in Table A.5. Notice the increasing values for r^2 and how the value of N increases until $N=N_0$. Using these numbers, the value $\ln (N_0/(N_0-N))$ was computed. Then, a plot of r^2 vs. $\ln (N_0/(N_0-N))$ was made for each experiment. This was done in Excel in order to take advantage of the linear regression line feature and also its ability to give the equation of the regression line. Also of interest was the R^2 or “coefficient of determination value” of the line. These plots are shown in Figure B.2. The slope and R^2 value of each linear regression line was then tabulated on a separate Excel spreadsheet and plotted as previously discussed.

CHAPTER 5

RESULTS AND DISCUSSION

5.1 Design Results

For each experimental trial, the particle was released from the exact same location on the board. Ideally, the particle should be released with no initial rotational or translational velocity. This could not be done by the simple method of releasing the particles by hand using tweezers. Thus, the release mechanism, described in Section 4.1.3, was designed and fabricated to drop particles one at a time. Because of the nature of this release device, the particles do have some, though very little, initial velocities. This was unavoidable. The only release mechanism that is capable of releasing particles with no rotational or translational velocity is an air suction device. This device would have used an air compressor to draw air through a thin plastic tube. The particle would have to be placed carefully on the end of the tube and be held in place by suction. To release the particle, the air suction would be turned off. This method was not used because of the lack of an air compression system.

Another unique feature of the particle release system was the hopper. The hopper was a small container with an open top where the particles were stored. In normal operation, the opening at the bottom of a hopper may get clogged with particles. This was realized, and so an agitator system was developed to allow for unclogged delivery of particles to the releaser mechanism. The agitator consisted of a small control servo mounted under the hopper. A nylon rotor was attached to the servo. The rotor blades oscillated back and forth over the hopper exit hole. This agitated the particles and broke

up any unwanted stagnation in the hopper. Since it wasn't necessary for the servo to work all of the time, an optical sensor was mounted high on the feed tube. This sensor signaled the servo to oscillate if the feed tube became empty, and to stop when the feed tube was full. This system worked flawlessly and there was never a problem with the hopper getting clogged.

It was very important in this experiment to release the particles onto the Galton board as near to the centerline of the Galton board as possible. This was accomplished by mounting the release mechanism onto a single axis movement stage. This stage had a precision of 0.001". By using this very precise movement device, particles were released very close to the centerline. Anything with less precision than this would have introduced an unwanted bias to the experiment.

Another innovation developed for this experiment was the use of light beams to detect the passing of a moving particle. Here, the issue was, how to detect such minute particles with the required accuracy and precision? As explained in Section 4.1.5, pinpoint optical beam sensor pairs were used. In this two-unit system, one unit emitted a very thin light beam, and the other unit was capable of detecting this light beam from a distance of up to one meter away. This was ideal for the Galton board, which was only about a half meter across. Two sets of optical sensors were used, one to start the digital timer and one to stop it. This was a great improvement over the stopwatch used by Sergeev [4] and is better suited for this experiment than the microphone system used by Bridgwater [3].

By far, the most ingenious part of the data collection system was the optical slot detectors. This solved the problem of how to automatically determine and record the exit

location of each of the particles. During the course of this work, many possible solutions were discussed, including very small mechanical switches, optical sensors, electrical contact devices, and even proximity switches. Most of these were eliminated either because of budget limitations or the fact that they would just not do the job. In the end, it was decided to use an opto-electronic system similar to the timer sensing units. Of course, monetary cost was of very high concern because not only two sensors were needed, but forty-nine of them. With a little research, inexpensive components were found which would do the job correctly. Each of the forty-nine sensors consists of an LED, an optical sensor, and a brass housing, all of which were discussed in more detail in Section 4.1.2. This system, developed by fellow NJIT student Mark Johnson, successfully provided the slot location of each of the percolating particles.

5.2 Experimental Results

Much data was collected from experiments on the Galton board. For each experimental parameter setting, approximately 150 separate trials were performed. Each trial consisted of dropping one ball down the Galton board and collecting two pieces of data. The two pieces of data were the residence time and the exit position. The time units were seconds and were given in thousandths of a second. The exit position was the number of the slot into which the ball fell. This value ranged from 1-49, where the center slot is numbered 25. The slot number could then be transformed into a horizontal location along the width of the board at the exit. Here, the radial distance (in centimeters) was defined as the horizontal distance traveled by the ball measured from its central release location on the board.

There were three different types of balls used in the experiment, i.e. aluminum, brass, and stainless steel. For each of these, the conditions of the experiment were changed in a number of ways. The board was tilted to five different angles. These angles ranged from 30° to 70° in 10° increments. Any angles steeper than 70° would cause the balls to jump off the surface of the board and any angles less than 30° would not give the balls enough energy to descend the board as they tended to get “stuck” on the pins. The balls were also dropped from different heights on the board. Five different heights were used ranging from 20-100 rows high with increments of 20 rows. The table below lists the correspondence between the rows and height measured from the bottom of the board.

Table 5.1 Rows of the Galton Board and Corresponding Heights in Centimeters.

Rows	Height (cm)
20	7.70
40	15.64
60	23.57
80	31.51
100	39.45

These parameter variations produced twenty-five experimental settings for each type of ball, thereby yielding a total of seventy-five experimental settings. This equates to a total of approximately 11,250 separate experiments (ball drops). All of this data was plotted and analyzed in different ways and certain behaviors have been deduced.

5.2.1 Average Radial Displacement

The first quantity that was determined from the data was the “average radial displacement” of the balls. Values were calculated for each of the seventy-five different parameter settings, using the equation,

$$\text{Radial Displacement (cm)} = (\text{Slot}-25) \times 0.79375 \quad (5.1)$$

This equation was explained in detail in Section 4.4 on Data Analysis and is equivalent to equation (4.2). As would be expected from this experiment, the average exit location of the balls was very near the centerline of the board. This was expected because the particle distribution of a Galton board is normal or Gaussian as can be seen in the following Figure 5.1.

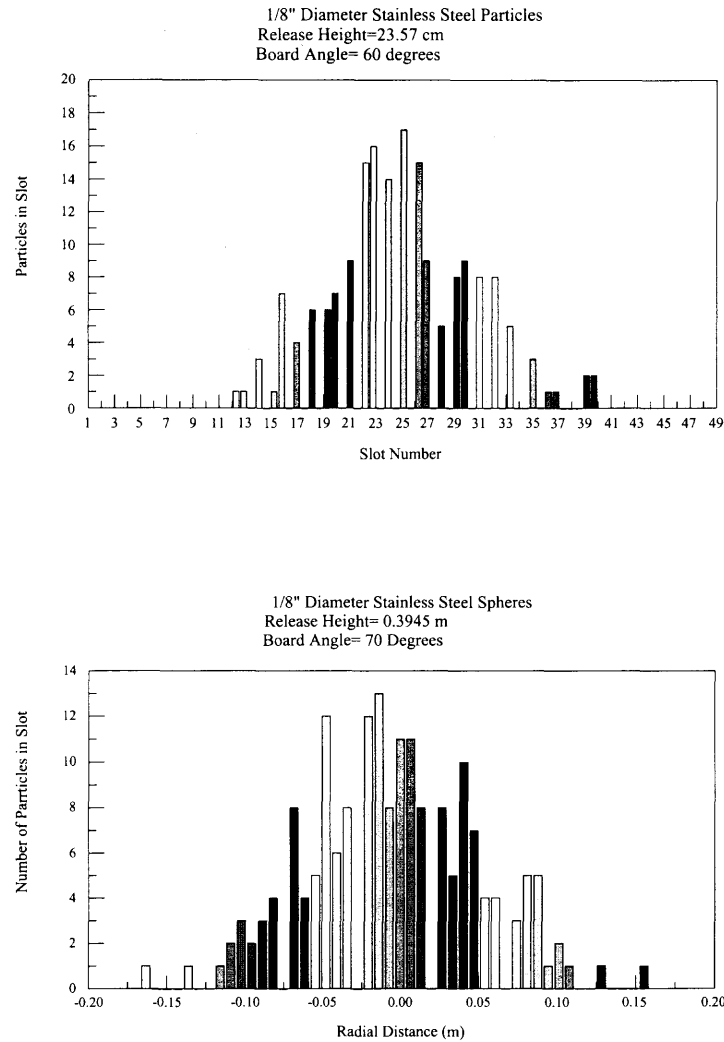


Figure 5.1 Typical particle distributions at the bottom of the Galton board.

Although most of the individual particles exited far from the center of the board, the average exit location of the particles was very near the center. The average exit location for all of the seventy-five parameter settings was -0.259 cm from the centerline of the board, as seen on Table A.7. This can be considered insignificant because it is less than half of the slot spacing, which is 0.6875 cm.

5.2.2 Standard Deviation of the Radial Displacement

The standard deviation of the exit location of the balls from the centerline is, in effect, a description of the spread of the Gaussian (or normal) shape of the ball distribution. The higher the standard deviation, the more shallow and spread out is the distribution.

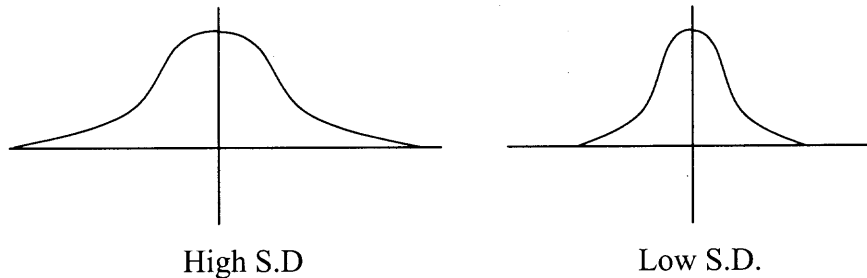


Figure 5.2 Gaussian distributions with a high and low standard deviations.

The lower values of the standard deviation result in a distribution that is sharper, more condensed, and higher in the center and less spread out.

For each of the three different material balls used, the standard deviation of the radial displacement was plotted versus the release height and the board angle. It is seen from Figures B.3, B.5, and B.7 that as the release height is increased, the standard deviation increased nearly linearly. This is what one would expect because the balls have time to collide with more pins at greater heights, and possibly also the balls reach higher kinetic energies and therefore have a greater tendency to spread. It is also noted in Figures B.4, B.6, and B.8 that the angle of the board does not seem to have any noticeable effect on the value of the standard deviation. This is contrary to intuition. One would think that at steeper angles, the standard deviation would be smaller and at shallower angles there would be more spread and the standard deviation would increase. This makes sense because the ball would travel slower and wander more at shallower

angles, thereby increasing the spread of the distribution. This conjecture doesn't appear to be supported by the data. It may be that even at shallow angles, the path of the ball is not very different from that at steep angles. This may be due to the small interstice space between the pins relative to the size of the balls. In this case, there was not much room for wandering in an interstice (gap or space between pins). Perhaps with more data, some effect of the board angle on the standard deviation can be seen. An examination of the data in Table A.8 and the associated Figures B.3-B.8 indicates little dependence of the standard deviation on the material of the balls. The data in Table A.8 suggests that the standard deviation is lowest for aluminum, while brass and stainless steel have about the same standard deviation. This seems reasonable from the observation of the coefficient of restitution in Table A.19, that the aluminum balls do not have as much bounce as the brass and stainless steel balls and therefore tend to have trajectories with less scatter down the board.

5.2.3 Average Residence Time

The average residence time in seconds was plotted against the release height (cm) and the board angle (degrees). From Figures B.9, B.11, and B.13, it is seen that there is a linear relationship between the release height and the residence time. The reason for this is that, assuming the ball has a nearly constant velocity, the greater the distance traveled, the greater the time required to traverse this distance. Figures B.10, B.12, and B.14 indicate that the residence time depends on the board angle, but the relationship is not linear. As the board angle increases, the residence time decreases. This is because of a greater effective force of gravity on the ball and the resulting increase in ball velocity. Also, as

the board angle increases, it is seen that the rate of change of the residence time decreases and goes toward zero at steep angles. Essentially,

$$\frac{dt}{d\theta} \rightarrow 0 \quad \text{as} \quad \theta \rightarrow 90^\circ \quad (5.2)$$

It is seen in Table A.9 that the residence times of the different material balls are noticeably different for the same parameter settings. The shortest residence times are the aluminum balls followed by the brass then the stainless steel. This is of course not all of the time. The percentage of aluminum parameter settings with the shortest residence times was 68%. The percentage of brass was 64% and 96% of the parameter settings of stainless steel had the longest residence times. This happens because the lower the coefficient of restitution of the particles from Table A.19, the less they will bounce around an interstice and will tend to move faster down the board.

5.2.4 Standard Deviation of the Residence Time

As for the standard deviation of the residence times, some expected and unexpected behaviors can be seen. First of all, it is noticed that in general, the standard deviation increases roughly linearly with increasing height. In other words, the variation of the residence times is greater for greater heights. This is what would be expected and can be seen in Figures B.15, B.17, and B.19. Another behavior that can be observed from these plots is that there is a tendency for the standard deviation of the residence time to increase with a decrease in the board angle. This is seen clearly in Figure B.16 for aluminum, but is not very clear in Figures B.18 and B.20 for brass and stainless steel respectively. Instead, there are some inconsistencies, which could probably be cleared up with some more data. It can be seen in the case of aluminum in Figure B.16, that for each release

height, the residence time standard deviation tends to decrease for an increase of the board angle. This seems true only for the higher board heights and is less noticeable for the lower board heights. In fact, what is seen for the cases of brass and stainless steel in Figures B.18 and B.20 is that there is little or no relationship between the residence time standard deviation and the board angle. It seems reasonable that the variation in residence time will increase with an increase in the board angle. As seen in Table A.10, the stainless steel balls have the largest variation of residence times, followed by brass, then aluminum. This seems natural since it correlates with the fact that the stainless steel balls have the longest residence times and therefore have the larger variation which is then followed by the brass then aluminum.

5.2.5 Confidence Interval for the Residence Time

Calculating the average residence time for each of the seventy-five different parameter settings is all well and good, but what is the precision of those averages? In other words, do the residence times really tell about the behavior of the Galton board system? To answer these questions, a statistical tool called a confidence interval is used.

In the data collection for the Galton board, the residence time in units of seconds was collected. Because of the limits of time and energy, only a finite number of data points were collected. This finite data collection is only a sampling set of data, since the whole population set of data is infinitely large. The standard deviation of this finite set, or sample set of data, could be found. It will be assumed that there is enough data collected to say that the standard deviation of the sample is the same as the standard deviation of the population. What is the certainty that the population average is within a specific

range? This certainty, or confidence, is a percentage between 0%-100%. It will not tell much if it states that there is a 50% certainty that the residence time is between, say 5 and 10 seconds. This will be a 50% confidence interval. This is not very certain. Typical values for confidence coefficients are 0.90, 0.95, and 0.99. If given a 100% confidence interval, the range will be too wide to tell of any important information. The equation for finding the interval at a certain confidence coefficient is,

$$\bar{x} \pm z s_{\bar{x}} \quad (5.3)$$

and because it is assumed that the sample standard deviation is equal to the population standard deviation, $s_{\bar{x}} = \sigma_{\bar{x}}$, equation (5.3) can be written as,

$$\bar{x} \pm z \sigma_{\bar{x}} \quad (5.4)$$

The confidence coefficient is described by z . Say, for example, that the chosen confidence coefficient is 95%, as in the results of this thesis. It is known that half of the 95% area under a normal probability distribution curve is 47.5% or 0.4750. From the z -chart for normal distributions, it was found that an area of 0.4750 corresponds to a z value of 1.96. The equation for a 95% confidence coefficient then becomes,

$$\bar{x} \pm 1.96 \sigma_{\bar{x}} \quad (5.5)$$

where \bar{x} is the sample average (average residence time) and $\sigma_{\bar{x}}$ is the sample standard deviation (S.D. of the residence time). The calculated values for this are shown in Table A.11.

It can be seen that none of the ranges intersect with values adjacent to them. This is a good thing. If the ranges did intersect with the adjacent values, then it would not be very certain where the true, or population, averages lie relative to one another. It is 95%

certain that the population average residence time is located in the ranges shown in the table for those given parameter settings.

5.2.6 Average Axial Velocity

From the experimental value of the average residence time and given the release height, the average axial velocity was calculated for each experimental parameter setting. The average axial velocity was found by:

$$V_A = H(\text{cm})/t_{\text{avg}}(\text{sec}) \quad (5.6)$$

This is the average velocity of the percolating particle from the entrance to the exit of the Galton board. First, it is immediately noticed from Figures B.21, B.23, and B.25 that the axial velocity is not dependent on the release height of the ball. In fact, for all three tested materials, the axial velocity seems to remain constant for all release heights. This means that the ball reaches its terminal (constant) velocity very quickly. It is also noticed from Figures B.22, B.24, and B.26 that the axial velocity increases linearly with increases in the board angle. This is true because at higher angles, there is a greater force of gravity acting along the plane of motion of the balls. It can also be seen from these figures that the axial velocity changes less for increases in the board angle. Put mathematically:

$$\frac{dV_A}{d\theta} \rightarrow 0 \quad \text{as} \quad \theta \rightarrow 90^\circ \quad (5.7)$$

This is the same result found in the plots for the average residence time. Comparing the axial velocities of the three different material particles at various experimental parameter settings as see in Table A.12, it can be concluded that the aluminum generally has the fastest axial velocity followed by the brass then the stainless steel.

5.2.7 Standard Deviation of the Axial Velocity

This section looks at how the standard deviation of the axial velocity behaves with changes in the release height, board angle, and ball material. From Figures B.27, B.29, and B.31 it is seen that the variation of the axial velocity decreases as the release height increases. Also, the rate of change of the axial velocity standard deviation approaches zero as the release height increases. In other words,

$$\frac{dS.D.V_A}{dH} \rightarrow 0 \quad \text{and} \quad S.D.V_A \rightarrow C \quad \text{as} \quad H \rightarrow \infty \quad (5.8)$$

This behavior goes against intuition. One would think that as the release height increased, the standard deviation of the axial velocity would also increase, i.e. have more variation. This is not so. The reason this happens may be that when the ball travels farther, the small interruptions in the travel tend to balance themselves out and lead to less variation in the axial velocity. It is also noticed from Figures B.28, B.30, and B.32 that as the board angle gets steeper, the standard deviation of the axial velocity increases. This is also counter-intuitive. One would think that there would be more variation in the axial velocity at shallower angles because of the increased sensitivity and slower travel of the balls. This is, however, not true. As a result of the increase of velocity from the steeper board angles, the ball impacts the pins at greater speeds and are then deflected back upward against the direction of travel. This produces a greater variation of axial velocities. When comparing the values of standard deviation of axial velocities for different materials from Table A.13, no relationship is noticed. Perhaps there is a relationship between these two and more data is required to see it.

5.2.8 Radial Velocity

The average radial velocity of the balls was found using the radial displacement of the balls from its release point on the centerline and its residence time. The formula used was,

$$V_R = D(\text{cm}) / T_{\text{avg}}(\text{sec}) \quad (5.9)$$

Where D is the radial displacement from the centerline. This is however not a true velocity, as the balls tend to change their direction of radial travel very often and rarely travel in only one direction radially. The average radial velocities were found for each parameter setting, but the results of this were expected. Obviously, the average radial velocity for all of the seventy-five different settings was approximately zero. The standard deviation of the radial velocities was interesting. It seems, from looking at Figures B.33-B.38 that the variation of the radial velocity decreased as the height increased. It is also seen that the standard deviation of the radial velocity increased as the board angle increased. There doesn't seem to be any relationship between the ball material and the standard deviation of the radial velocity in Table A.15.

5.2 Radial Dispersion

Following the method used by Bridgwater et al. [2], this section begins with the PDE that describes the radial dispersion of particles from a centerline. This equation is,

$$\frac{\partial n}{\partial t} = E_r \left(\frac{\partial^2 n}{\partial r^2} + \frac{1}{r} \frac{\partial n}{\partial r} \right) = E_r \nabla^2 n(r, t) \quad (5.10)$$

where n is the number of particles per unit area perpendicular to the percolation direction, t is the time, r is the radial distance from the center, and E_r is the radial dispersion coefficient. Using the following boundary conditions,

$$n \rightarrow 0 \quad \text{as} \quad r \rightarrow \infty \quad \text{for} \quad t > 0 \quad (5.11)$$

$$n = 0 \quad \text{for} \quad r > 0 \quad \text{at} \quad t = 0 \quad (5.12)$$

$$\int_0^{\infty} 2\pi r n dr = N_0 \quad \text{for} \quad t > 0 \quad (5.13)$$

It is found that the equation for the number of particles per unit area at a radial distance r , at time t , and with a given value of E_r is,

$$n = \frac{N_0}{4\pi E_r t} \exp\left(\frac{-r^2}{4E_r t}\right) \quad (5.14)$$

It is also known that the number of particles having centers within a radius r is,

$$N = \int_0^r 2\pi r n dr \quad (5.15)$$

Combining and rearranging the previous two equations gives,

$$\frac{r^2}{4E_r t} = \ln\left(\frac{N_0}{N_0 - N}\right) \quad \text{or} \quad 4E_r t = \frac{r^2}{\ln\left(\frac{N_0}{N_0 - N}\right)} \quad (5.16)$$

Remember that this is under the false assumption that the residence times are constant. Under this assumption, if the plot of r^2 vs. $\ln(N_0/(N_0-N))$ is a straight line, the radial dispersion coefficient is constant. If it is found that r^2 is proportional to $\ln(N_0/(N_0-N))$, it can be concluded that the radial dispersion mechanism is a diffusional, or random walk mechanism.

Values of r^2 vs. $\ln(N_0/(N_0-N))$ have been plotted for all seventy-five different experimental parameter settings. Although the data is rough, it seems that all the plots form a straight line. The data points all fall very close to a least-squares line displayed on

each plot as can be seen in Figure B.2. Thus it can be said that the Galton board system is a diffusional or random walk mechanism for all heights and board angles.

The R-squared value was found for each of the seventy-five best-fit lines. This value, also known as the coefficient of determination, is an indicator that ranges in value from 0 to 1 and it reveals how closely the values for the trend line correspond to the actual data. The trend line is most reliable when its R-squared value is at or near 1. It can be seen from Table A.17, that most R-squared values are very near to 1 or exactly at 1. The average of all seventy-five R-squared values is 0.980. This tells quantitatively that the dispersion mechanism in the Galton board is very close to a diffusive, or random walk mechanism. The slope of the plots of r^2 vs. $\ln(N_0/(N_0-N))$ is given in Table A.16. Since it is known from the analysis that the slope of these plots is equal to $4E_r t$, these numbers don't tell anything directly. After dividing the numbers in Table A.13 by $4t$, where t is the average residence time given in Table A.9, some possible patterns can be seen for the radial dispersion coefficient in Table A.18. Although it is not very evident from the data, it seems that the aluminum particles tend to have the higher values of the radial dispersion coefficient. For the same parameter settings, 40%, or ten out of twenty-five of the aluminum experiments were the highest value of radial dispersion coefficient compared to the brass and stainless steel. This may correspond with the fact that the aluminum particles have a distinctly lower coefficient of restitution than the brass and the stainless steel as seen in Table A.19. This occurs not because the aluminum particles have a larger distribution spread, but because the mean residence time is significantly lower than the other particles. It is the residence time that has the relationship with the coefficient of restitution. In Section 5.2.3, this relationship was explained in greater

detail. So, because the aluminum balls move faster down the Galton board, the values for the radial dispersion coefficient increase. Looking at the data for brass and stainless steel on Table A.18, no clear patterns can be seen. This may be because the value of coefficient of restitution for the brass and stainless steel are very close in value, but are quite different from aluminum.

If one thinks about it, the value of the radial dispersion coefficient should remain the same for any release height. To see if this is true, look at Figures B.45, B.47, and B.49 for aluminum, brass, and stainless steel respectively. The values of the radial dispersion coefficient tend to jump around quite a bit for the board set at the same angle. There does not, however, appear to be any noticeable trend or slope to these lines. It all seems to roughly oscillate around a constant value. It cannot be said with any confidence that there is any relationship between the radial dispersion coefficient and the release height.

How about the board angle? Does this somehow affect the value of the radial dispersion coefficient? The data to find the answers to these questions is plotted in Figures B.46, B.48, and B.50. For the aluminum and stainless steel Figures B.46 and B.50, no noticeable trends in the plotted data can be seen. All of the lines seem to be quite flat with not much of a trend up or down. From Figure B.48 for brass, something different can be seen. It is seen that in general, the radial dispersion coefficient increases with an increase in the board angle. This phenomenon is quite distinct in this figure. All graphs of the data in this plot tend to slope upward on average.

Of course, any observed relationships in this section are simply unvalidated hypotheses. With the small amount of data collected in the experiments, no solid

quantitative conclusions can be made here. All that is given here is a qualitative explanation for trend patterns observed in the collected data. In order to verify these patterns, much more data must be collected and analyzed.

CHAPTER 6

CONCLUSIONS

6.1 Conclusions

From the previously detailed experiments conducted with a Galton board, some conclusions have been made. It has been found that the width, or standard deviation, of the distribution of particles at the exit of the Galton board is linearly dependent on the release height of the particles. As the release height increases, the standard deviation of the resulting Gaussian, or normal, distribution formed by the exiting particles increases. This is because of the higher number of collisions associated with a greater release height, which then result in a greater tendency to spread. It has also been found that there is no relationship between the standard deviation of the resulting distribution and the board tilt angle. This is because with a small interstice, the percolating particle has very little room for wandering and probably tends to take the same path regardless of board angle. The particles with lower coefficient of restitution had a lower standard deviation of exit distribution. This is in accordance with the work done by Bridgwater et al. [2 and 3].

As expected, the average residence time increased linearly with the release height. Also as expected, the average residence time decreased with increasing board angle. The particles go faster at steeper angles. It can be concluded that the change in residence time with board angle is greater for lower angles and approaches zero for steeper angles near 90° or vertical. The particles with lower coefficient of restitution tended to descend the board quicker than particles with high coefficient of restitution.

The standard deviation of the residence times increased linearly with the release height. It was also seen that the standard deviation of the residence time decreased with increasing board angle for particles with a lower coefficient of restitution. For particles with a higher coefficient of restitution, there was not a clear relationship between the standard deviation of the residence time and the board angle.

The average axial velocity was found to be constant for all release height settings. This tells that the particles reached a constant average velocity in a very short time. It was also seen that the average axial velocity of the particles increased nearly linearly with the board angle. The particles with the lower coefficient of restitution tended to have a higher average axial velocity. The standard deviation of the axial velocity decreased for increasing release height. This counter-intuitive result happens because when the particles travel further, the small interruptions in travel tend to balance themselves out and lead to less variation in axial velocity. Also, it was found that the standard deviation of the axial velocity increases as the board angle increases because of the greater speed of impact with the pins and therefore larger rebound against the direction of travel.

The standard deviation of the average radial velocity decreased as release height increased and increased as the board angle increased. Although this is an interesting result, no conclusions can be made from this behavior.

From the analysis of the radial dispersion coefficient, it was found that the particles percolating on the Galton board used in these experiments are subject to not only a radial dispersion mechanism, but also to a diffusional, or random walk mechanism.

6.2 Ideas for Future Work

After performing the experiments presented in this thesis, it has been realized how much more can be done to investigate the phenomenon and behavior of Galton board systems. In these experiments, only three parameters were adjustable; the particle release height, the board tilt angle, and the particle material. All other variables remained constant. There are many more parameters that can be changed in order to find the dependence of certain behaviors with a change in those parameters. Here are just a few other parameters that can be changed and experimented with for a Galton board.

- Ratio of Pin Diameter to Particle Diameter (D/d): For the experiments detailed in this thesis, the ratio was $\frac{1}{2}$. It would be interesting to alter this ratio and see how values such as the particle distribution and the residence time are affected.
- Pins Per Area (Pins/m^2): This is a measure of the density of the pins on the board. There can be very few pins or very many pins on the board. It is certain that changing this value will affect the path of travel of the descending particles.
- Packing Ratio of the Pins ($\text{m}^2(\text{pins})/\text{m}^2(\text{board})$): This is a measure of the tightness of the pin array. For cylindrical obstacles, this value can range from close to zero where the pins are spread very far apart or are very small to a maximum value of 0.7854 where the pins are touching one another and the packing doesn't allow particles to pass. For the Galton board used in the previously detailed experiments, the packing ratio was 0.0628.
- Particle and Pin Material: Although three different materials were used in these experiments, there are many more materials that may have been used. Another variable that was not investigated here is the pins, or obstacles made from

different materials. These two variables together affect the coefficient of restitution of the collisions and this coefficient is a very important variable to look at in this system.

- **Shape of the Pins and Particles:** There is no rule that states that the pins are to have a circular cross section. It would be just as valid to use pins with different shapes such as triangular, oval, square, or even thin plates. Also, the particles need not be spherical. Cubic or elliptical particles may be used and would probably give interesting results. Why even use discrete particles? The Galton board would work with fluids as well, under the proper experimental conditions.
- **Distribution of Pins:** In the previous experiments, the distribution of pins was even. That is, the spacing of all the rows and columns was constant. In Galton board experiments conducted by Sergeev et al. [4], the horizontal spacing of the columns varied linearly with the horizontal distance and the resulting distribution was observed. This can also be done with the vertical spacing between rows.
- **Vibration:** There have been many experiments conducted to study the effect of vibration on the inter-particle percolation of particles. Why not study the effect of vibrations on the spontaneous inter-particle percolation in a Galton board system? Of course, the vibrations can have variable amplitude and frequency.
- **External Forces:** Studies have been done on the effect of external forces other than gravity on the movement of particles through a viscous fluid. The same can be done on a Galton board. How, for example, would the presence of a large magnetic field affect the travel of particles in the system?

- More Data Points: There were only about 180 trials run for each of the parameter settings in the experiments conducted for this thesis. The results would be much clearer if one thousand or more trials were performed for each setting. More trials would have also made it possible to make more in depth conclusions about the behaviors of the Galton board system.

The experiments and results presented here are just the beginning of looking at the mechanics and behavior of the Galton board system. These experiments were performed more out of scientific curiosity than for use in some industrial application. It is hoped that someday the behaviors of the Galton board system can be utilized by industry to improve some process or by the educational community to pique the curiosity of students and inspire them to make their own investigations into the many different phenomenon of nature.

APPENDIX A

TABLES

The following appendix contains tables giving the characteristics of the experimental apparatus, samples of experimental data, and numerical results of the performed experiments.

Table A.1 Radial Displacement Distances (r) for Slot Numbers of the Galton Board.

Slot	n	r (cm)
1	-24	19.05
2	-23	18.26
3	-22	17.46
4	-21	16.67
5	-20	15.88
6	-19	15.08
7	-18	14.29
8	-17	13.49
9	-16	12.70
10	-15	11.91
11	-14	11.11
12	-13	10.32
13	-12	9.53
14	-11	8.73
15	-10	7.94
16	-9	7.14
17	-8	6.35
18	-7	5.56
19	-6	4.76
20	-5	3.97
21	-4	3.18
22	-3	2.38
23	-2	1.59
24	-1	0.79
25	0	0.00

Slot	n	r (cm)
26	1	0.79
27	2	1.59
28	3	2.38
29	4	3.18
30	5	3.97
31	6	4.76
32	7	5.56
33	8	6.35
34	9	7.14
35	10	7.94
36	11	8.73
37	12	9.53
38	13	10.32
39	14	11.11
40	15	11.91
41	16	12.70
42	17	13.49
43	18	14.29
44	19	15.08
45	20	15.88
46	21	16.67
47	22	17.46
48	23	18.26
49	24	19.05

Table A.2 Height (H) Conversion for Row Numbers of the Galton Board.

H (Rows)	H (cm)
100	39.45
90	35.48
80	31.51
70	27.54
60	23.57
50	19.61
40	15.64
30	11.67
20	7.70
18	6.91
16	6.11
14	5.32
12	4.52
10	3.73
8	2.94
6	2.14
4	1.35
2	0.56

Table A.3 Sample Excel Data for Brass Balls Dropped from a Height of 60 Rows and an Angle of 40 Degrees.

Slot	Time (s)
21	4.851
18	5.167
21	4.517
22	5.377
34	5.104
27	4.855
14	4.877
30	5.225
27	5.648
21	5.021
15	5.030
14	5.373
20	4.459
27	5.523
28	5.675
25	5.309
21	5.443
17	4.999
29	5.177
22	5.031
22	5.066
34	4.575
24	5.291
19	5.170
34	5.304
33	4.969
25	4.908
30	5.316
15	5.371
24	5.868
34	4.898
31	5.335

Table A.4 Sample of Data from the Automatic Data Collection System.

RESTART
,0,1,28,4731
,0,2,24,4464
,0,3,19,5588
,0,4,21,5288
,0,5,25,5229
,0,6,23,4949
,0,7,36,4666
E2-WARNING- Ball got stuck on board !
,1,9,26,5066
,1,10,25,5221
,1,11,33,4535
E3-WARNING- Ball was not detected !
E2-WARNING- Ball got stuck on board !
,3,14,23,5089
,3,15,23,4889
,3,16,22,4643
,3,17,24,4578
,3,18,31,5709
,3,19,25,4914
,3,20,28,5380
,3,21,20,5264
E3-WARNING- Ball was not detected !
,4,23,19,5240
,4,24,32,4816
,4,25,16,4708
,4,26,28,5260
,4,27,15,5096
,4,28,20,4858
,4,29,12,4811
,4,30,23,5472
,4,31,28,4879
,4,32,28,4323
,4,33,32,5999
,4,34,25,5190

Table A.5 Values to Find the Radial Dispersion Coefficient (1/8" Brass, Release Height 60 rows).

Angle (degrees)= 70
No= 170

r^2 (cm) ²	N	ln (No/(No-N))
0.630	34	0.223
10.080	105	0.961
30.872	142	1.804
63.004	164	3.344
106.477	169	5.136
161.290	170	X
227.444	X	X
304.939	X	X

Angle (degrees)= 60
No= 176

r^2 (cm) ²	N	ln (No/(No-N))
0.630	31	0.194
10.080	102	0.866
30.872	141	1.615
63.004	165	2.773
106.477	175	5.170
161.290	176	X
227.444	X	X
304.939	X	X

Angle (degrees)= 50
No= 176

r^2 (cm) ²	N	ln (No/(No-N))
0.630	42	0.273
10.080	94	0.764
30.872	143	1.674
63.004	169	3.225
106.477	174	4.477
161.290	176	X
227.444	X	X
304.939	X	X

Angle (degrees)= 40
No= 169

r^2 (cm) ²	N	ln (No/(No-N))
0.630	36	0.240
10.080	94	0.812
30.872	133	1.546
63.004	156	2.565
106.477	166	4.031
161.290	167	4.437
227.444	168	5.130
304.939	169	X

Angle (degrees)= 30
No= 163

r^2 (cm) ²	N	ln (No/(No-N))
0.630	38	0.265
10.080	99	0.935
30.872	138	1.875
63.004	157	3.302
106.477	163	X
161.290	X	X
227.444	X	X
304.939	X	X

Table A.6 Number of Data Points Collected for Each Parameter Setting.

	Height (cm)					
Angle	39.45	31.51	23.57	15.64	7.70	
70	176	174	182	183	182	Aluminum
60	182	173	183	185	181	
50	179	178	182	185	185	
40	171	175	181	179	184	
30	148	166	174	176	184	

	Height (cm)					
Angle	39.45	31.51	23.57	15.64	7.70	
70	341	359	170	180	177	Brass
60	361	174	176	177	179	
50	363	358	176	168	182	
40	357	167	169	178	182	
30	345	154	163	177	181	

	Height (cm)					
Angle	39.45	31.51	23.57	15.64	7.70	
70	180	173	183	177	179	Stainless
60	184	180	183	182	184	
50	184	184	182	183	185	
40	176	176	178	181	182	
30	172	168	172	179	183	

Table A.7 Radial Displacement from the Centerline in Centimeters.

Angle	Height (cm)					
	39.45	31.51	23.57	15.64	7.70	
70	-0.857	-0.465	-1.090	-0.395	-0.423	Aluminum Avg = -0.352 cm
60	-0.419	-0.284	-0.017	-0.206	-0.079	
50	-0.106	-0.936	-0.301	-0.180	0.112	
40	0.269	-0.776	-0.895	0.102	-0.604	
30	-0.542	-0.430	0.100	0.099	-0.466	

Angle	Height (cm)					
	39.45	31.51	23.57	15.64	7.70	
70	0.335	-0.696	0.079	-0.013	0.081	Brass Avg = -0.210 cm
60	0.213	-0.347	0.325	-0.466	0.133	
50	-0.330	-0.242	0.465	-0.558	-0.371	
40	-0.678	-0.480	-0.587	-0.210	0.105	
30	-1.084	-0.211	-0.691	-0.081	0.123	

Angle	Height (cm)					
	39.45	31.51	23.57	15.64	7.70	
70	-0.516	-0.262	-0.095	-0.072	-0.310	Stainless Avg = -0.215 cm
60	-0.505	-0.282	-0.100	-0.048	-0.190	
50	0.561	-0.345	0.209	-0.035	-0.129	
40	-0.370	-0.392	0.276	0.057	-0.314	
30	-0.951	-0.657	-0.849	-0.067	0.004	

Total Avg = -0.259 cm

Table A.8 Standard Deviation of the Radial Displacement from the Centerline in Centimeters.

Angle	Height (cm)					
	39.45	31.51	23.57	15.64	7.70	
70	5.241	4.997	4.340	3.202	2.416	Aluminum
60	5.575	5.525	4.210	3.747	2.344	
50	5.125	5.300	4.111	3.605	2.416	28%
40	5.350	5.211	4.344	3.518	2.370	16%
30	5.111	4.835	4.409	3.542	2.455	56%

Angle	Height (cm)					
	39.45	31.51	23.57	15.64	7.70	
70	5.754	5.099	4.118	3.368	2.528	Brass
60	5.961	4.936	4.466	3.498	2.578	
50	5.835	5.147	4.410	4.071	2.630	40%
40	5.576	4.973	4.768	3.677	2.704	36%
30	5.712	4.869	4.002	3.590	2.374	24%

Angle	Height (cm)					
	39.45	31.51	23.57	15.64	7.70	
70	5.530	4.843	4.183	3.495	2.468	Stainless
60	5.874	5.368	4.361	3.682	2.766	
50	6.085	4.746	4.266	4.118	2.385	32%
40	6.095	5.201	5.147	3.689	2.510	48%
30	4.848	4.679	4.326	3.651	2.375	20%



 1st (Highest)
 2nd
 3rd (Lowest)

Table A.9 Average Residence Time in Seconds.

Angle	Height (cm)					
	39.45	31.51	23.57	15.64	7.70	
70	6.836	5.394	4.134	2.750	1.350	Aluminum
60	7.189	5.723	4.386	2.918	1.417	
50	7.675	6.162	4.715	3.120	1.516	0%
40	8.472	6.852	5.146	3.453	1.685	32%
30	9.446	7.641	5.815	3.842	1.912	68%

Angle	Height (cm)					
	39.45	31.51	23.57	15.64	7.70	
70	6.805	5.647	4.209	2.795	1.349	Brass
60	7.150	5.881	4.397	2.902	1.432	
50	7.752	6.219	4.671	3.085	1.520	4%
40	8.584	6.947	5.144	3.435	1.695	64%
30	9.690	8.005	5.919	3.938	2.014	32%

Angle	Height (cm)					
	39.45	31.51	23.57	15.64	7.70	
70	7.218	5.734	4.338	2.951	1.413	Stainless
60	7.508	5.989	4.554	3.070	1.488	
50	7.948	6.384	4.885	3.247	1.583	96%
40	8.835	7.032	5.308	3.551	1.742	4%
30	10.038	8.034	6.190	4.073	1.956	0%



 1st (Highest)
 2nd
 3rd (Lowest)

Table A.10 Standard Deviation of the Residence Time in Seconds.

Angle	Height (cm)					
	39.45	31.51	23.57	15.64	7.70	
70	0.451	0.425	0.330	0.267	0.177	Aluminum
60	0.465	0.393	0.354	0.277	0.199	
50	0.474	0.411	0.349	0.289	0.189	20%
40	0.582	0.449	0.382	0.320	0.207	24%
30	0.741	0.579	0.481	0.360	0.250	56%

Angle	Height (cm)					
	39.45	31.51	23.57	15.64	7.70	
70	0.478	0.438	0.436	0.318	0.207	Brass
60	0.461	0.431	0.389	0.287	0.218	
50	0.512	0.462	0.379	0.312	0.212	24%
40	0.514	0.419	0.377	0.329	0.227	52%
30	0.608	0.505	0.407	0.368	0.218	24%

Angle	Height (cm)					
	39.45	31.51	23.57	15.64	7.70	
70	0.485	0.466	0.386	0.318	0.202	Stainless
60	0.512	0.482	0.411	0.353	0.230	
50	0.463	0.494	0.345	0.337	0.214	56%
40	0.511	0.509	0.411	0.329	0.234	24%
30	0.556	0.524	0.435	0.337	0.250	20%


 1st (Highest)
 2nd
 3rd (Lowest)

Table A.11 95% Confidence Interval of the Residence Time.

	Height (cm)					
Angle	39.45	31.51	23.57	15.64	7.70	
70	6.77-6.90	5.33-5.46	4.09-4.18	2.71-2.79	1.32-1.38	Aluminum
60	7.12-7.26	5.66-5.78	4.33-4.44	2.88-2.96	1.39-1.45	
50	7.60-7.74	6.10-6.22	4.66-4.77	3.08-3.16	1.49-1.54	
40	8.38-8.56	6.79-6.92	5.09-5.20	3.41-3.50	1.65-1.71	
30	9.32-9.57	7.55-7.73	5.74-5.89	3.79-3.90	1.88-1.95	

	Height (cm)					
Angle	39.45	31.51	23.57	15.64	7.70	
70	6.75-6.86	5.60-5.69	4.14-4.28	2.75-2.84	1.32-1.38	Brass
60	7.10-7.20	5.82-5.95	4.34-4.45	2.86-2.95	1.40-1.46	
50	7.70-7.81	6.17-6.27	4.61-4.73	3.04-3.13	1.49-1.55	
40	8.53-8.64	6.88-7.01	5.09-5.20	3.39-3.48	1.66-1.73	
30	9.63-9.75	7.92-8.09	5.86-5.98	3.88-3.99	1.98-2.05	

	Height (cm)					
Angle	39.45	31.51	23.57	15.64	7.70	
70	7.15-7.29	5.66-5.80	4.28-4.39	2.90-3.00	1.38-1.44	Stainless
60	7.43-7.58	5.92-6.06	4.49-4.61	3.02-3.12	1.45-1.52	
50	7.88-8.02	6.31-6.46	4.83-4.94	3.20-3.30	1.55-1.61	
40	8.76-8.91	6.96-7.11	5.25-5.37	3.50-3.60	1.71-1.78	
30	10.00-10.17	7.95-8.11	6.12-6.26	4.02-4.12	1.92-1.99	

Table A.12 Average Axial Velocity in Centimeters/Second.

Angle	Height (cm)					
	39.45	31.51	23.57	15.64	7.70	
70	5.796	5.879	5.787	5.741	5.807	Aluminum 64% 36% 0%
60	5.511	5.532	5.408	5.410	5.550	
50	5.160	5.136	5.027	5.057	5.162	
40	4.679	4.619	4.605	4.569	4.643	
30	4.203	4.148	4.082	4.107	4.099	

Angle	Height (cm)					
	39.45	31.51	23.57	15.64	7.70	
70	5.826	5.613	5.658	5.670	5.848	Brass 36% 60% 4%
60	5.541	5.387	5.403	5.444	5.512	
50	5.111	5.095	5.081	5.122	5.169	
40	4.613	4.552	4.607	4.595	4.631	
30	4.087	3.952	4.001	4.007	3.870	

Angle	Height (cm)					
	39.45	31.51	23.57	15.64	7.70	
70	5.490	5.532	5.477	5.364	5.564	Stainless 0% 4% 96%
60	5.279	5.297	5.218	5.163	5.309	
50	4.980	4.966	4.849	4.870	4.951	
40	4.480	4.504	4.467	4.443	4.501	
30	3.923	3.939	3.827	3.867	4.005	




 1st (Highest)
 2nd
 3rd (Lowest)

Table A.13 Standard Deviation of the Axial Velocity in Centimeters/Second.

Angle	Height (cm)						
	39.45	31.51	23.57	15.64	7.70		
70	0.383	0.473	0.460	0.566	0.806	Aluminum	
60	0.365	0.383	0.438	0.535	0.858		
50	0.323	0.348	0.375	0.476	0.675		32%
40	0.330	0.312	0.348	0.432	0.599		28%
30	0.348	0.323	0.348	0.395	0.561		40%

Angle	Height (cm)						
	39.45	31.51	23.57	15.64	7.70		
70	0.410	0.437	0.575	0.668	0.932	Brass	
60	0.362	0.399	0.488	0.572	0.925		
50	0.343	0.382	0.430	0.522	0.760		44%
40	0.280	0.275	0.343	0.448	0.679		32%
30	0.259	0.261	0.282	0.383	0.450		24%

Angle	Height (cm)						
	39.45	31.51	23.57	15.64	7.70		
70	0.364	0.460	0.492	0.607	0.837	Stainless	
60	0.365	0.443	0.478	0.610	0.891		
50	0.293	0.399	0.339	0.525	0.670		24%
40	0.263	0.329	0.348	0.418	0.618		40%
30	0.218	0.270	0.273	0.330	0.551		36%




 1st (Highest)
 2nd
 3rd (Lowest)

Table A.14 Average Radial Velocity in Centimeters/Second.

	Height (cm)					
Angle	39.45	31.51	23.57	15.64	7.70	
70	-0.130	-0.092	-0.272	-0.152	-0.330	Aluminum
60	-0.059	-0.042	-0.003	-0.065	-0.034	Avg = -0.093 cm/s
50	-0.011	-0.153	-0.058	-0.056	0.058	
40	0.033	-0.113	-0.179	0.028	-0.361	
30	-0.068	-0.061	0.018	0.022	-0.250	

	Height (cm)					
Angle	39.45	31.51	23.57	15.64	7.70	
70	0.055	-0.123	0.042	-0.021	0.025	Brass
60	0.029	-0.063	0.088	-0.166	0.112	Avg = -0.036 cm/s
50	-0.039	-0.038	0.099	-0.172	-0.262	
40	-0.076	-0.076	-0.127	-0.060	0.068	
30	-0.111	-0.027	-0.109	-0.020	0.065	

	Height (cm)					
Angle	39.45	31.51	23.57	15.64	7.70	
70	-0.077	-0.052	-0.022	-0.038	-0.212	Stainless
60	-0.061	-0.042	-0.024	0.000	-0.145	Avg = -0.051 cm/s
50	0.074	-0.053	0.045	-0.001	-0.098	
40	-0.037	-0.060	0.055	0.013	-0.208	
30	-0.096	-0.084	-0.138	-0.009	0.003	


Total Avg = -0.060 cm/s

Table A.15 Standard Deviation of the Radial Velocity in Centimeters/Second.

Angle	Height (cm)					
	39.45	31.51	23.57	15.64	7.70	
70	0.774	0.963	1.066	1.190	1.828	Aluminum
60	0.794	0.985	0.977	1.333	1.743	
50	0.681	0.879	0.884	1.190	1.650	40%
40	0.654	0.776	0.869	1.050	1.471	28%
30	0.577	0.665	0.776	0.949	1.408	32%

Angle	Height (cm)					
	39.45	31.51	23.57	15.64	7.70	
70	0.856	0.926	0.994	1.231	2.021	Brass
60	0.844	0.849	1.022	1.243	1.888	
50	0.766	0.845	0.958	1.343	1.805	44%
40	0.662	0.725	0.951	1.099	1.722	40%
30	0.609	0.632	0.690	0.948	1.247	16%

Angle	Height (cm)					
	39.45	31.51	23.57	15.64	7.70	
70	0.777	0.872	0.954	1.211	1.804	Stainless
60	0.794	0.915	0.974	1.232	2.004	
50	0.776	0.751	0.883	1.285	1.577	16%
40	0.698	0.750	0.995	1.059	1.511	32%
30	0.493	0.590	0.714	0.938	1.234	52%



 1st (Highest)

 2nd

 3rd (Lowest)

Table A.16 Slope of R^2 vs. $\ln(N/(N-N_0))$ in Units of cm^2 .

	Height (cm)					
Angle	39.45	31.51	23.57	15.64	7.70	
70	21.16	41.53	27.15	15.34	7.44	Aluminum
60	47.15	43.08	21.57	19.95	5.56	
50	42.17	35.34	31.63	16.61	6.38	
40	40.02	41.91	36.91	18.16	7.56	
30	21.16	34.44	25.31	15.08	7.48	
Avg.	34.44	39.26	28.51	17.03	6.88	

32%
28%
40%

	Height (cm)					
Angle	39.45	31.51	23.57	15.64	7.70	
70	47.60	38.19	21.89	13.05	8.68	Brass
60	42.35	31.49	21.99	14.85	10.20	
50	41.89	47.19	24.54	21.70	8.94	
40	46.04	31.07	42.56	20.79	9.53	
30	47.97	32.03	20.94	14.21	7.62	
Avg.	45.17	35.99	26.38	16.92	8.93	

40%
24%
36%

	Height (cm)					
Angle	39.45	31.51	23.57	15.64	7.70	
70	48.61	40.25	22.14	17.06	8.39	Stainless
60	37.99	48.14	29.84	21.93	8.16	
50	38.76	28.21	25.97	22.93	6.24	
40	42.42	32.59	31.22	20.67	8.18	
30	47.46	24.93	21.18	19.68	7.58	
Avg.	43.05	34.82	26.07	20.45	7.71	

28%
48%
24%

 1st (Highest)
 2nd
 3rd (Lowest)

Table A.17 R^2 or Coefficient of Determination of the Linear Regression Line of the Radial Dispersion Coefficient.

	Height (cm)					
Angle	39.45	31.51	23.57	15.64	7.70	
70	0.957	0.964	0.980	0.989	0.991	Aluminum avg=0.977
60	0.990	0.989	0.987	0.972	1.000	
50	0.941	0.974	0.857	0.996	0.998	
40	0.986	0.984	0.945	0.985	0.999	
30	0.957	0.986	0.992	0.997	1.000	

	Height (cm)					
Angle	39.45	31.51	23.57	15.64	7.70	
70	0.986	0.989	0.996	0.992	0.999	Brass avg=0.985
60	0.973	0.987	0.991	0.997	0.958	
50	0.988	0.979	0.988	0.992	0.994	
40	0.989	0.980	0.919	0.964	0.987	
30	0.992	0.993	0.994	1.000	0.996	

	Height (cm)					
Angle	39.45	31.51	23.57	15.64	7.70	
70	0.951	0.920	0.997	0.989	0.986	Stainless avg=0.979
60	0.996	0.981	0.974	0.982	1.000	
50	0.977	0.977	0.989	0.947	0.999	
40	0.983	0.996	0.986	0.962	0.975	
30	0.970	0.997	0.998	0.957	0.992	

Total Avg=0.980

Table A.18 Radial Dispersion Coefficient in Units of cm²/s.

Angle	Height (cm)					
	39.45	31.51	23.57	15.64	7.70	
70	0.77	1.92	1.64	1.39	1.38	Aluminum 40% 28% 32%
60	1.64	1.88	1.23	1.71	0.98	
50	1.37	1.43	1.68	1.33	1.05	
40	1.18	1.53	1.79	1.32	1.12	
30	2.24	1.13	1.09	0.98	0.98	

Angle	Height (cm)					
	39.45	31.51	23.57	15.64	7.70	
70	1.75	1.69	1.30	1.17	1.61	Brass 36% 32% 32%
60	1.48	1.34	1.25	1.28	1.78	
50	1.35	1.90	1.31	1.76	1.47	
40	1.34	1.12	2.07	1.51	1.41	
30	1.24	1.00	0.88	0.90	0.95	

Angle	Height (cm)					
	39.45	31.51	23.57	15.64	7.70	
70	1.68	1.75	1.28	1.45	1.48	Stainless 24% 40% 36%
60	1.26	2.01	1.64	1.79	1.37	
50	1.22	1.10	1.33	1.77	0.99	
40	1.20	1.16	1.47	1.45	1.17	
30	1.18	0.78	0.86	1.21	0.97	




 1st (Highest)
 2nd
 3rd (Lowest)

Table A.19 Coefficient of Restitution ($e=H_2/H_1$) of the Collision of 1/8" Diameter Spheres on a 2" Thick Block of Alloy steel.

Brass			Aluminum			Stainless Steel		
H1 (cm)	H2 (cm)	e	H1 (cm)	H2 (cm)	e	H1 (cm)	H2 (cm)	e
25	13.25	0.53	25	12.25	0.49	25	12.00	0.48
24	13.30	0.55	24	11.75	0.49	24	11.75	0.49
20	11.25	0.56	20	8.75	0.44	20	10.25	0.51
17	10.00	0.59	17	8.00	0.47	17	9.00	0.53
16	9.50	0.59	16	8.00	0.50	16	8.75	0.55
15	9.25	0.62	15	7.50	0.50	15	8.50	0.57
14	8.70	0.62	14	7.00	0.50	14	7.50	0.54
13	8.25	0.63	13	6.50	0.50	13	7.00	0.54
12	7.25	0.60	12	6.50	0.54	12	6.50	0.54
10	6.25	0.63	10	4.25	0.43	10	6.00	0.60

Average=0.59

Average=0.49

Average=0.53

APPENDIX B

FIGURES

The following appendix contains figures of the flowchart for the automatic data collection system and plots showing the variation of statistical values with changes of the release height and board angle.

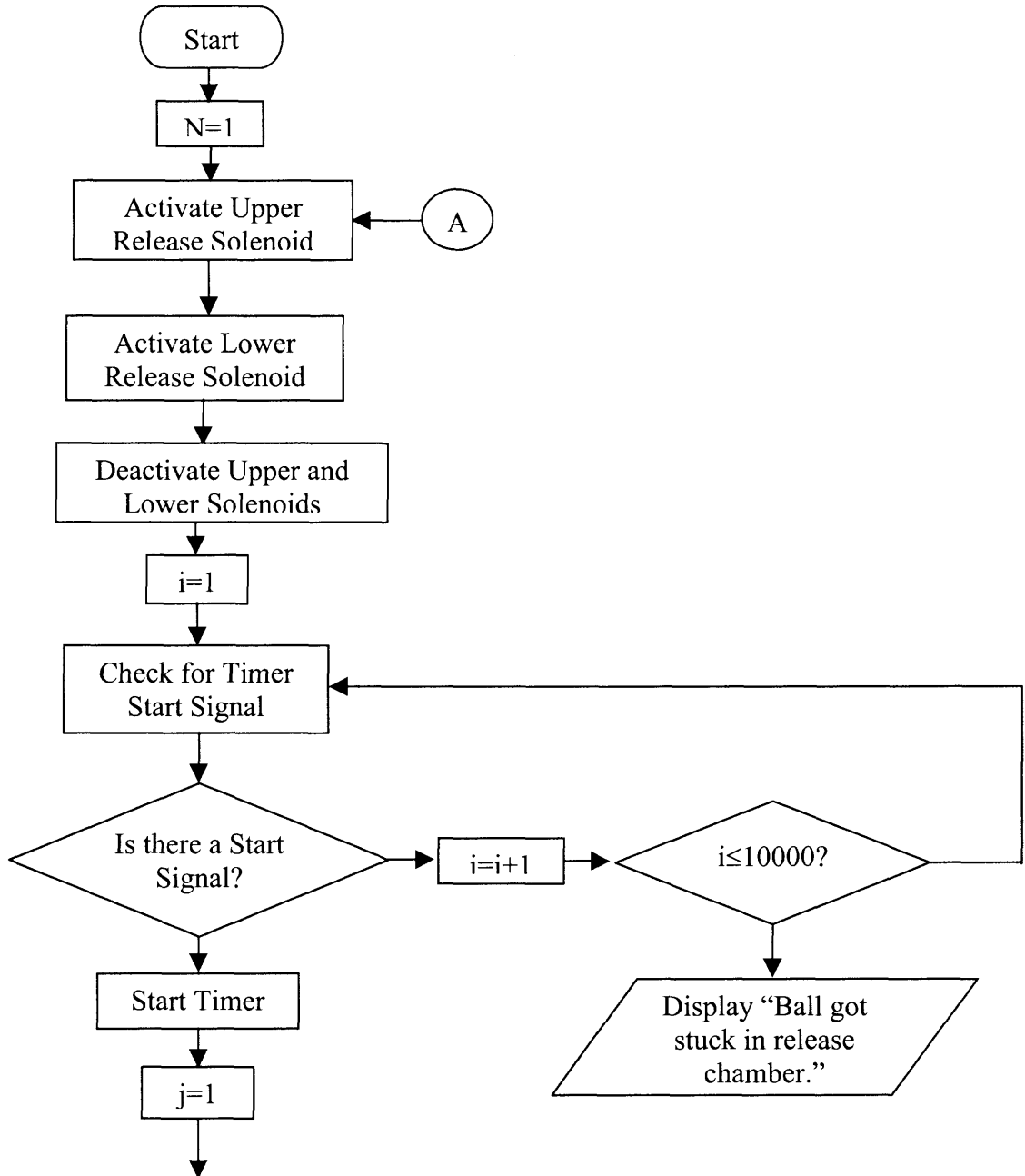


Figure B.1 Logic flowchart for the automatic data collection system.

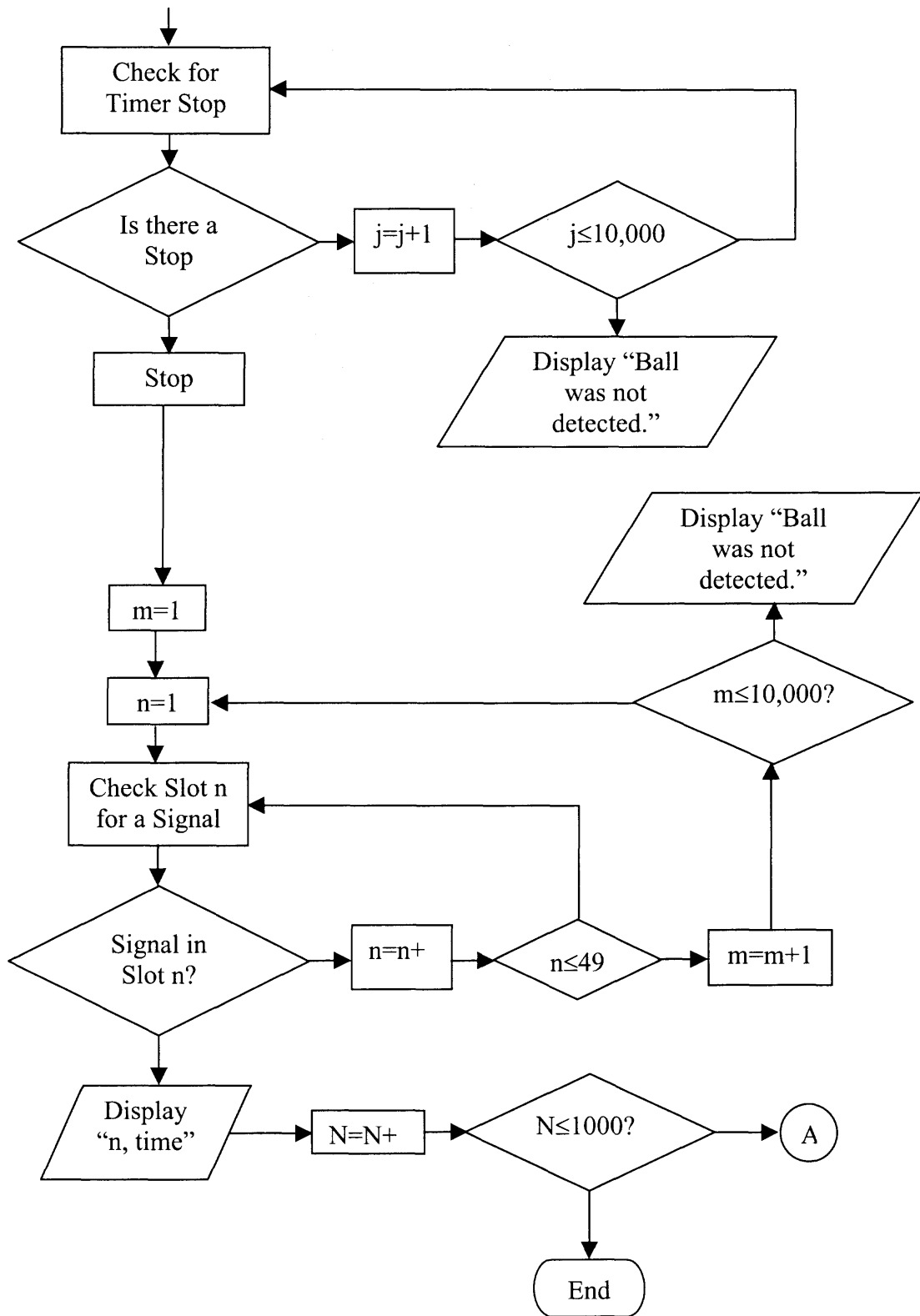


Figure B.1 (Continued) Logic flowchart for the automatic data collection system.

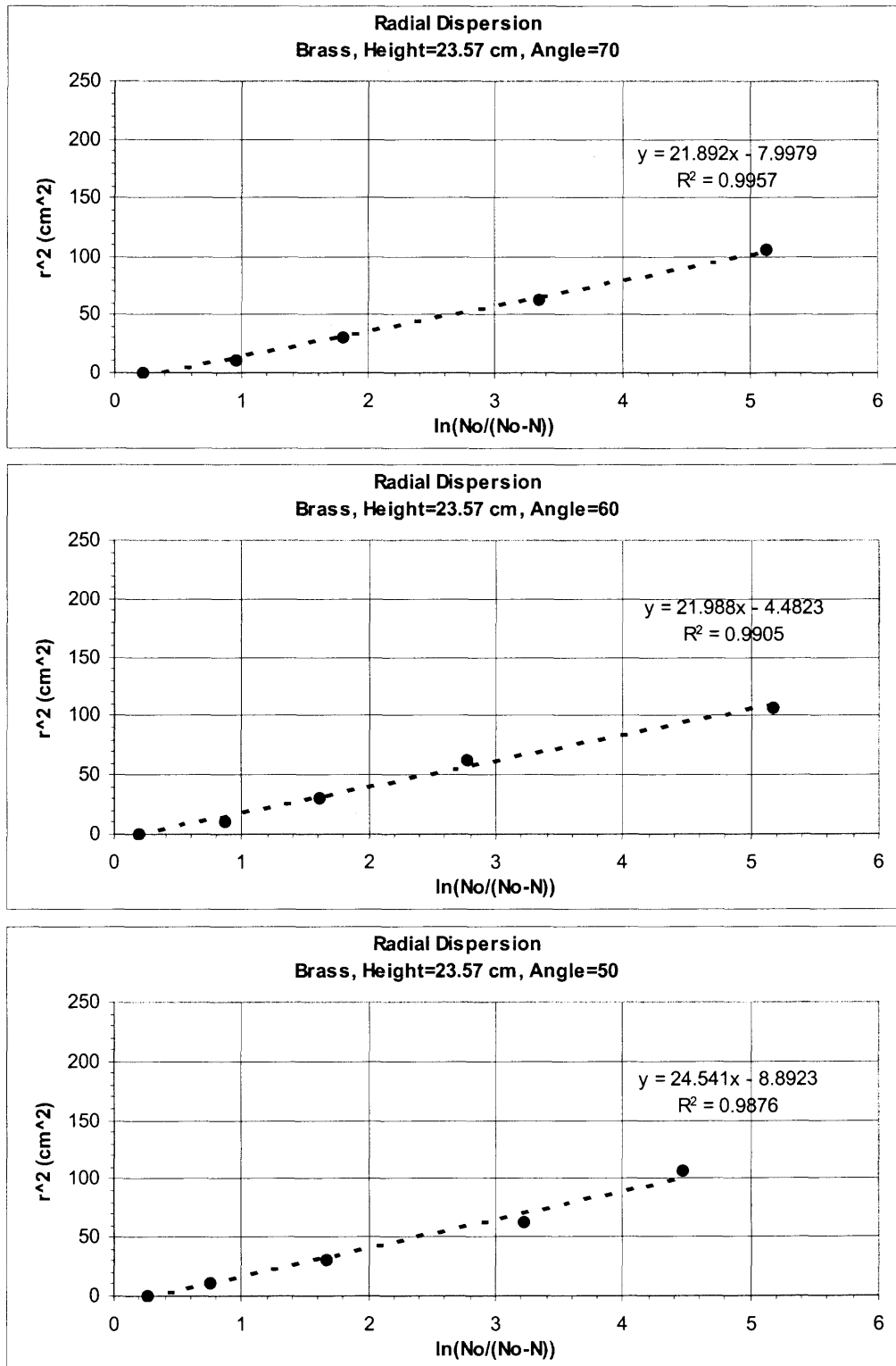


Figure B.2 Plots of the radial dispersion coefficient.

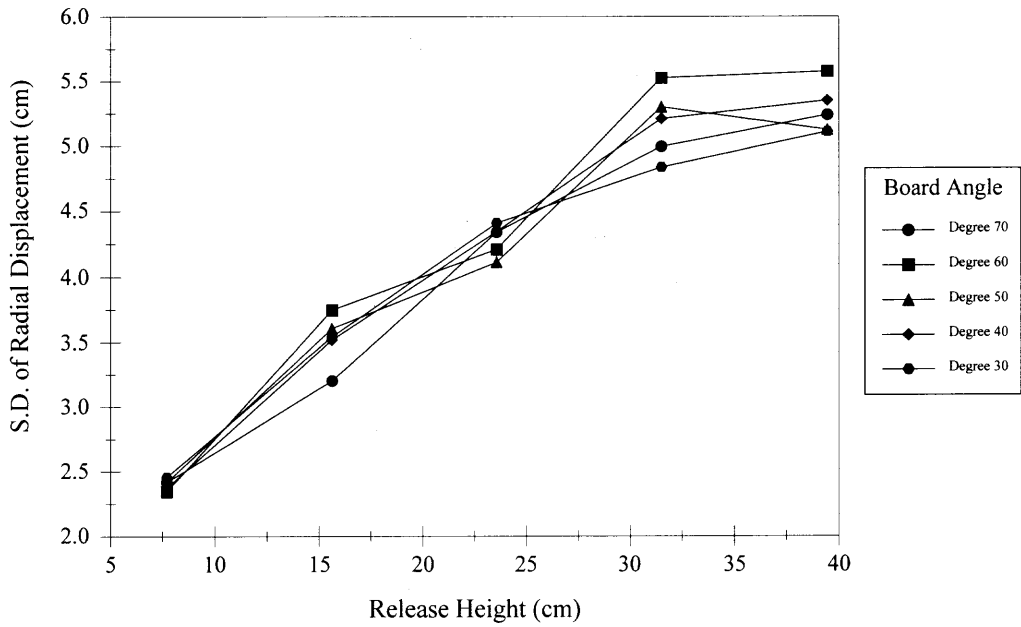


Figure B.3 Standard deviation of the radial displacement vs. release height of 1/8" diameter aluminum spheres for various board angles.

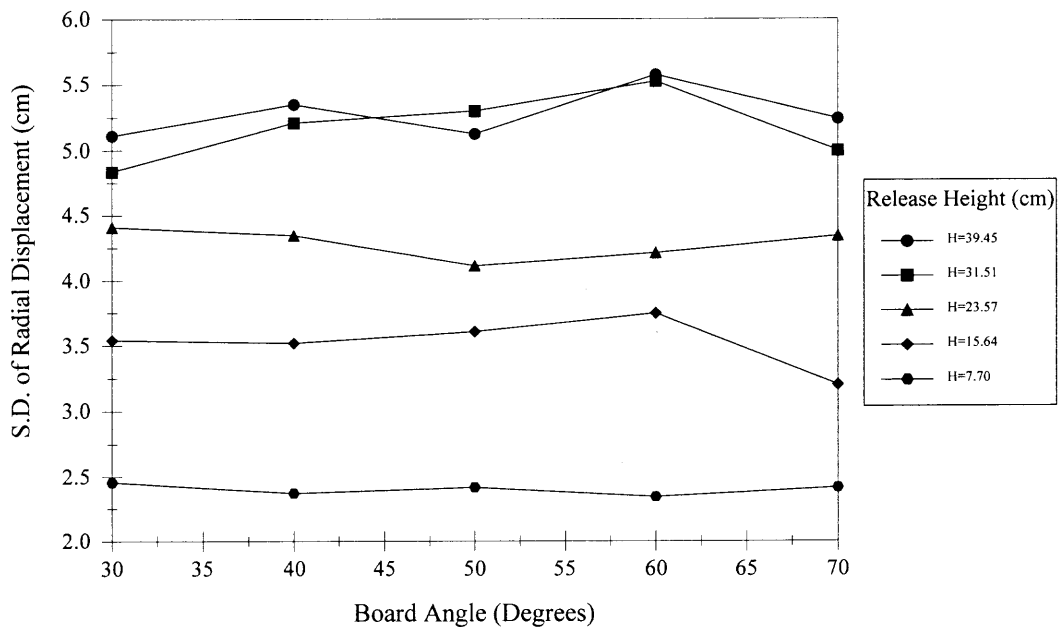


Figure B.4 Standard deviation of the radial displacement vs. board angle of 1/8" diameter aluminum spheres for various release heights.

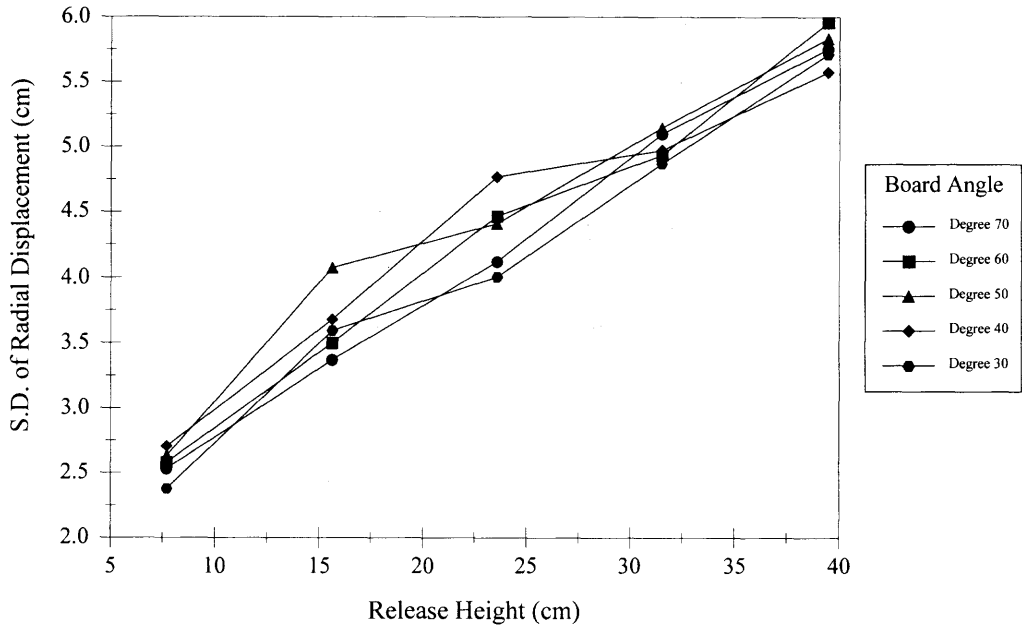


Figure B.5 Standard deviation of the radial displacement vs. release height of 1/8” diameter brass spheres for various board angles.

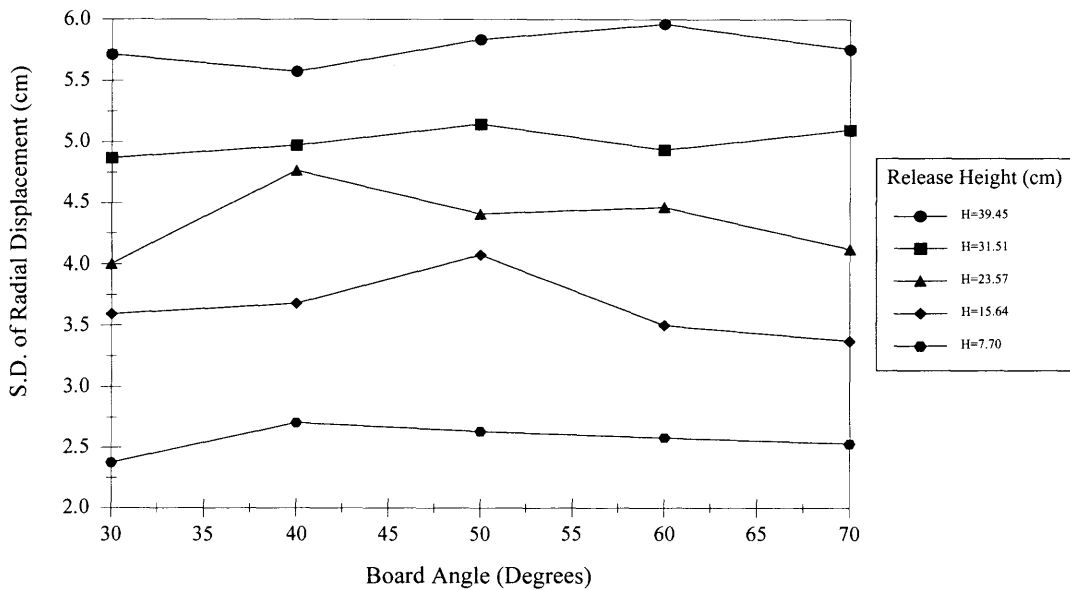


Figure B.6 Standard deviation of the radial displacement vs. board angle of 1/8” diameter brass spheres for various release heights.

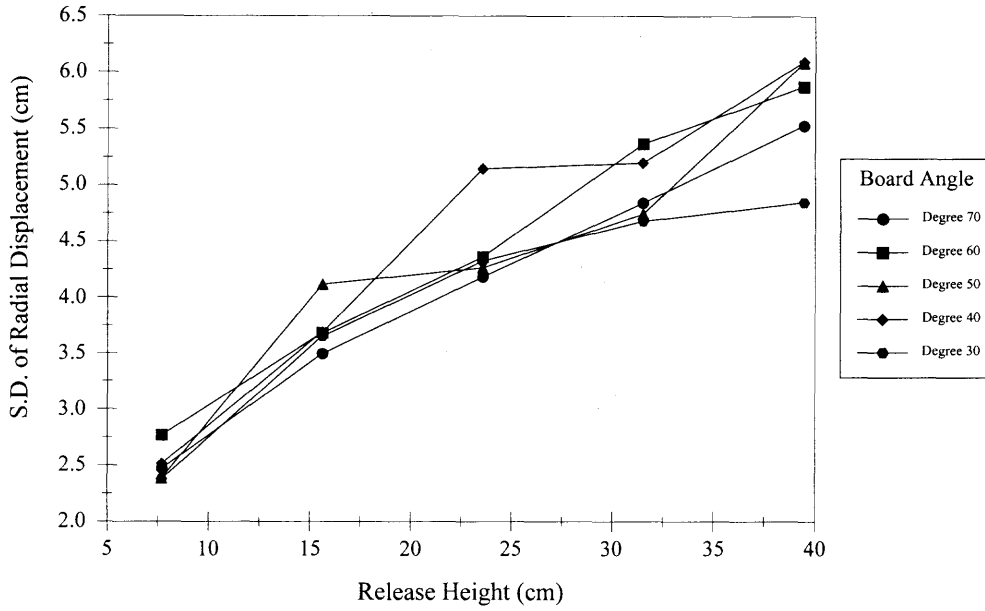


Figure B.7 Standard deviation of the radial displacement vs. release height of 1/8” diameter stainless steel spheres for various board angles.

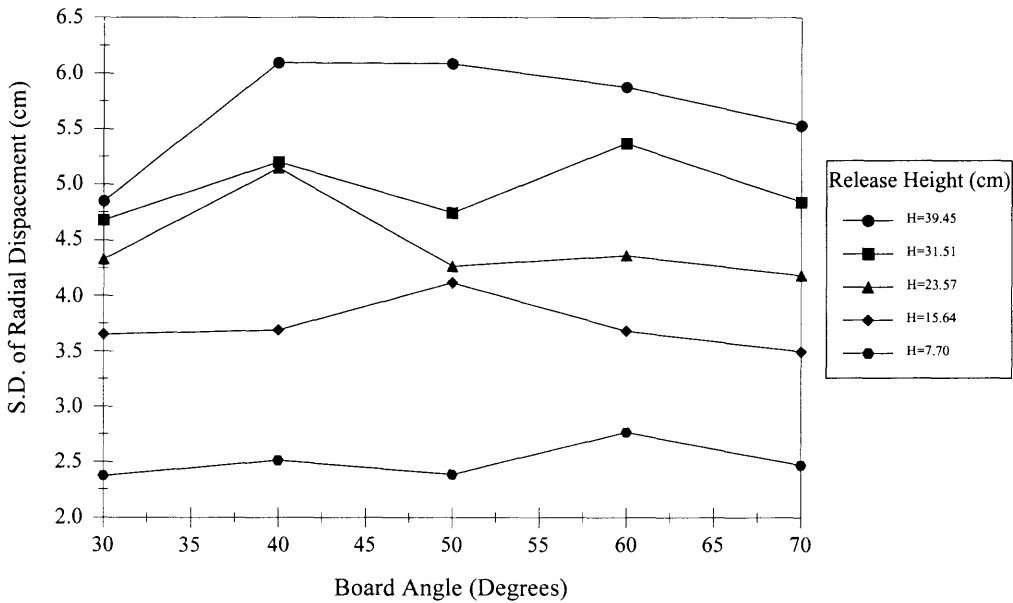


Figure B.8 Standard deviation of the radial displacement vs. board angle of 1/8” diameter stainless steel spheres for various release heights.

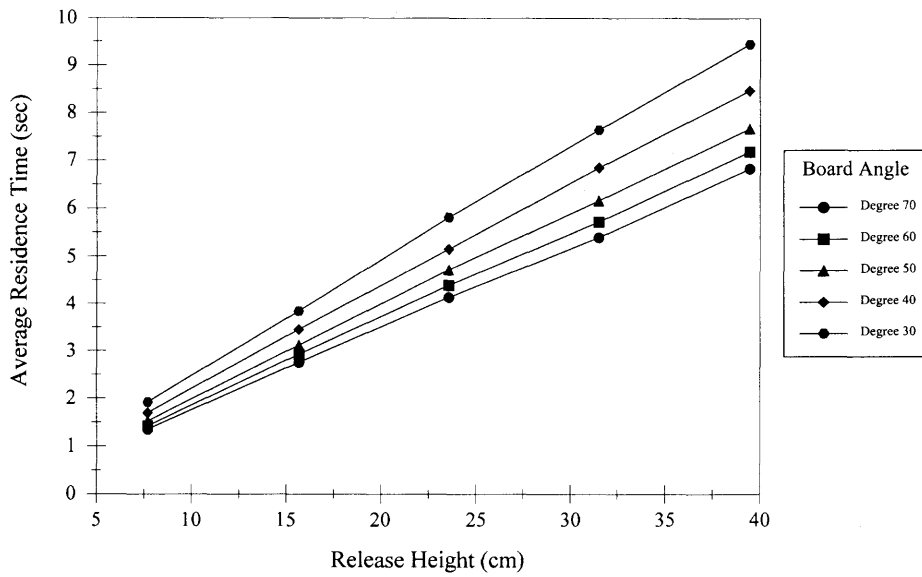


Figure B.9 Average residence time vs. release height of 1/8" diameter aluminum spheres for various board angles.

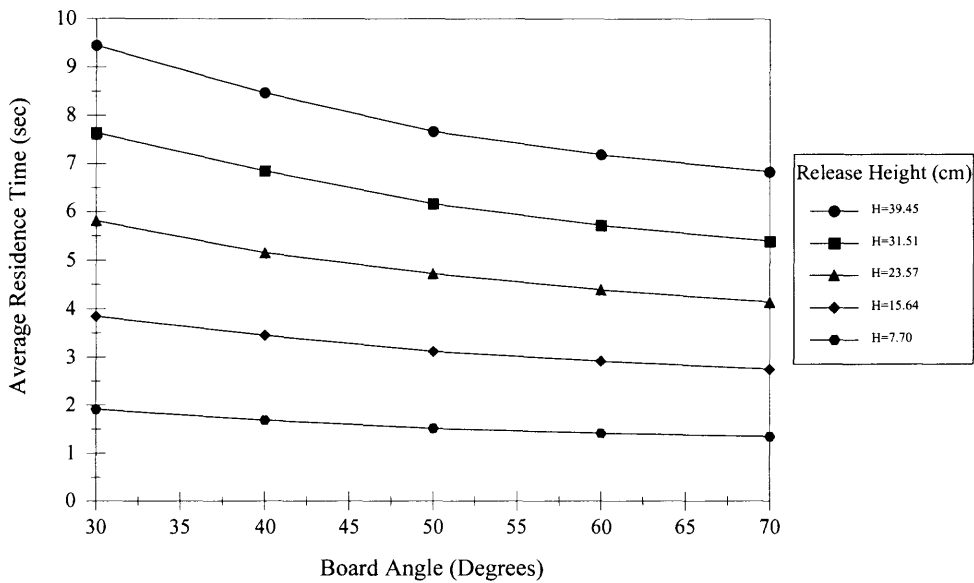


Figure B.10 Average residence time vs. board angle of 1/8" diameter aluminum spheres for various release heights.

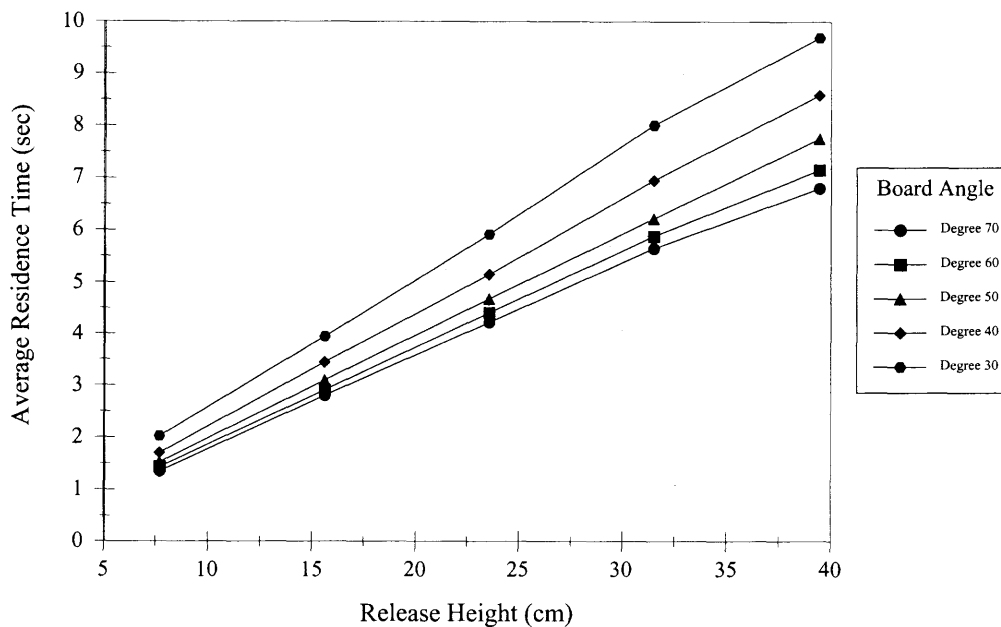


Figure B.11 Average residence time vs. release height of 1/8'' diameter brass spheres for various board angles.

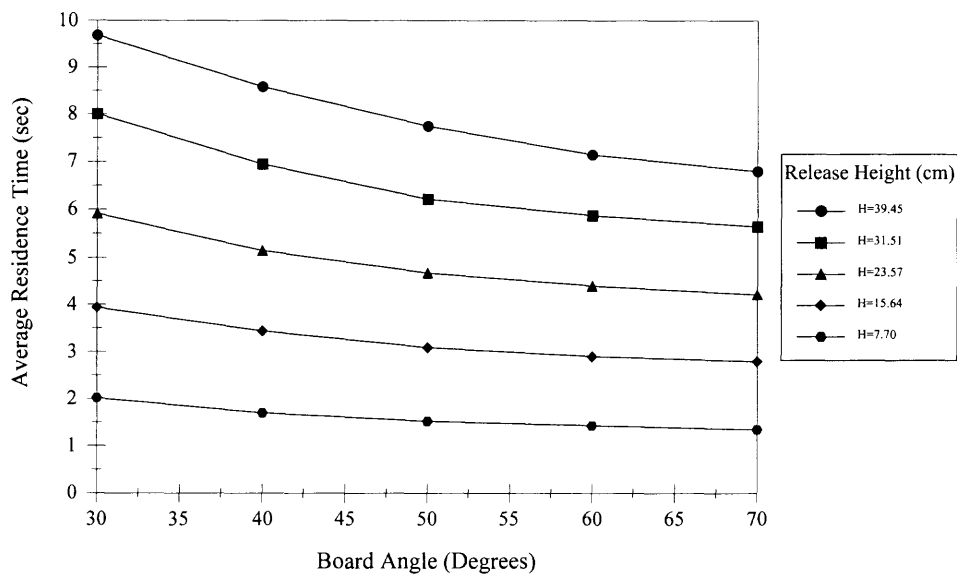


Figure B.12 Average residence time vs. board angle of 1/8'' diameter brass spheres for various release heights.

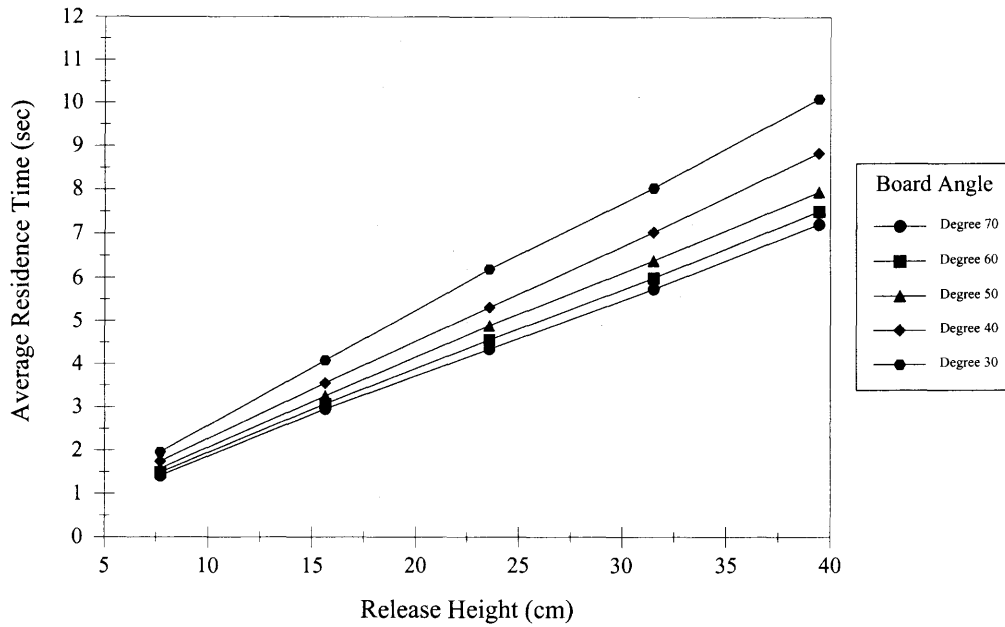


Figure B.13 Average residence time vs. release height of 1/8" diameter stainless steel spheres for various board angles.

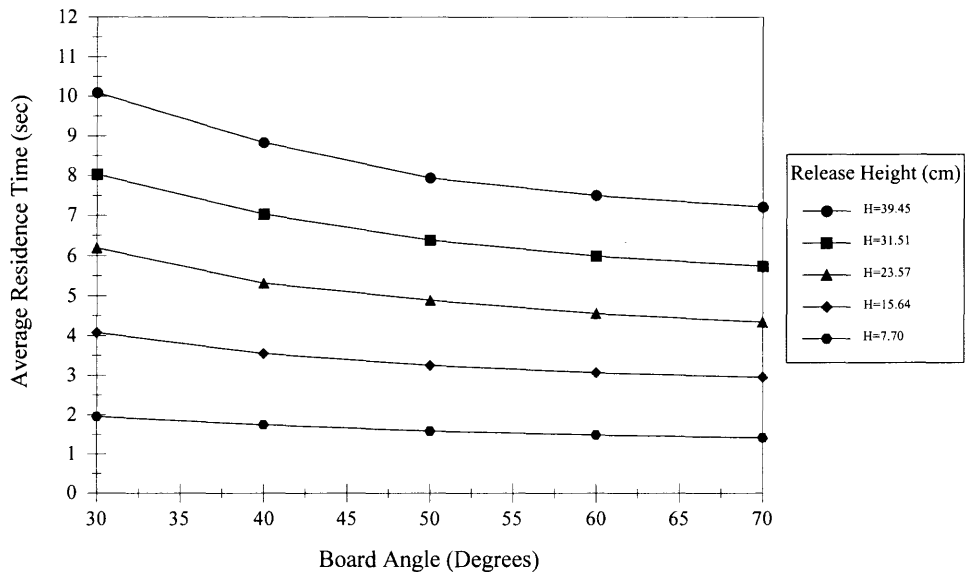


Figure B.14 Average residence time vs. board angle of 1/8" diameter stainless steel spheres for various release heights.

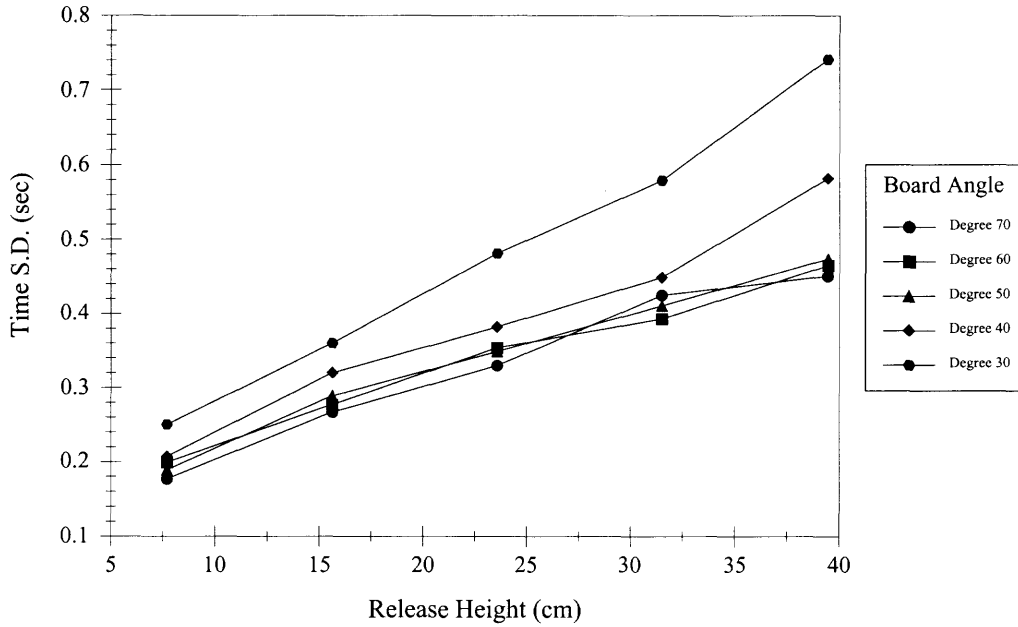


Figure B.15 Standard deviation of the residence time vs. release height of 1/8” aluminum spheres for various board angles.

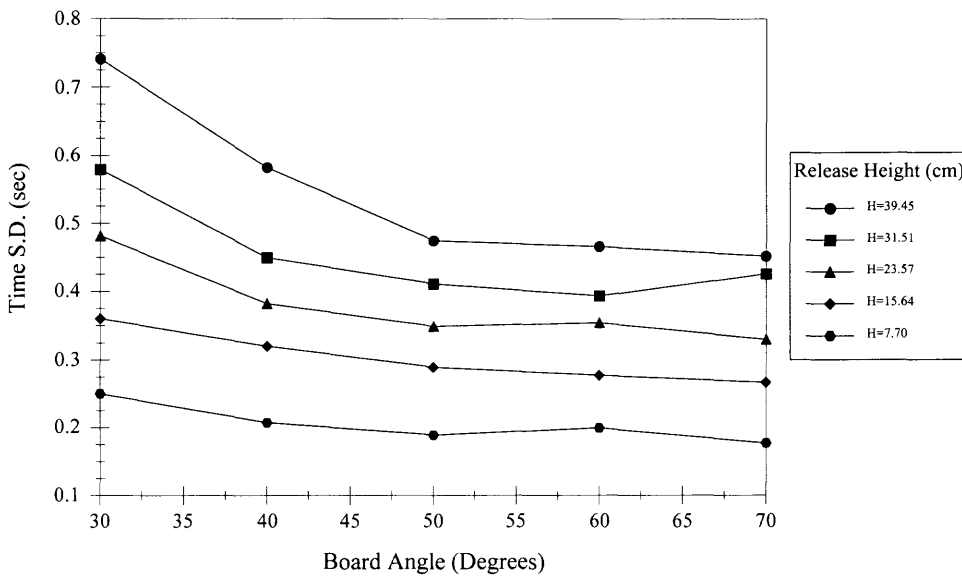


Figure B.16 Standard deviation of the residence time vs. board angle of 1/8” aluminum spheres for various release heights.

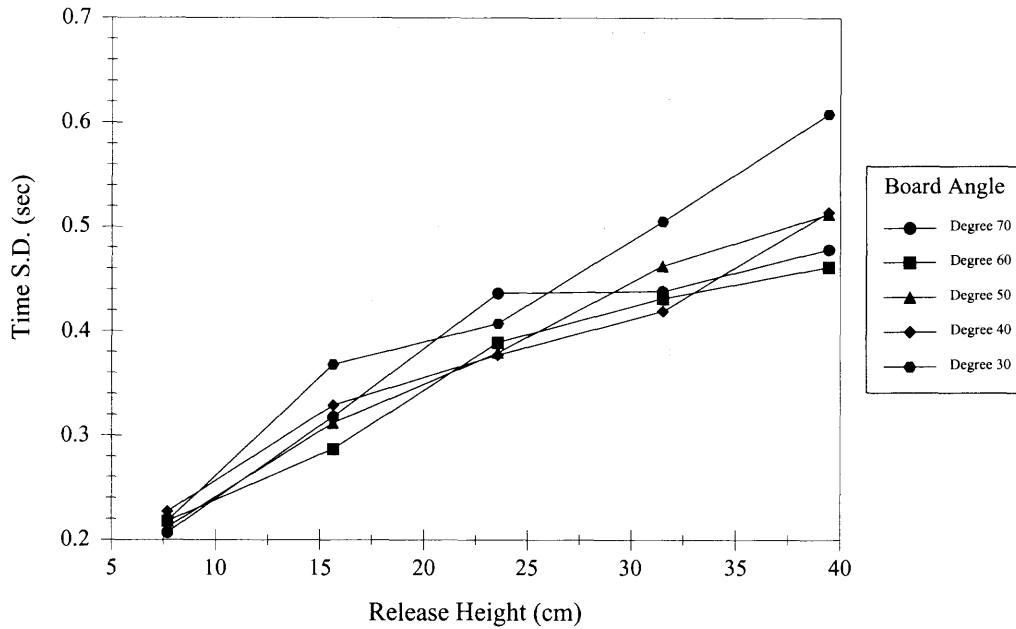


Figure B.17 Standard deviation of the residence time vs. release height of 1/8" brass spheres for various board angles.

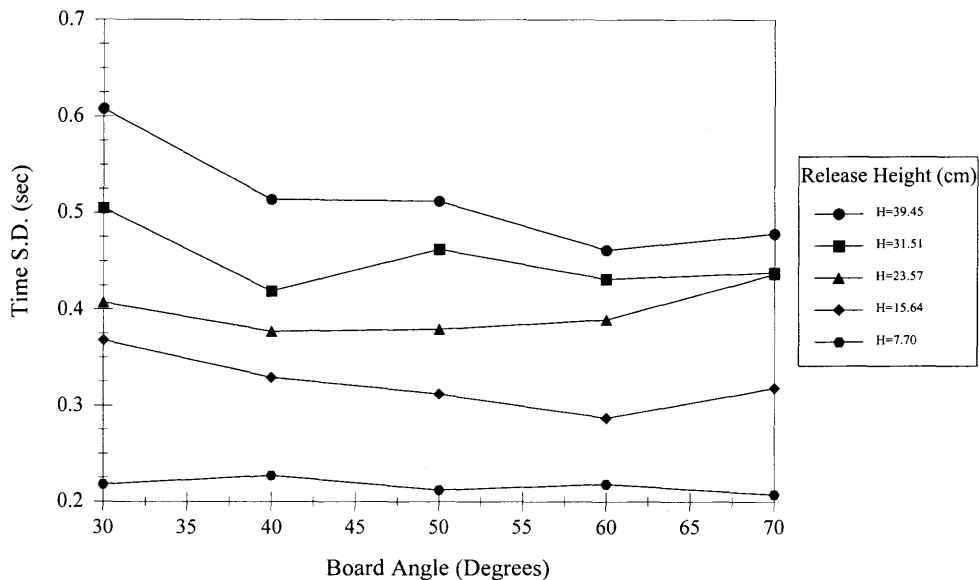


Figure B.18 Standard deviation of the residence time vs. board angle of 1/8" brass spheres for various release heights.

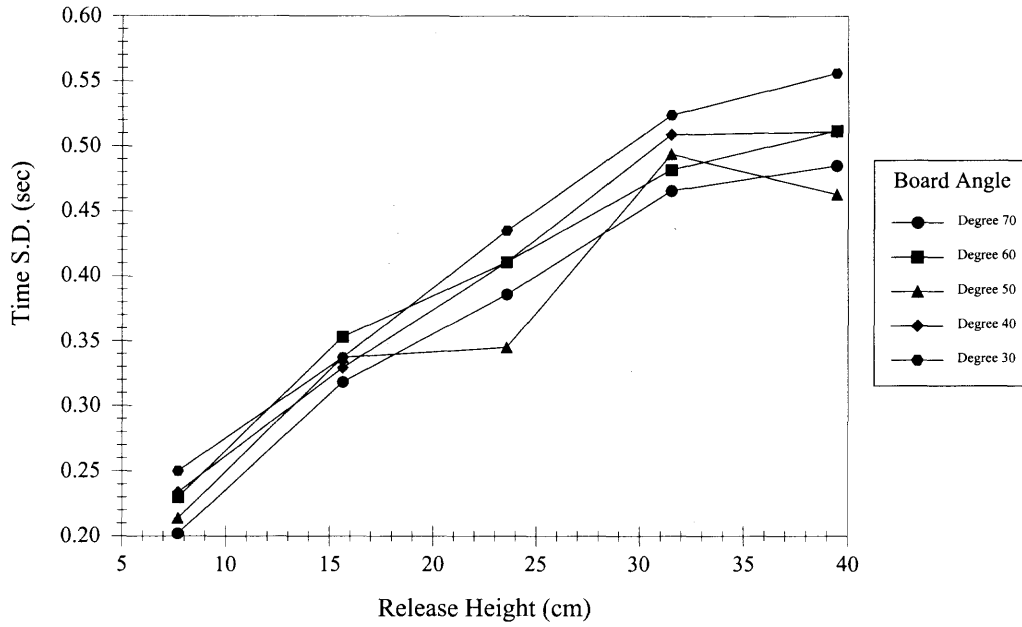


Figure B.19 Standard deviation of the residence time vs. release height of 1/8" stainless steel spheres for various board angles.

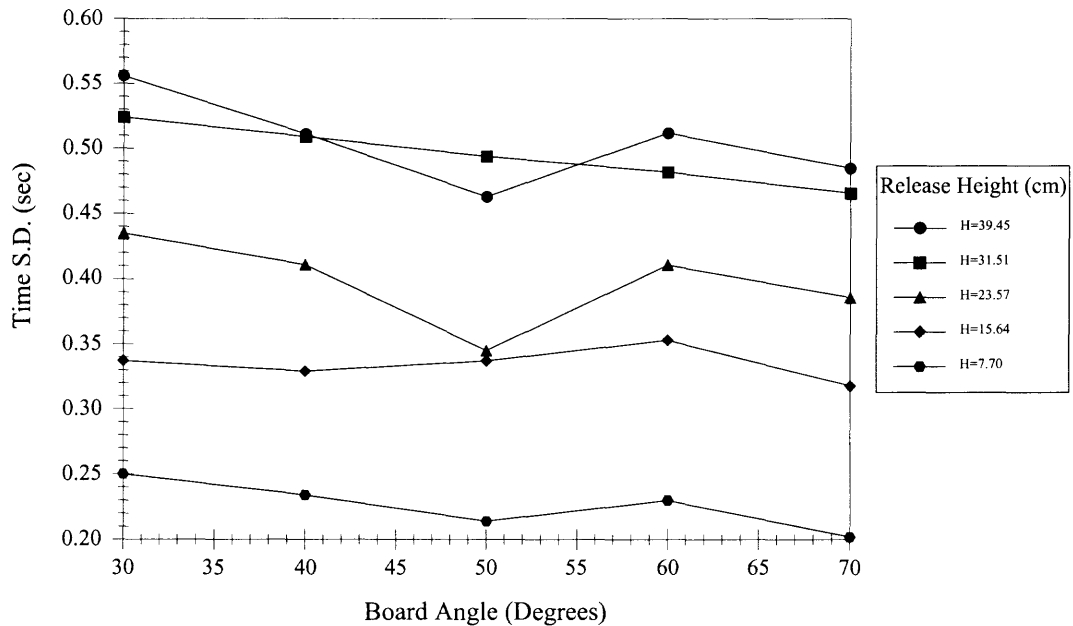


Figure B.20 Standard deviation of the residence time vs. board angle of 1/8" stainless steel spheres for various release heights.

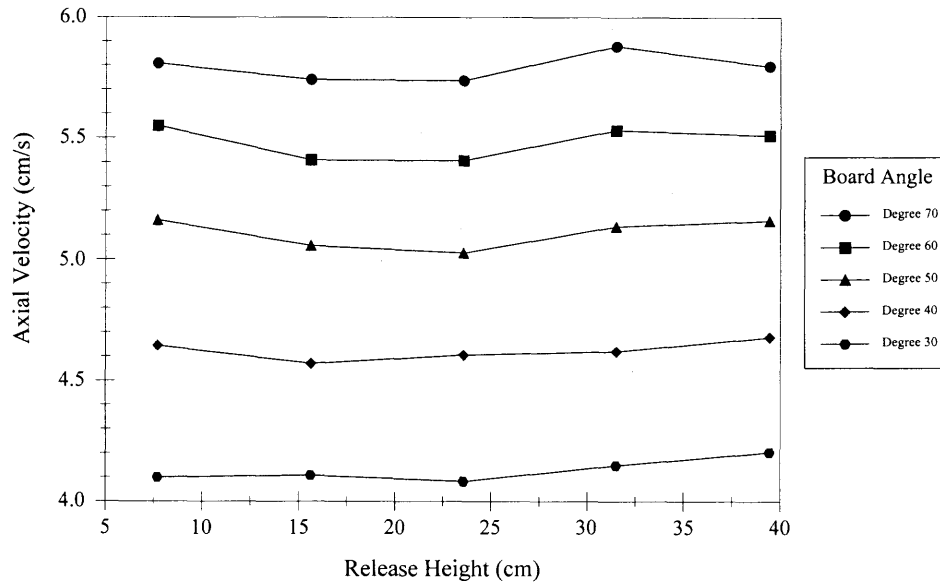


Figure B.21 Average axial velocity vs. release height of 1/8" aluminum spheres for various board angles.

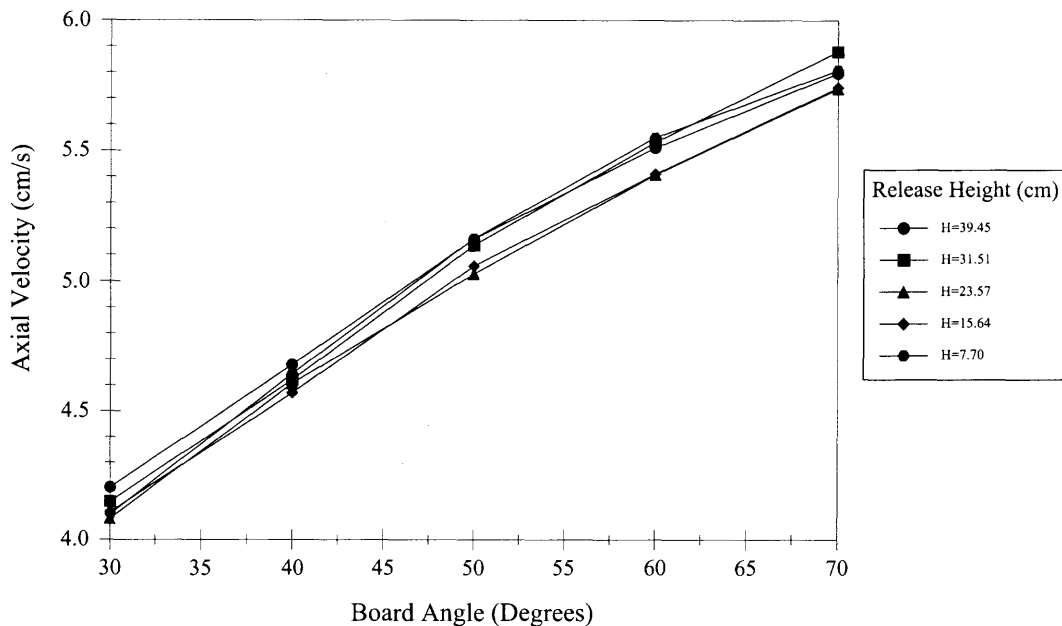


Figure B.22 Average axial velocity vs. board angle of 1/8" aluminum spheres for various release heights.

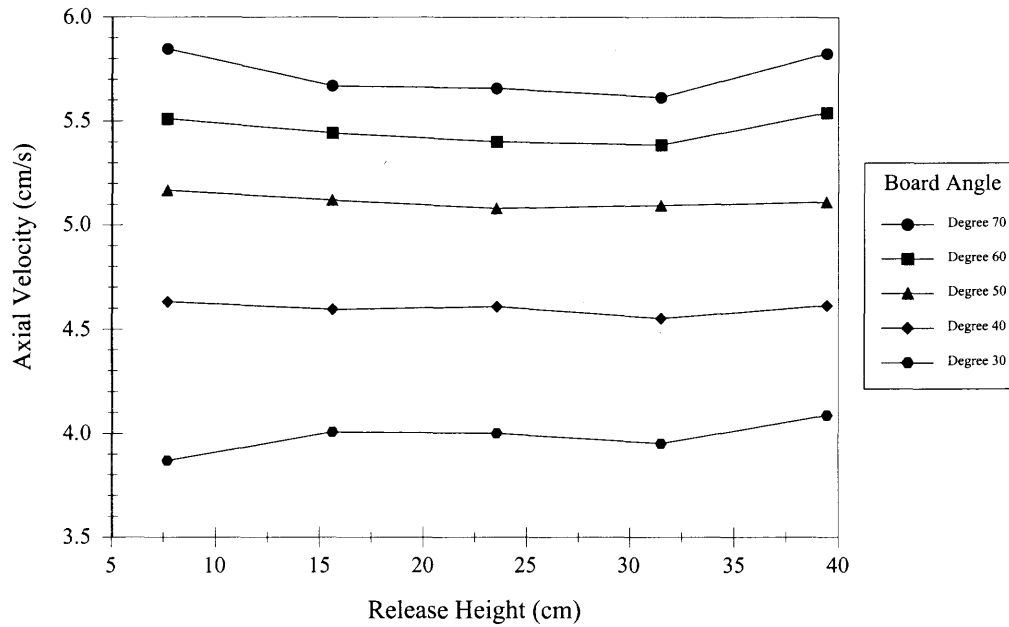


Figure B.23 Average axial velocity vs. release height of 1/8" brass spheres for various board angles.

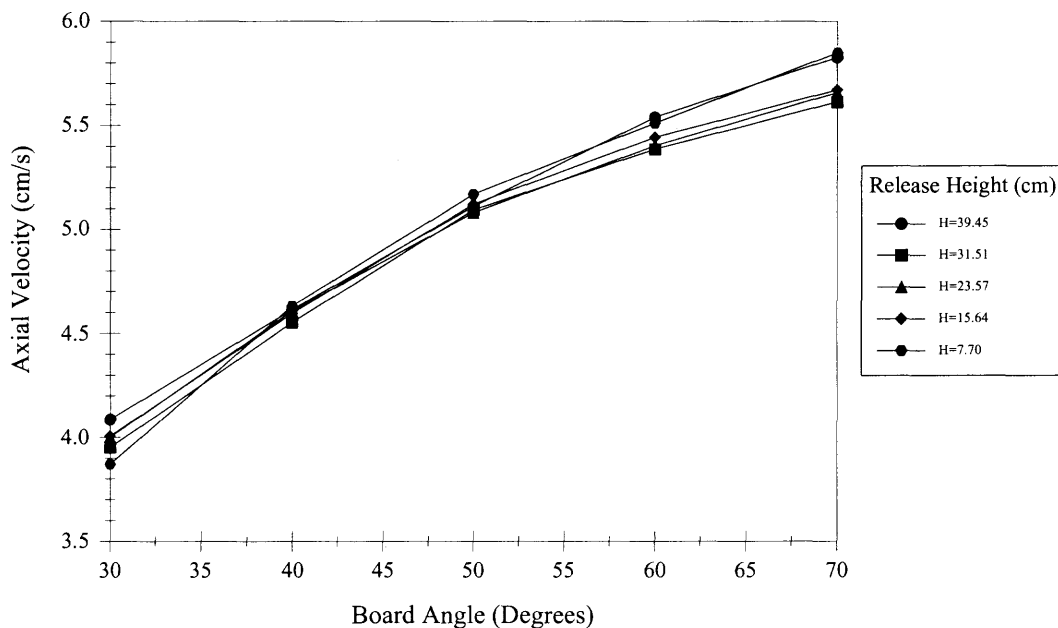


Figure B.24 Average axial velocity vs. board angle for 1/8" brass spheres for various release heights.

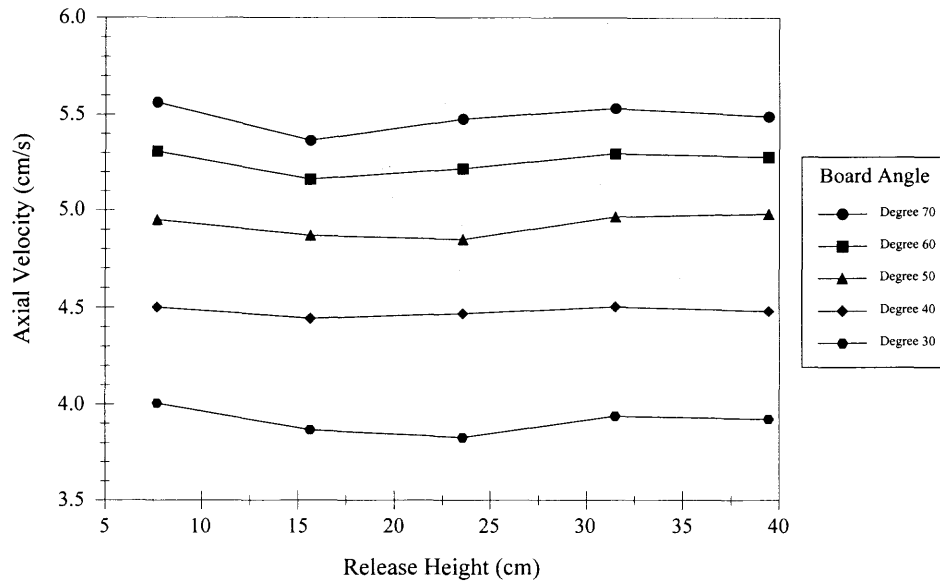


Figure B.25 Average axial velocity vs. release height of 1/8" stainless steel spheres for various board angles.

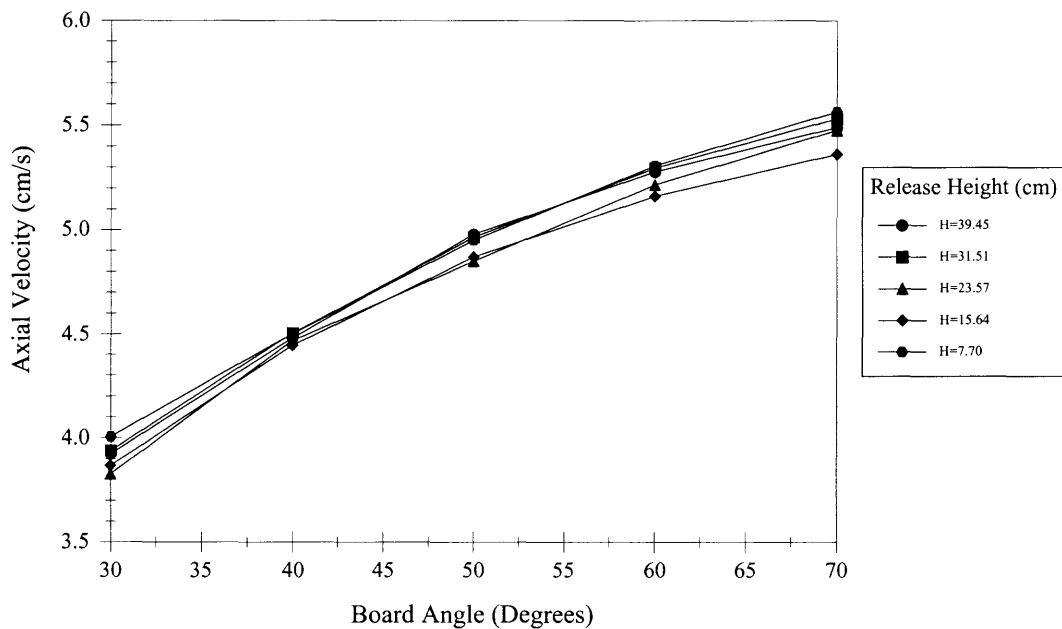


Figure B.26 Average axial velocity vs. board angle of 1/8" stainless steel spheres for various release heights.

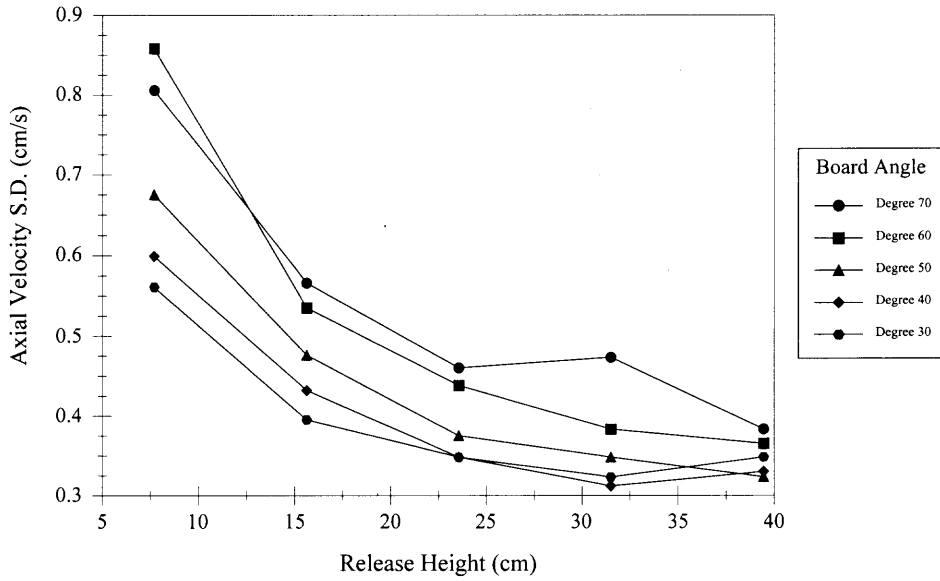


Figure B.27 Standard deviation of the axial velocity vs. release height of 1/8" aluminum spheres for various board angles.

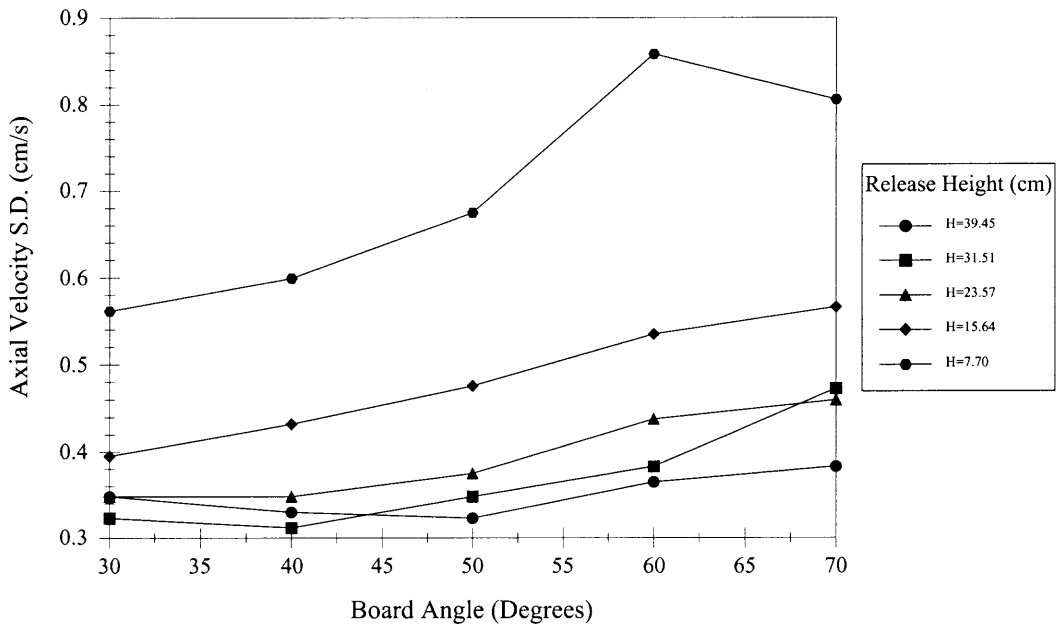


Figure B.28 Standard deviation of the axial velocity vs. board angle of 1/8" aluminum spheres for various release heights.

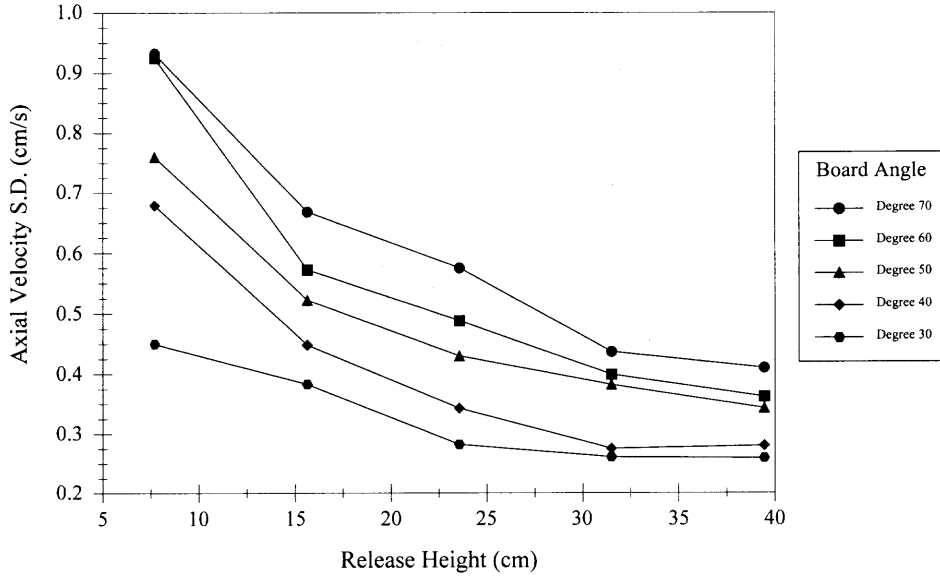


Figure B.29 Standard deviation of the axial velocity vs. release height of 1/8” brass spheres for various board angles.

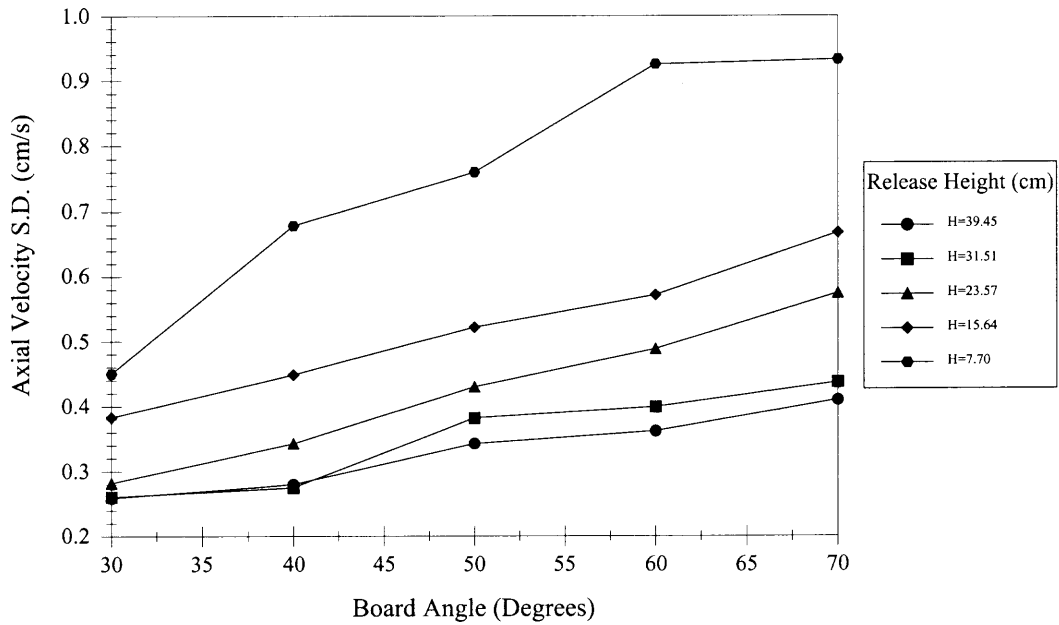


Figure B.30 Standard deviation of the axial velocity vs. board angle of 1/8” brass spheres for various release heights.

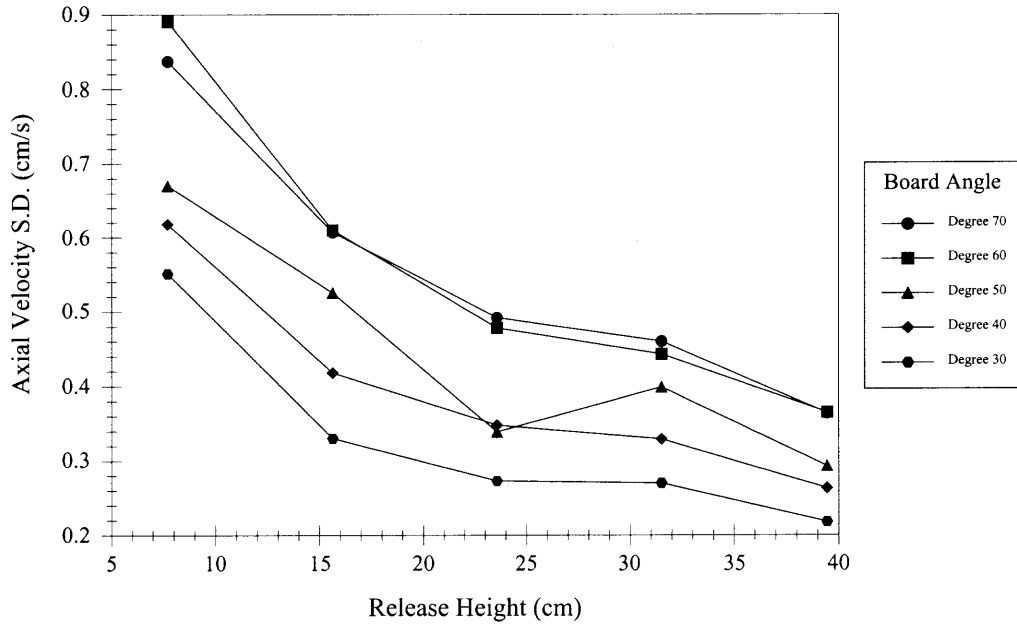


Figure B.31 Standard deviation of the axial velocity vs. release height of 1/8” stainless steel spheres for various board angles.

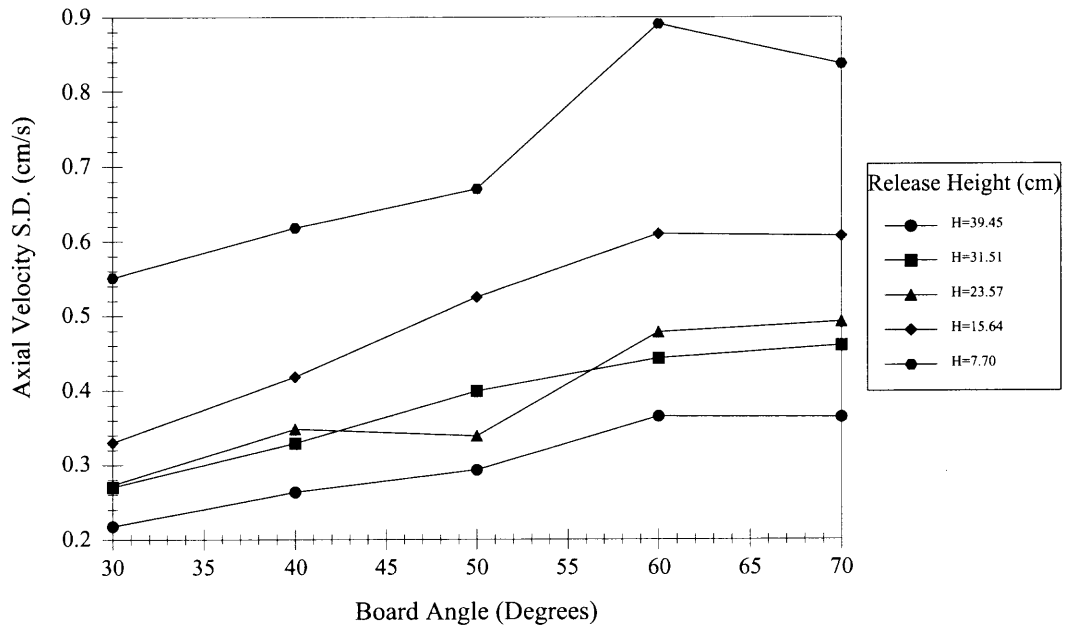


Figure B.32 Standard deviation of the axial velocity vs. board angle of 1/8” stainless steel spheres for various release heights.

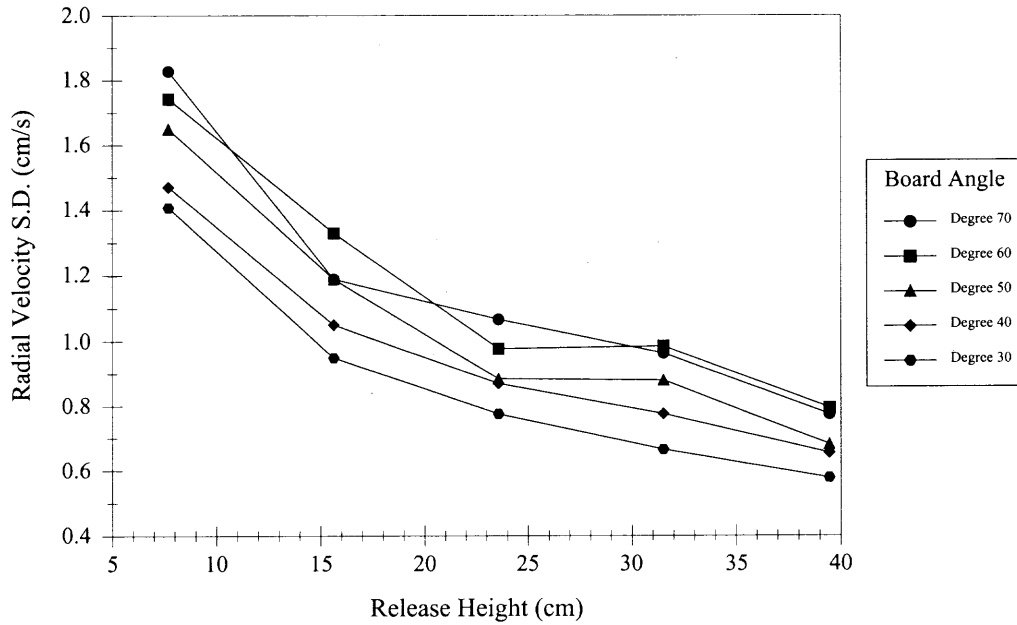


Figure B.33 Standard deviation of the radial velocity vs. release height of 1/8'' aluminum spheres for various board angles.

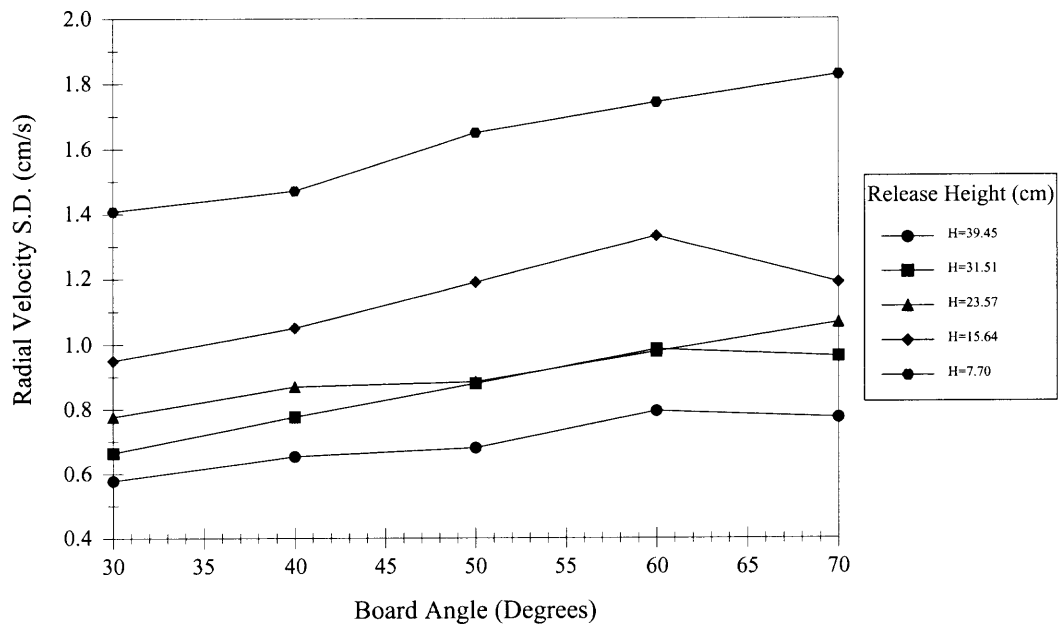


Figure B.34 Standard deviation of the radial velocity vs. board angle of 1/8'' aluminum spheres for various release heights.

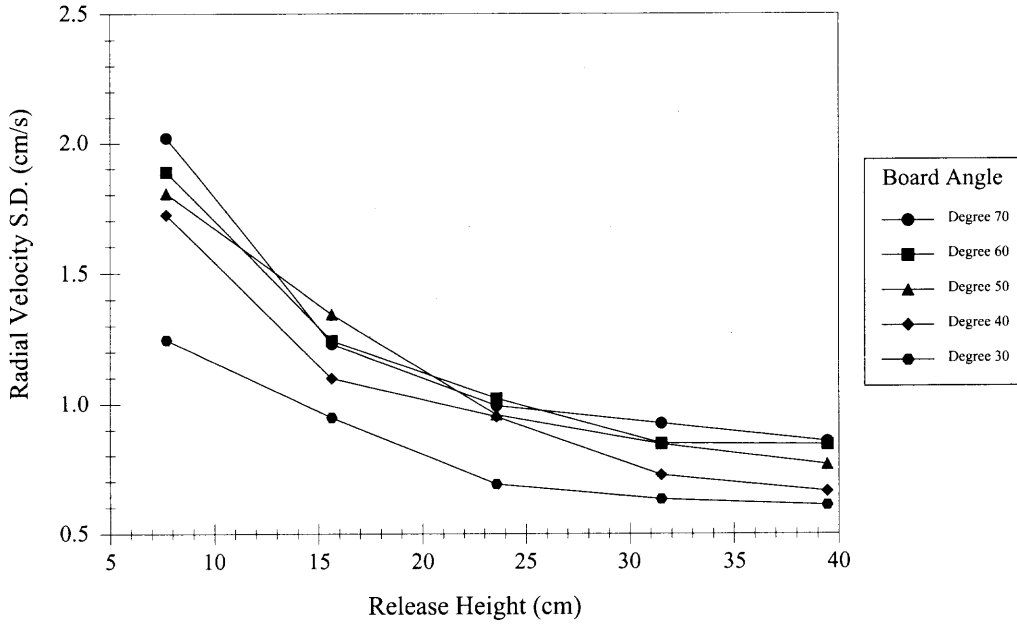


Figure B.35 Standard deviation of the radial velocity vs. release height of 1/8" brass spheres for various board angles.

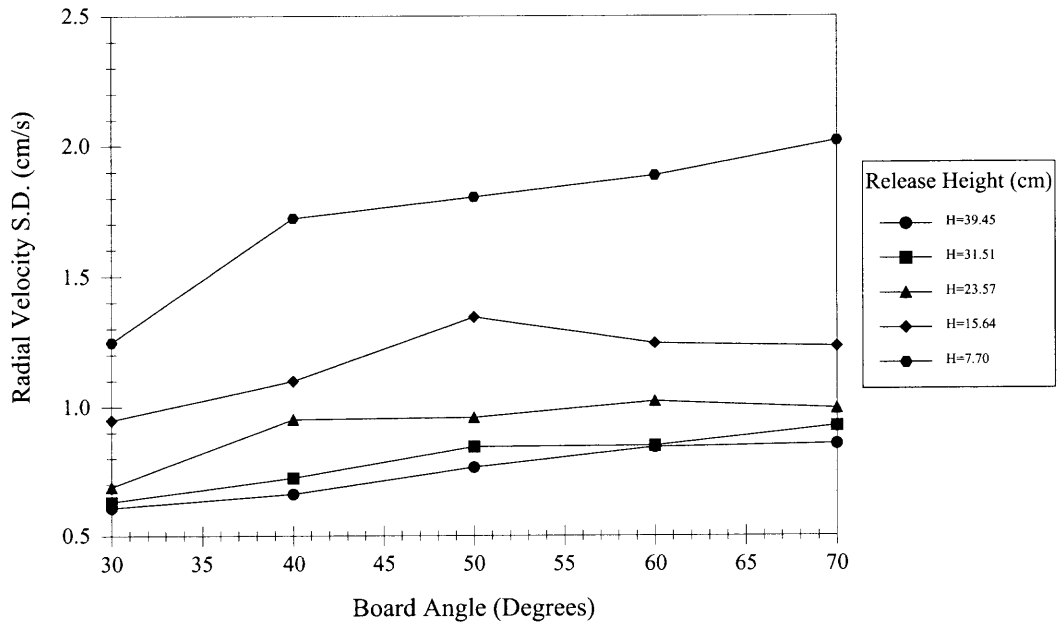


Figure B.36 Standard deviation of the radial velocity vs. board angle of 1/8" brass spheres for various release heights.

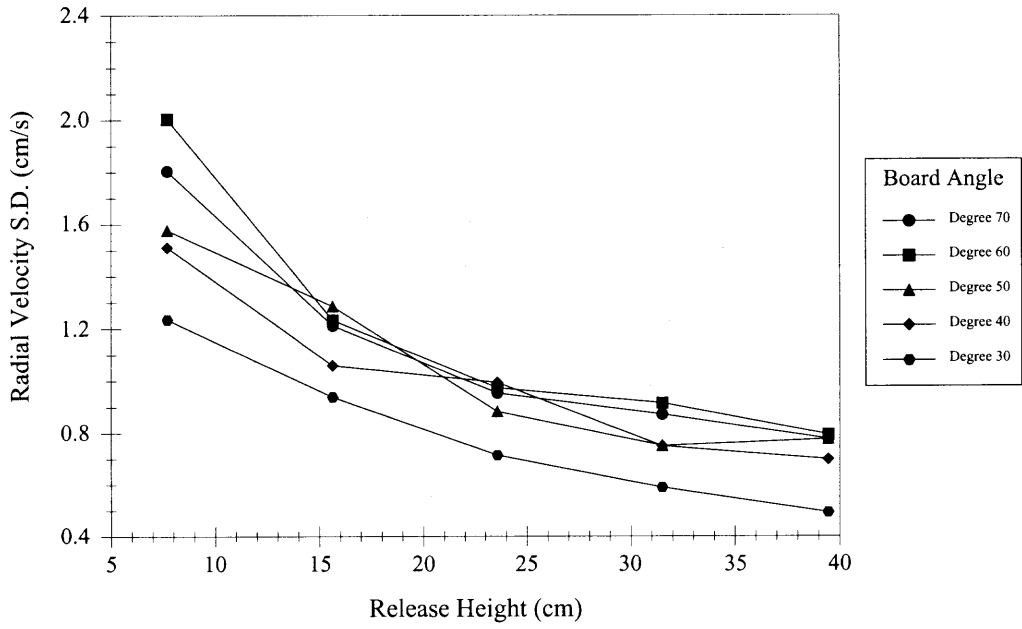


Figure B.37 Standard deviation of the radial velocity vs. release height of 1/8” stainless steel spheres for various board angles.

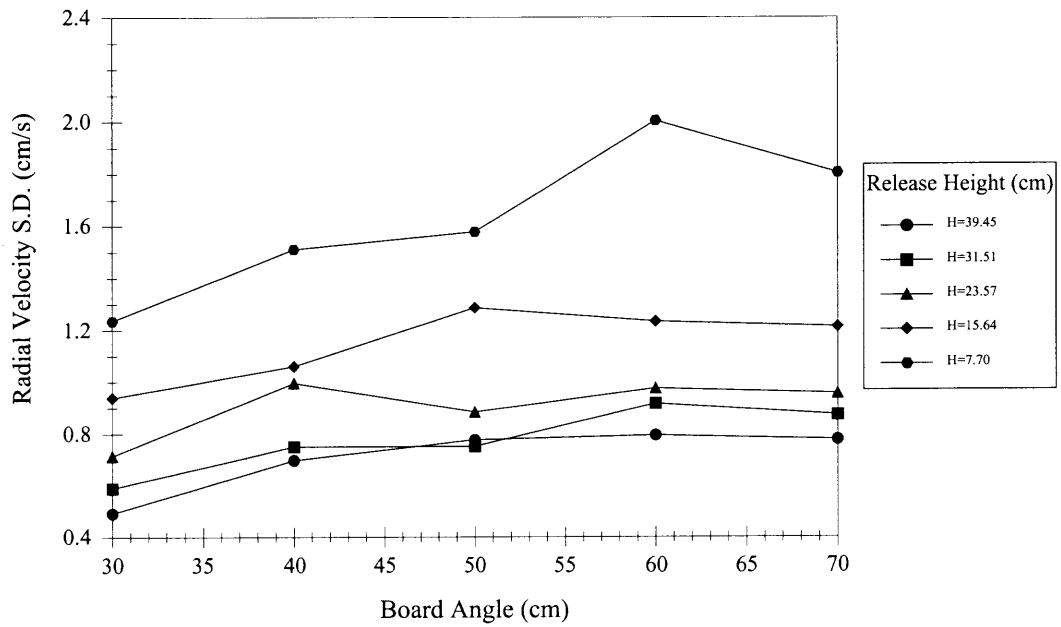


Figure B.38 Standard deviation of the radial velocity vs. board angle of 1/8” stainless steel spheres for various release heights.

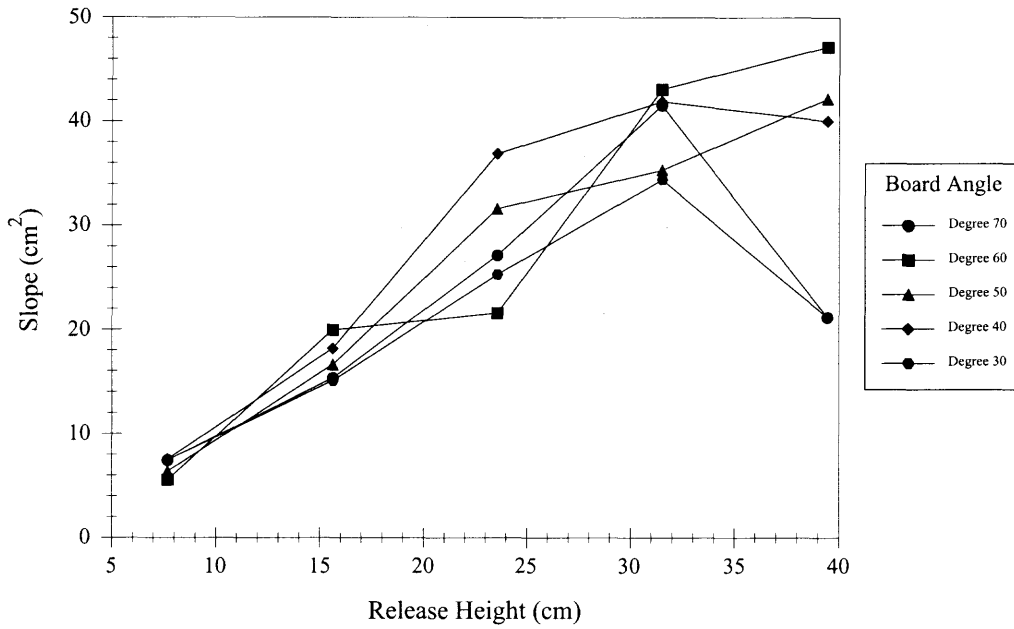


Figure B.39 Slope of $[r^2 \text{ vs. } \ln(N_0/(N_0-N))]$ vs. release height of 1/8" aluminum spheres for various board angles.

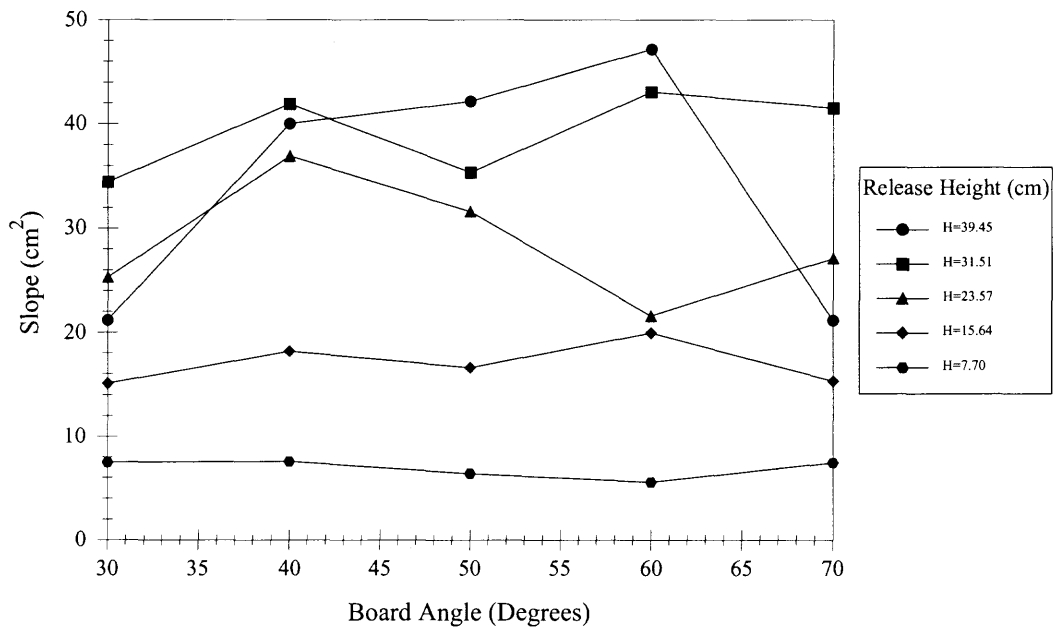


Figure B.40 Slope of $[r^2 \text{ vs. } \ln(N_0/(N_0-N))]$ vs. board angle of 1/8" aluminum spheres for various release heights.

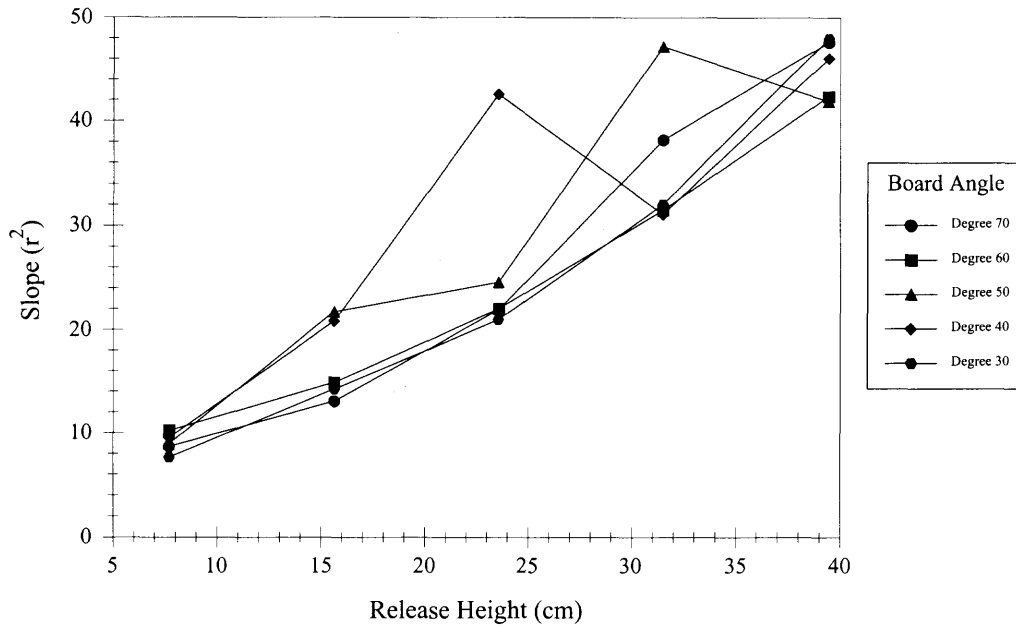


Figure B.41 Slope of $[r^2 \text{ vs. } \ln(N_0/(N_0-N))]$ vs. release height of 1/8" brass spheres for various board angles.

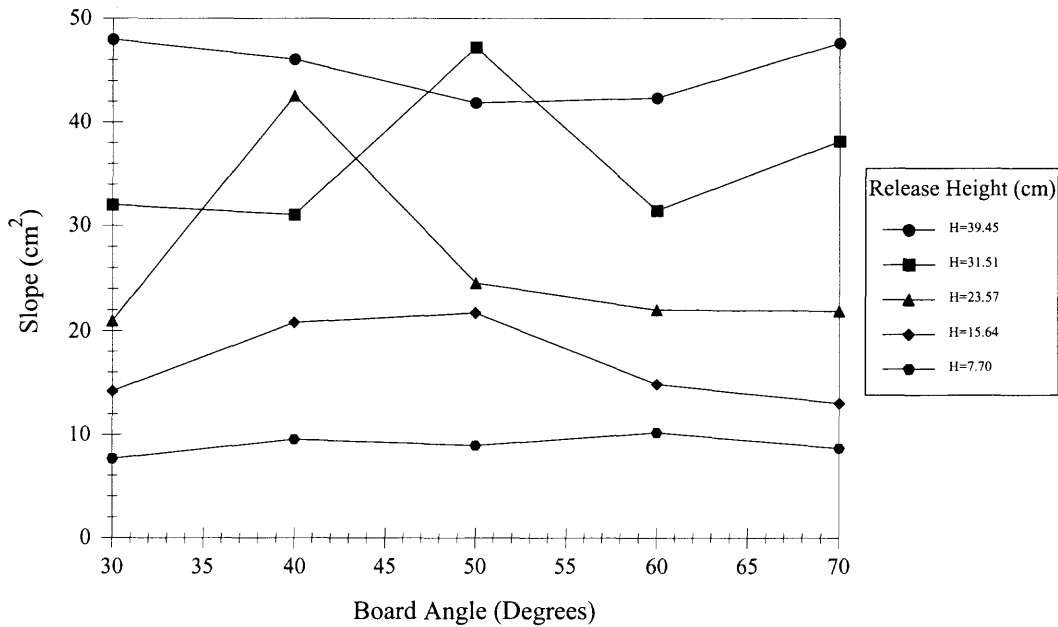


Figure B.42 Slope of $[r^2 \text{ vs. } \ln(N_0/(N_0-N))]$ vs. board angle of 1/8" brass spheres for various release heights.

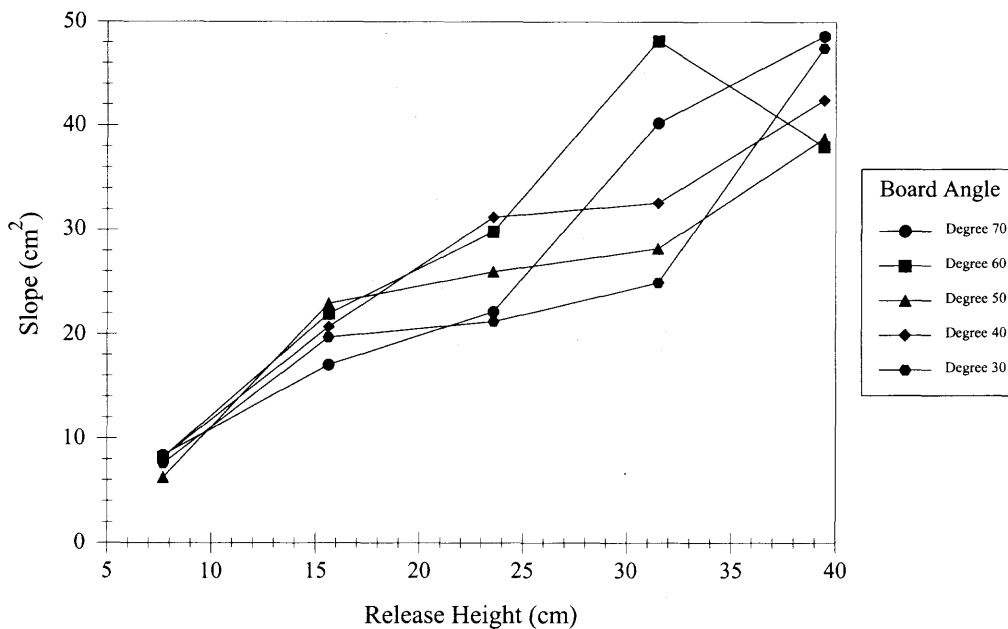


Figure B.43 Slope of $[r^2 \text{ vs. } \ln(N_0/(N_0-N))]$ vs. release height of 1/8" stainless steel spheres for various board angles.

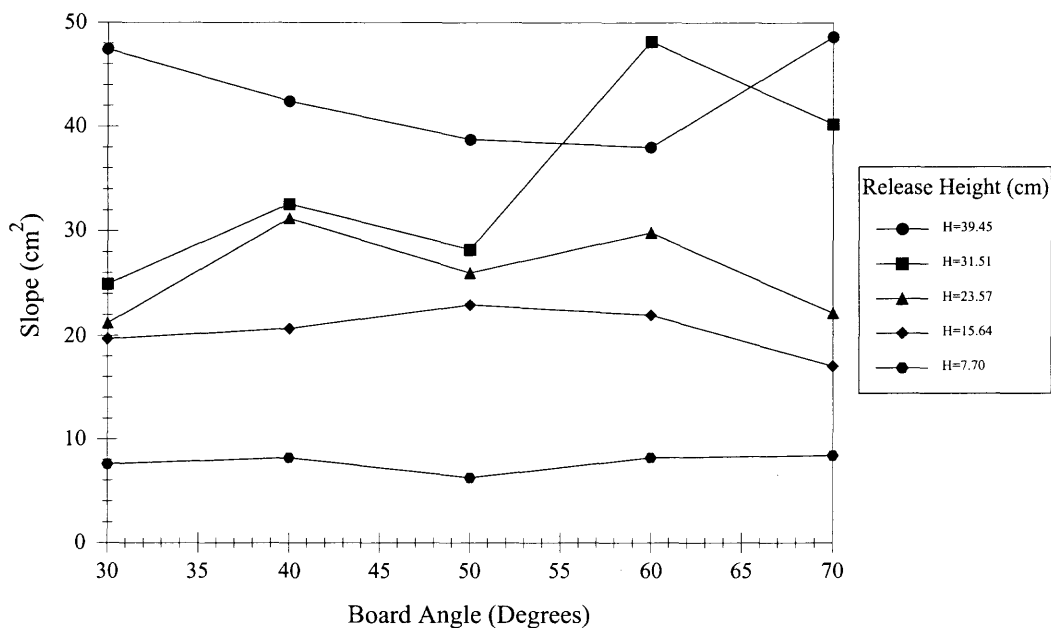


Figure B.44 Slope of $[r^2 \text{ vs. } \ln(N_0/(N_0-N))]$ vs. board angle of 1/8" stainless steel spheres for various release heights.

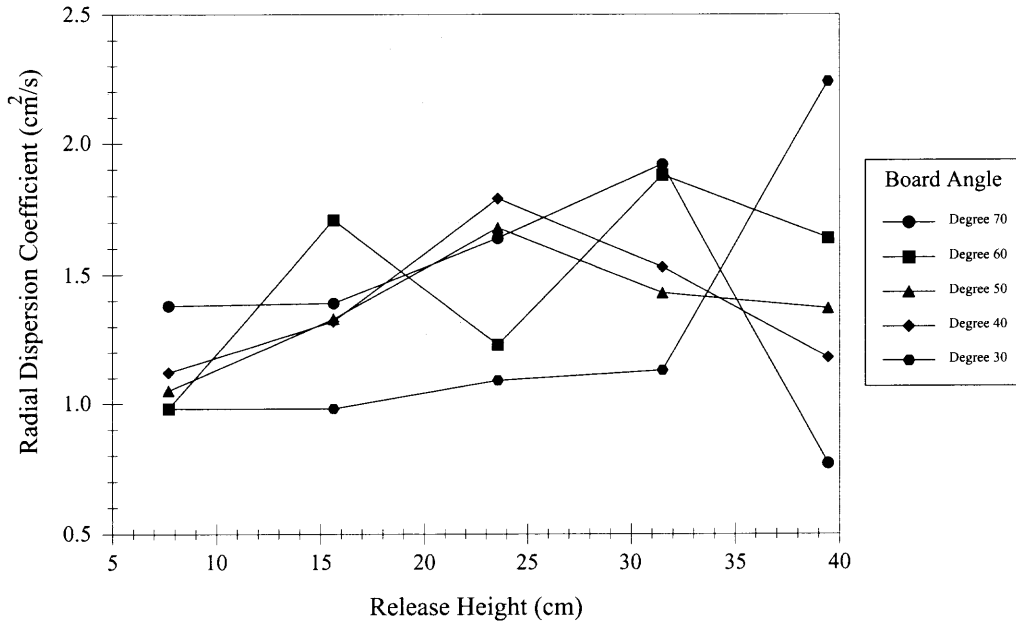


Figure B.45 Radial Dispersion Coefficient vs. release height of 1/8" aluminum spheres for various board angles.

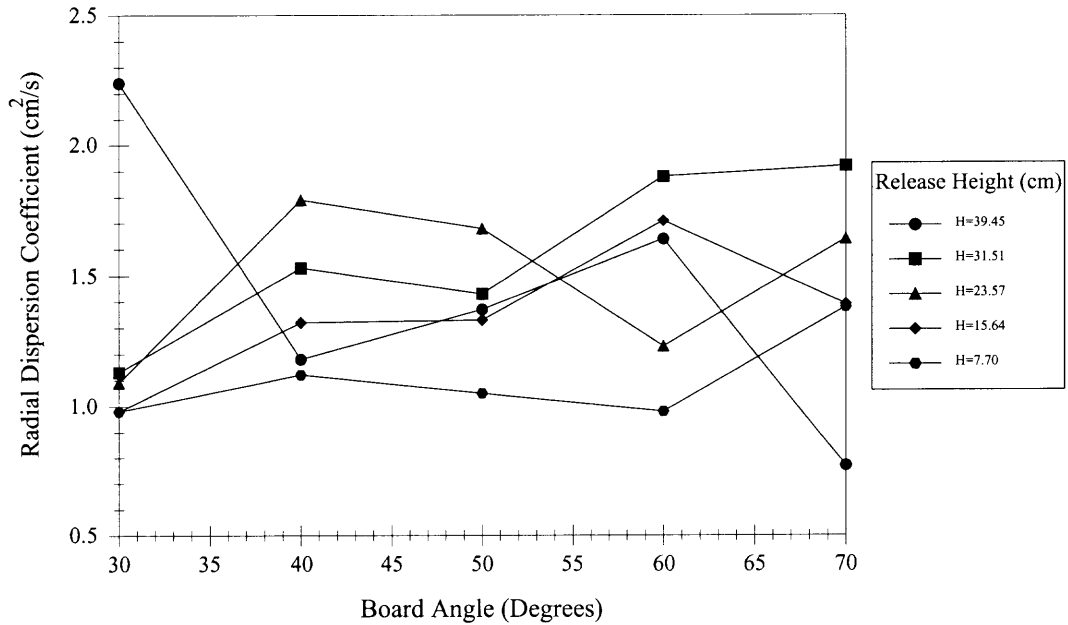


Figure B.46 Radial Dispersion Coefficient vs. board angle of 1/8" aluminum spheres for various release heights.

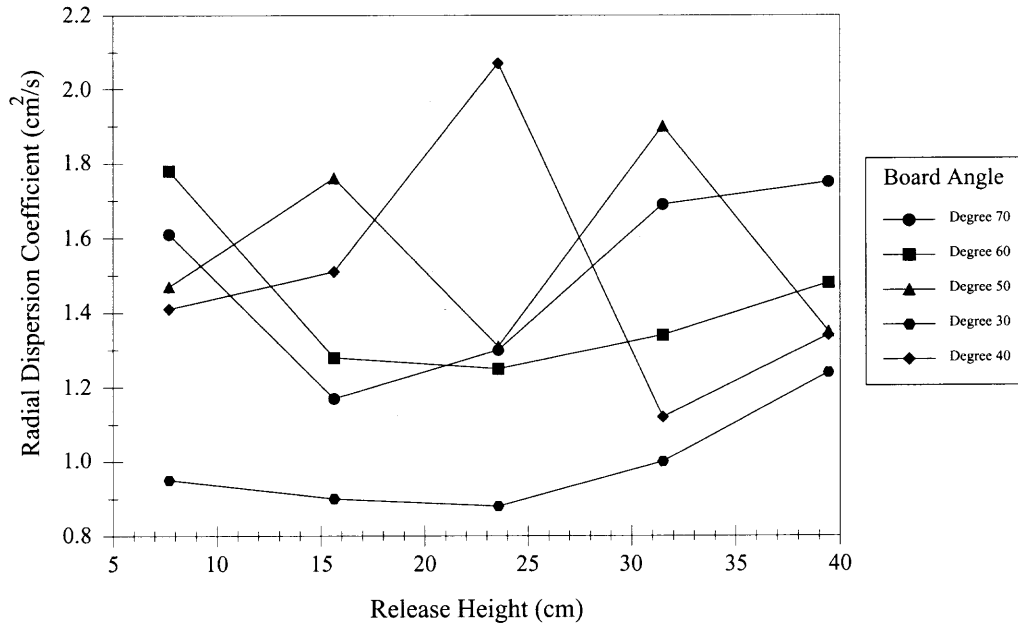


Figure B.47 Radial Dispersion Coefficient vs. release height of 1/8” brass spheres for various board angles.

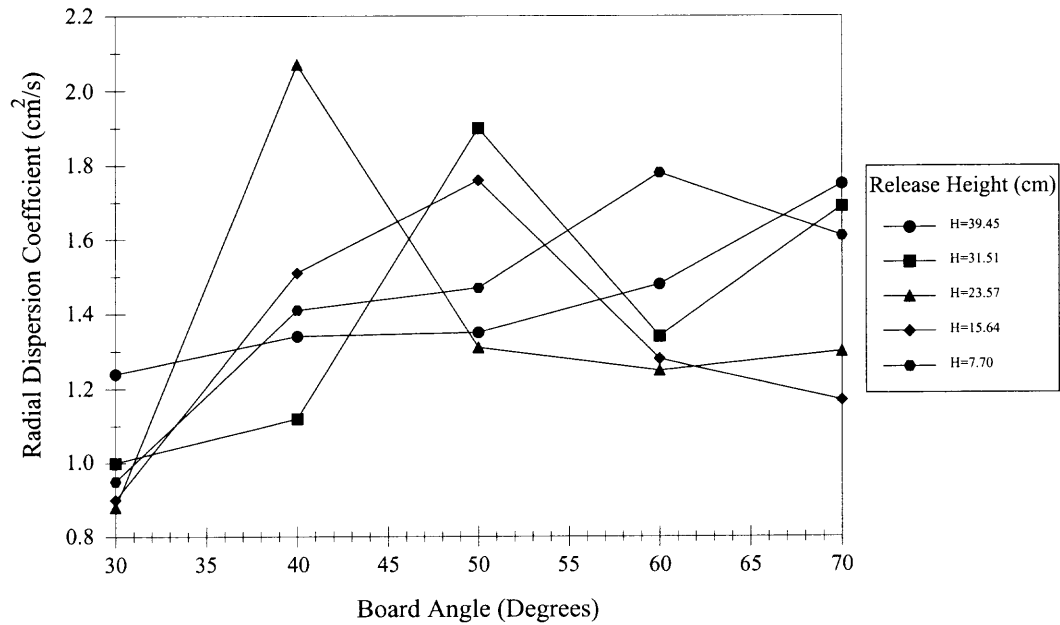


Figure B.48 Radial Dispersion Coefficient vs. board angle of 1/8” brass spheres for various release heights.

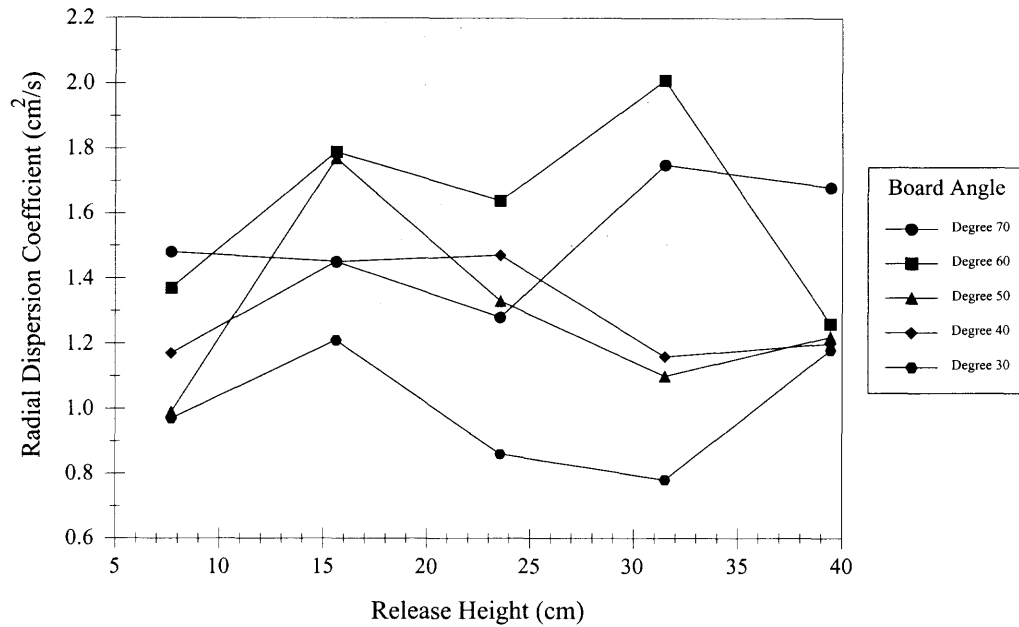


Figure B.49 Radial Dispersion Coefficient vs. release height of 1/8" stainless steel spheres for various board angles.

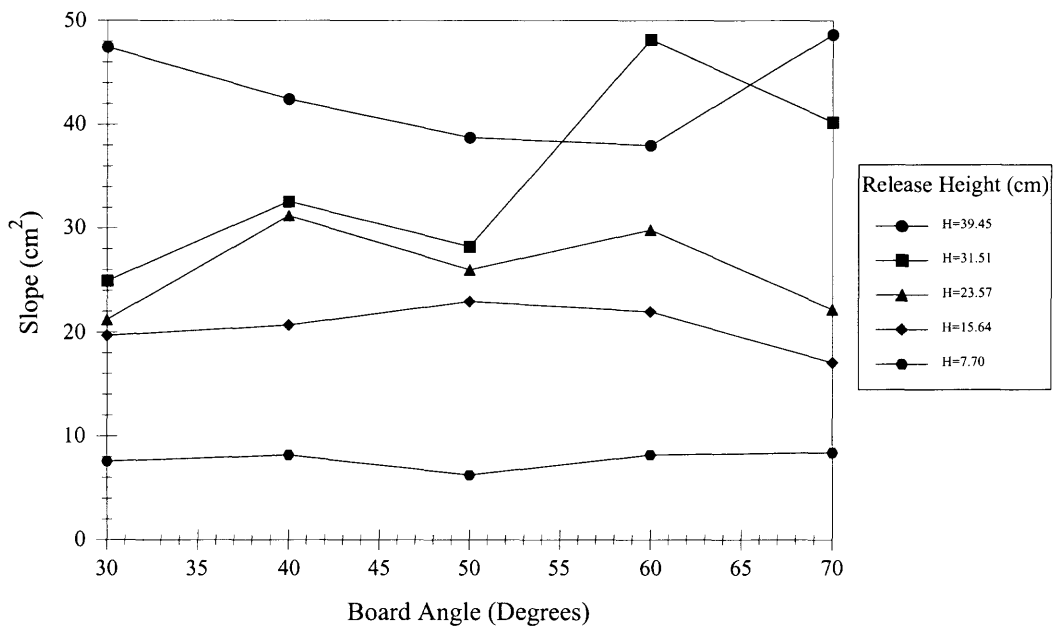
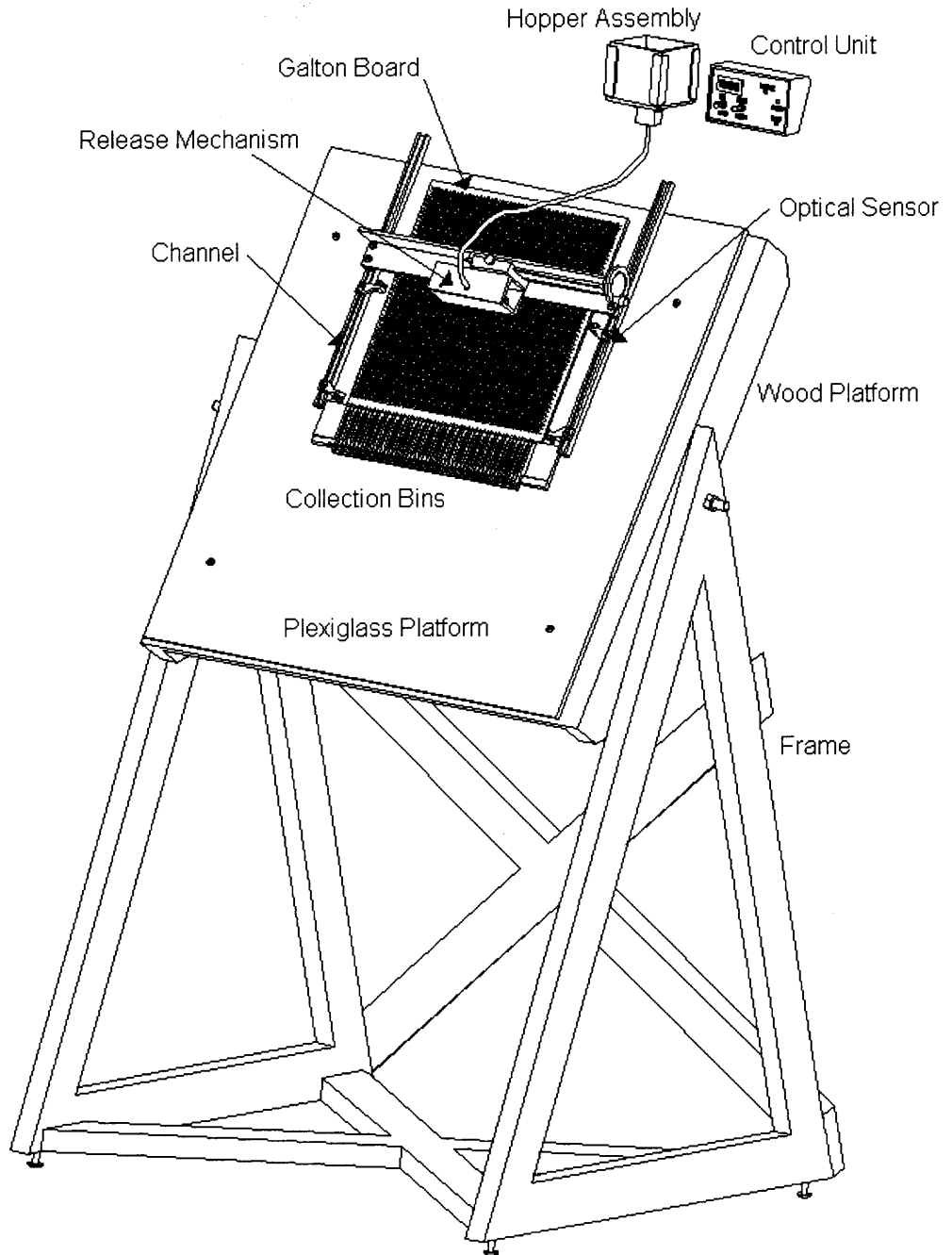


Figure B.50 Radial Dispersion Coefficient vs. board angle of 1/8" stainless steel spheres for various release heights.

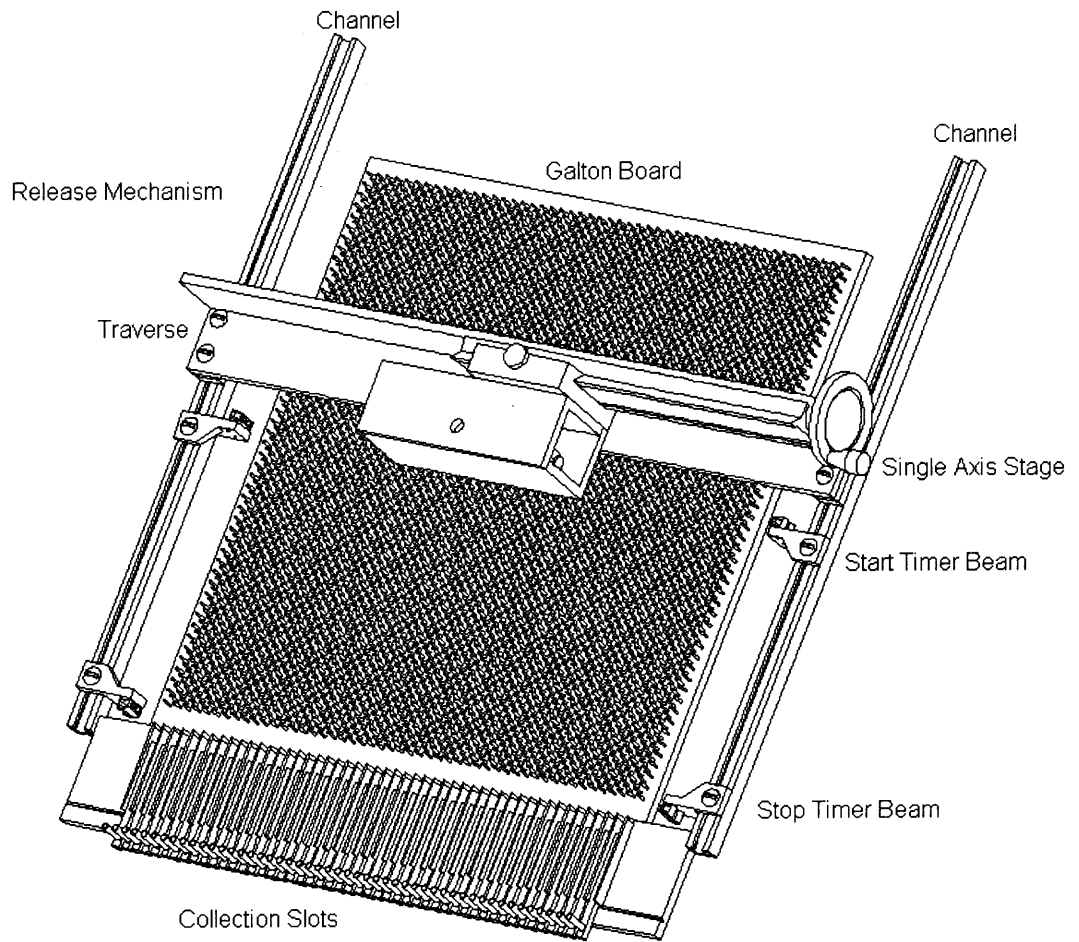
APPENDIX C

TECHNICAL DRAWINGS

The following appendix contains assembly drawings of the experimental apparatus and detail drawings of individual parts of the apparatus.

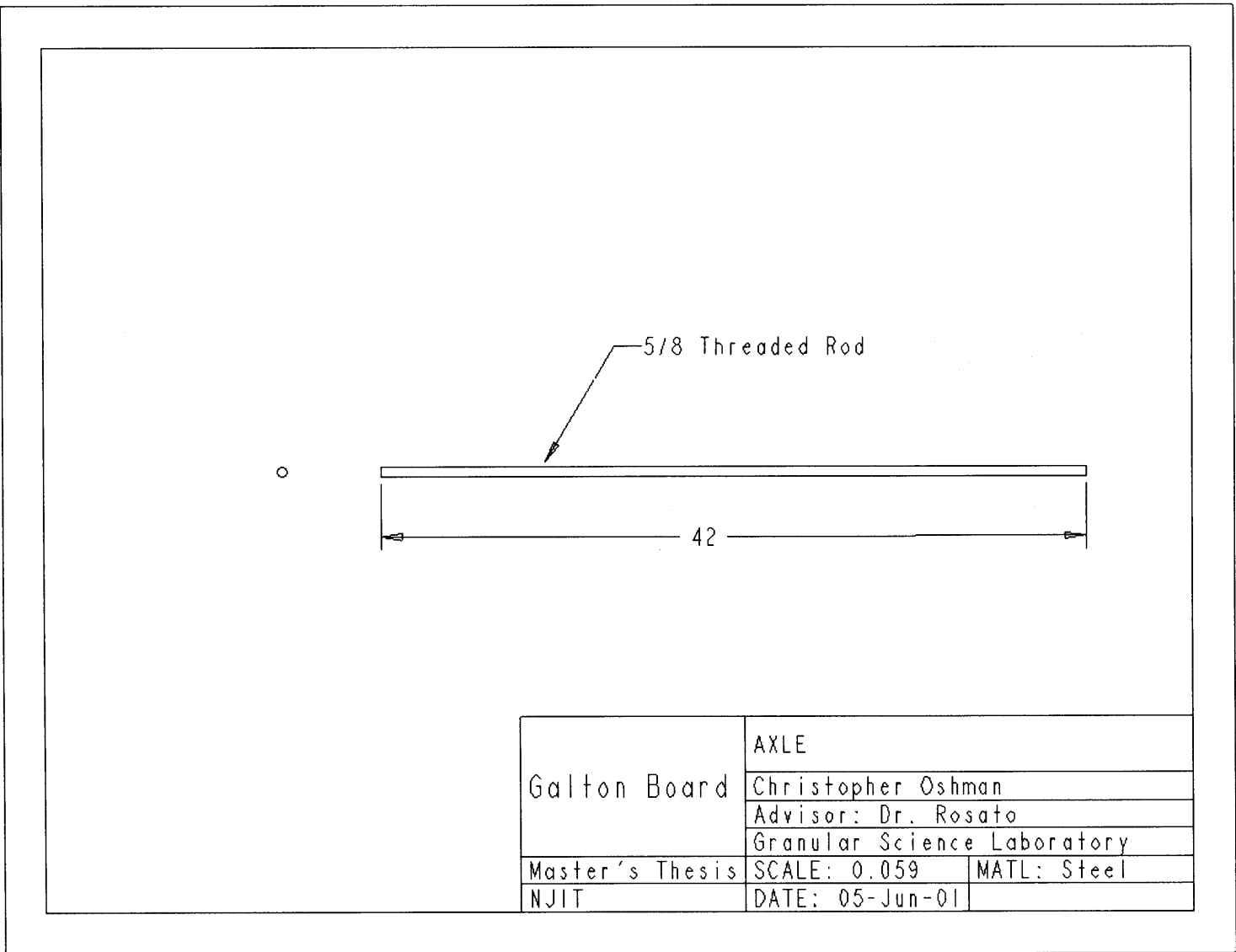


Drawing C.1 Assembly of Galton board system.



Drawing C.2 Close up of Galton board assembly.

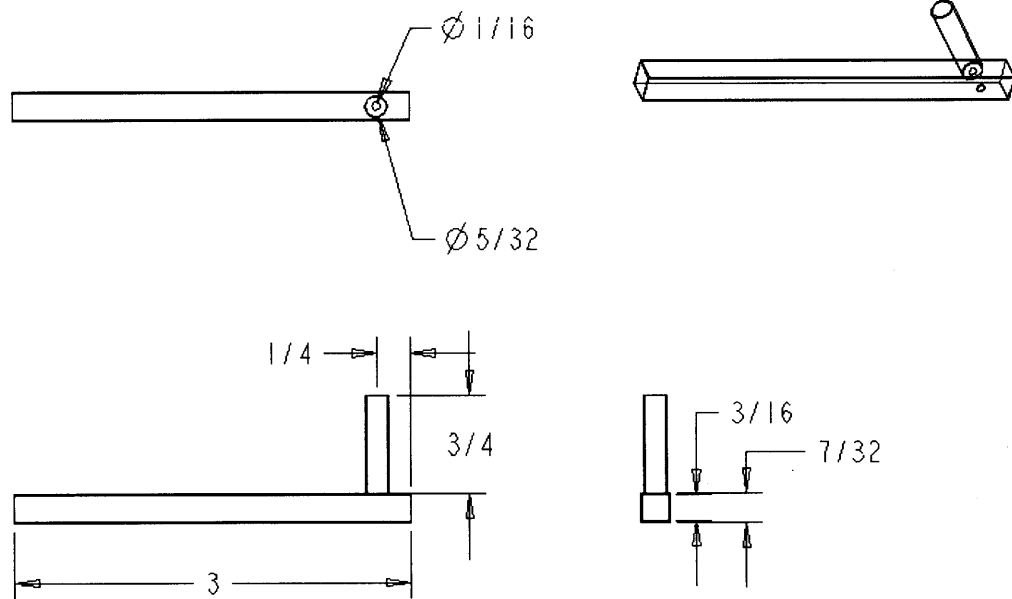
Drawing C.3 Axle.



	AXLE	
Galton Board	Christopher Oshman	
	Advisor: Dr. Rosato	
	Granular Science Laboratory	
Master's Thesis	SCALE: 0.059	MATL: Steel
NJIT	DATE: 05-Jun-01	

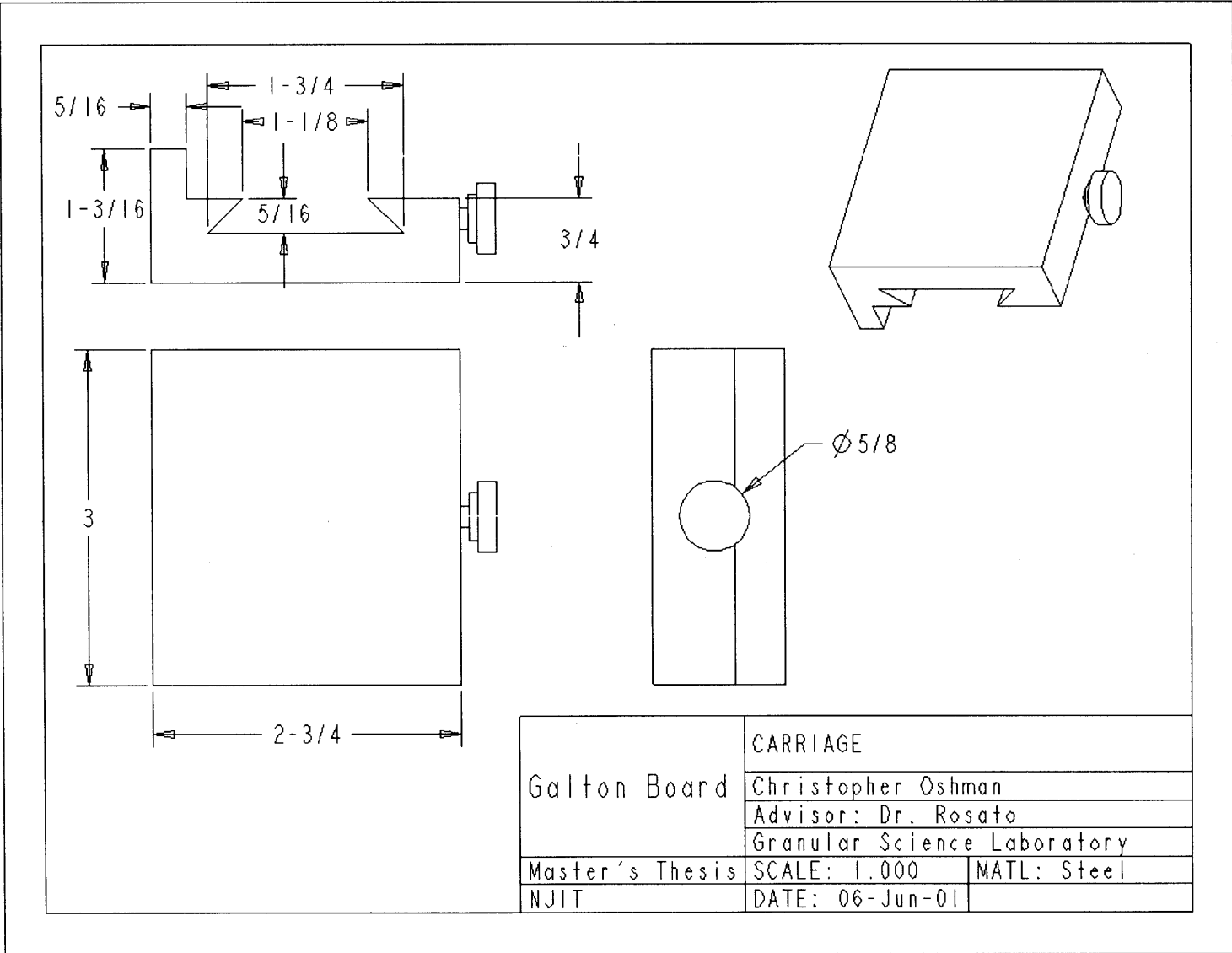
Drawing C.4 Brass Sensor Housing.

NOTE: Two Pieces are soldered together using a propane torch



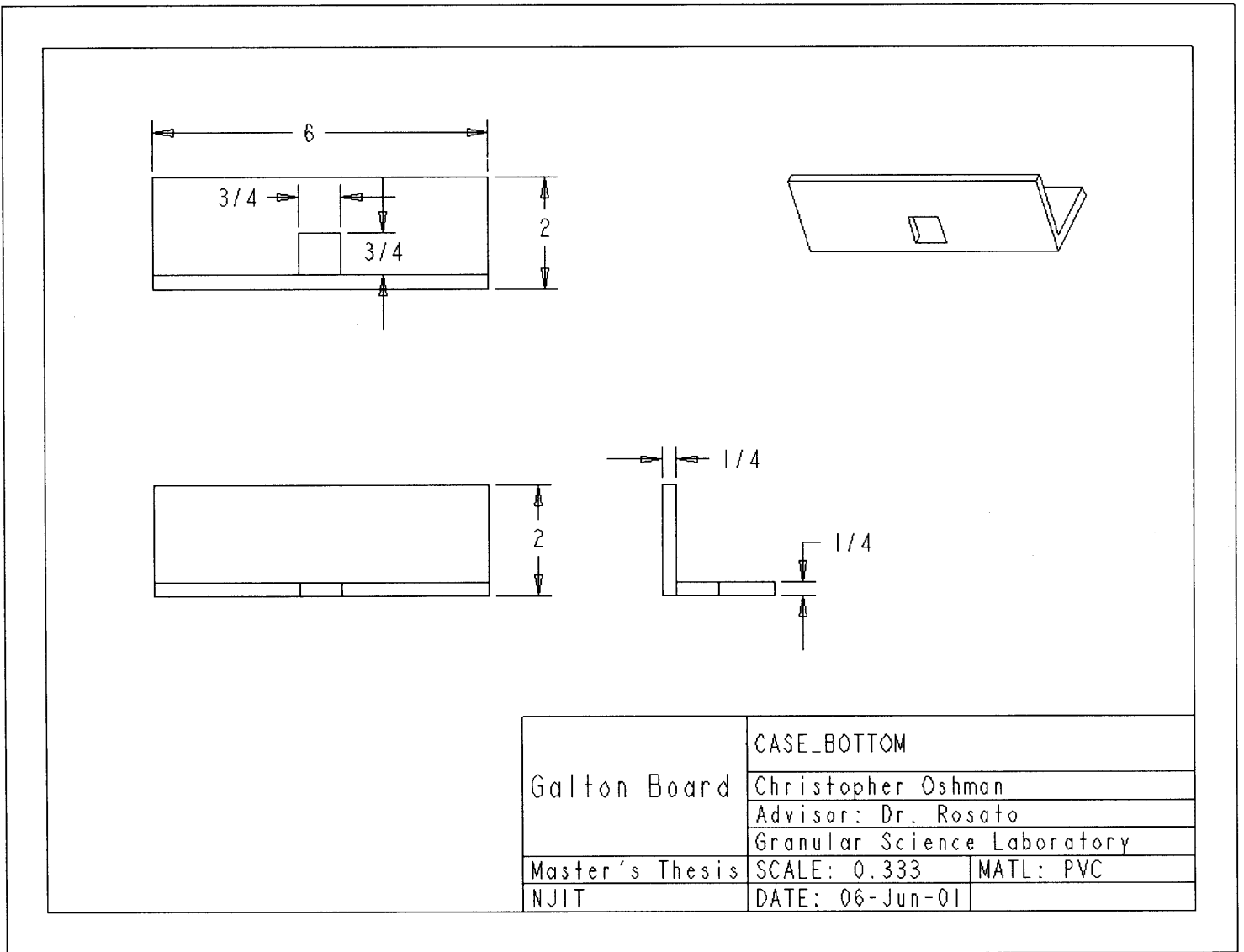
	BRASS SENSOR	
Galton Board	Christopher Oshman	
	Advisor: Dr. Rosato	
	Granular Science Laboratory	
Master's Thesis	SCALE: 1.000	MATL: Brass
NJIT	DATE: 05-Jun-01	

Drawing C.5 Carriage.

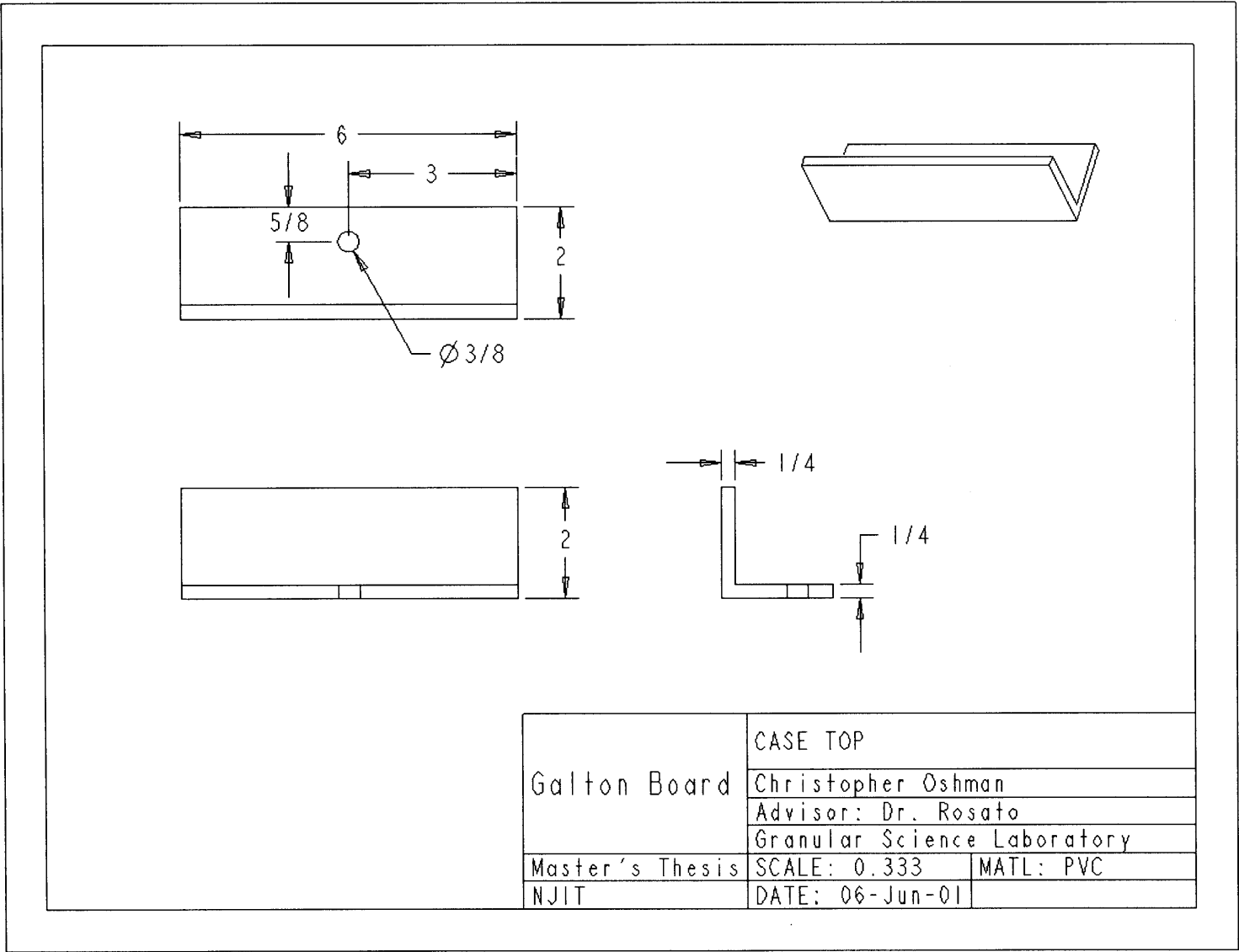


	CARRIAGE	
Galton Board	Christopher Oshman	
	Advisor: Dr. Rosato	
	Granular Science Laboratory	
Master's Thesis	SCALE: 1.000	MATL: Steel
NJIT	DATE: 06-Jun-01	

Drawing C.6 Bottom of the release housing.

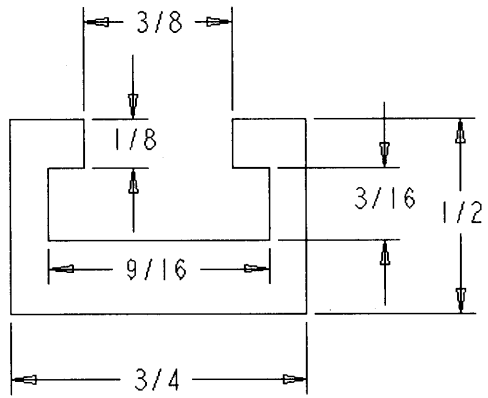


Drawing C.7 Top of the release housing.



Galton Board	CASE TOP	
	Christopher Oshman	
	Advisor: Dr. Rosato	
Master's Thesis NJIT	Granular Science Laboratory	
	SCALE: 0.333	MATL: PVC
	DATE: 06-Jun-01	

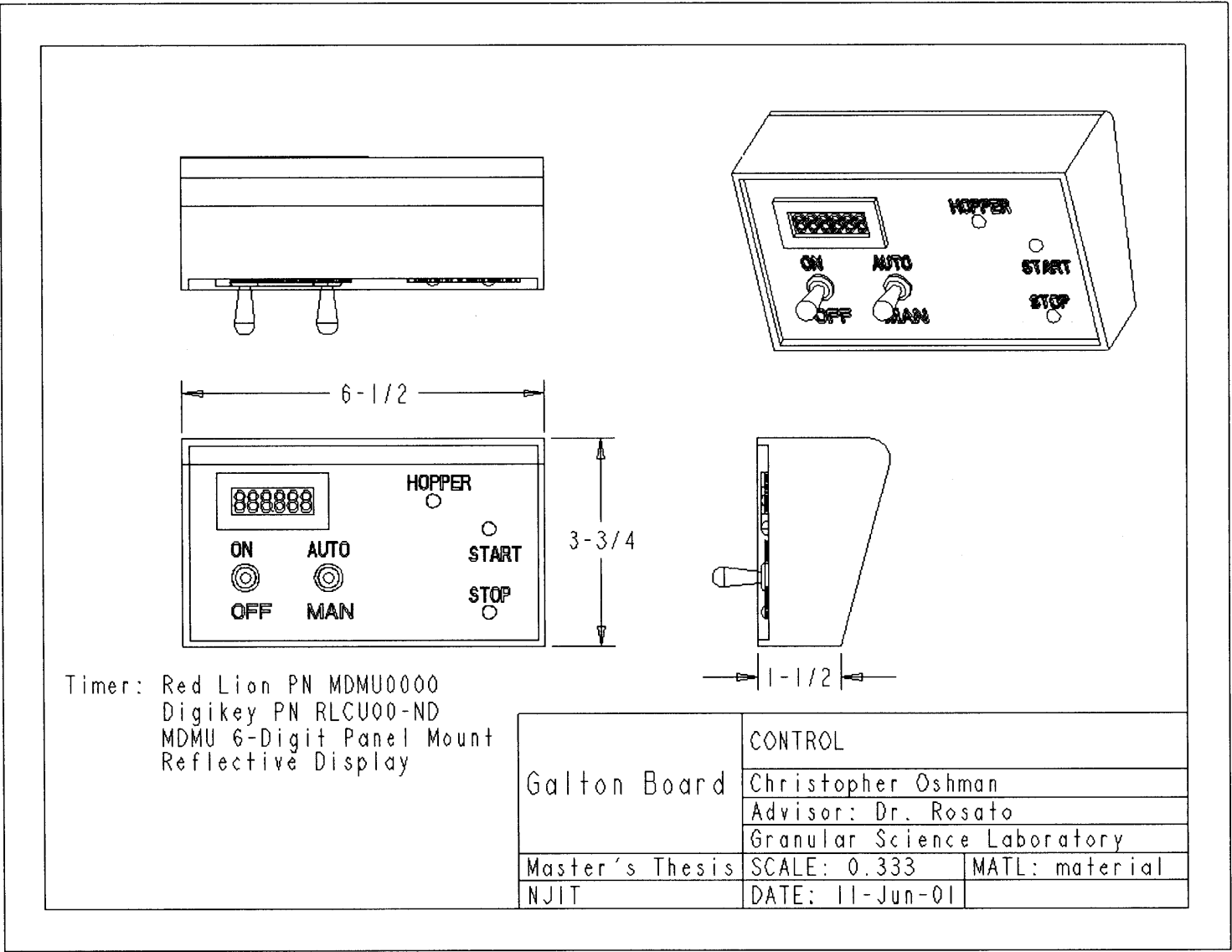
Drawing C.8 Channel.



NOTE: LENGTH= 20"

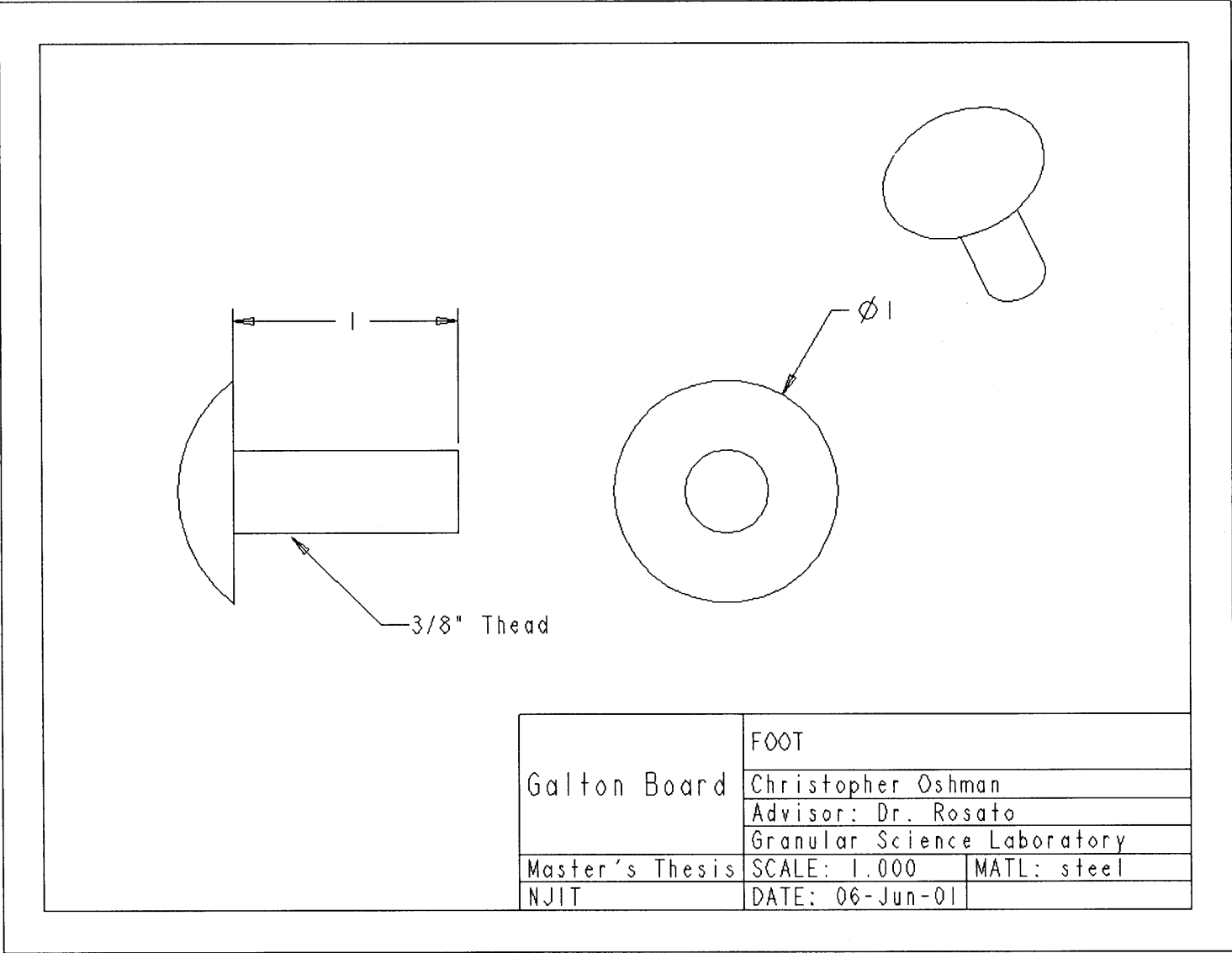
Galton Board	CHANNEL	
	Christopher Oshman	
	Advisor: Dr. Rosato Granular Science Laboratory	
Master's Thesis	SCALE: 0.125	MATL: Aluminum
NJIT	DATE: 05-Jun-01	

Drawing C.9 Control Panel



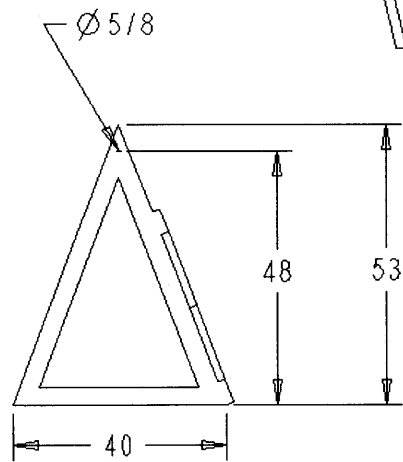
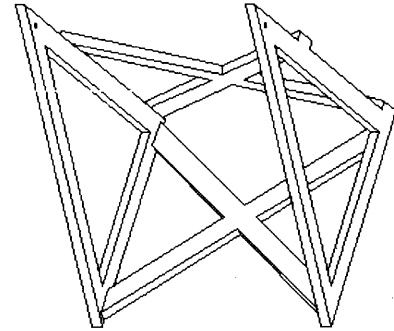
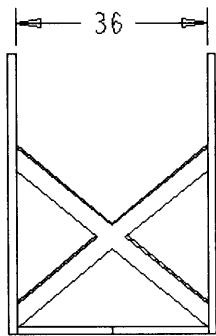
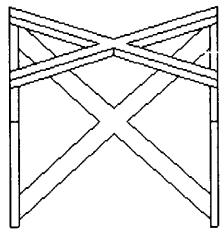
Galton Board	CONTROL	
	Christopher Oshman	
	Advisor: Dr. Rosato Granular Science Laboratory	
Master's Thesis	SCALE: 0.333	MATL: material
NJIT	DATE: 11-Jun-01	

Drawing C.10 Foot.



	FOOT	
Galton Board	Christopher Oshman	
	Advisor: Dr. Rosato	
	Granular Science Laboratory	
Master's Thesis	SCALE: 1.000	MATL: steel
NJIT	DATE: 06-Jun-01	

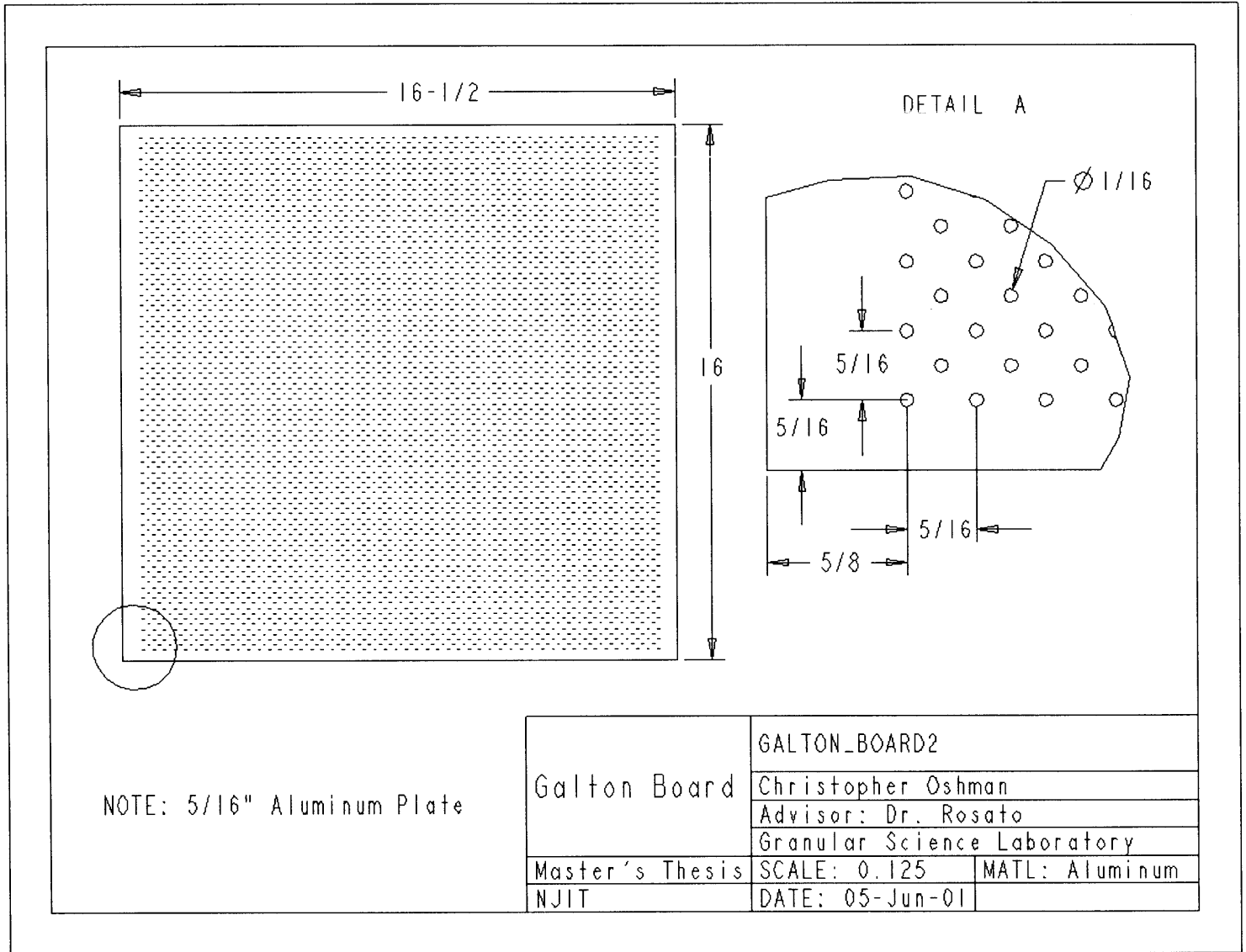
Drawing C.11 Frame.



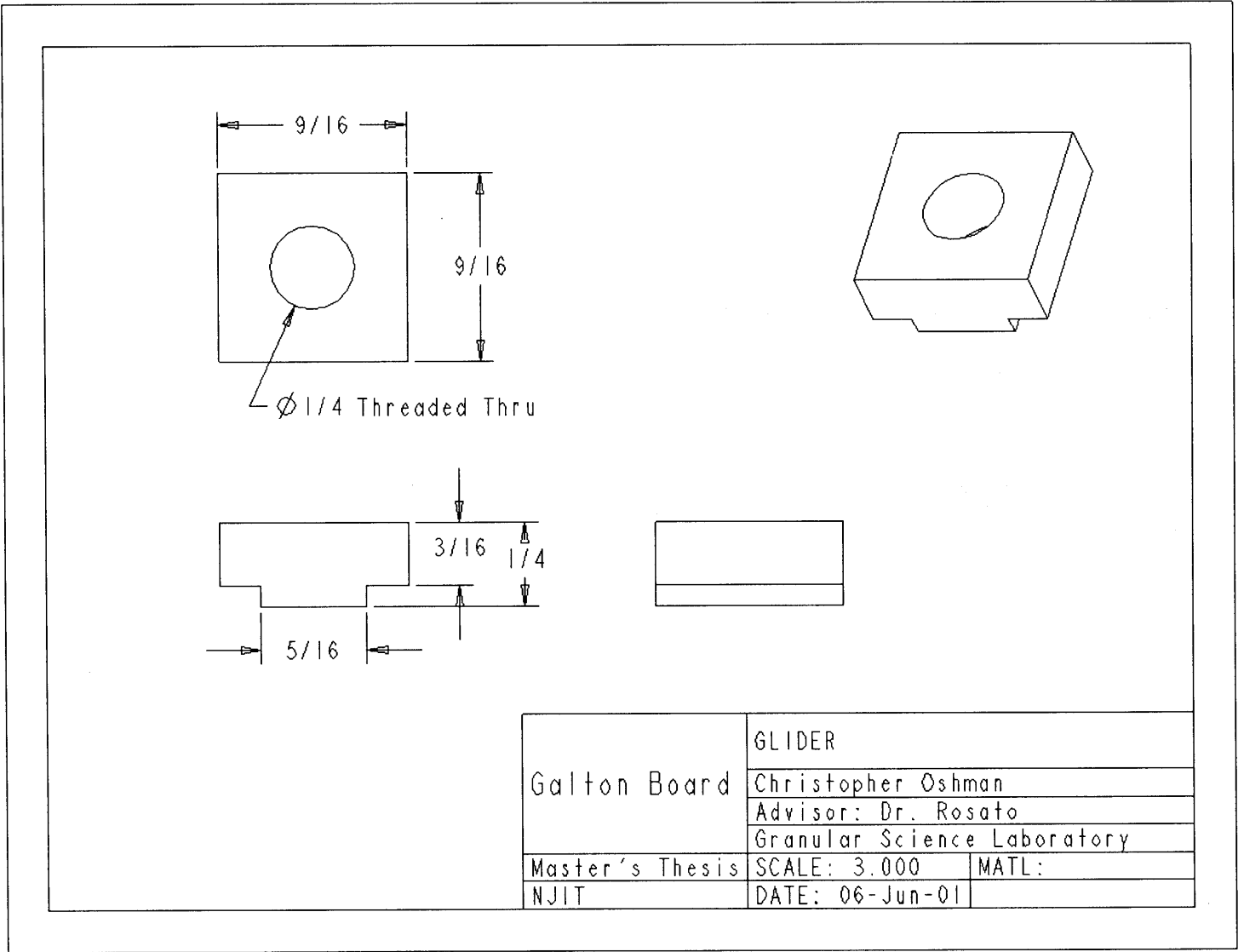
NOTE: 2x4 Lumber

	FRAME	
Galton Board	Christopher Oshman	
	Advisor: Dr. Rosato	
	Granular Science Laboratory	
Master's Thesis	SCALE: 0.040	MATL: Wood
NJIT	DATE: 05-Jun-01	

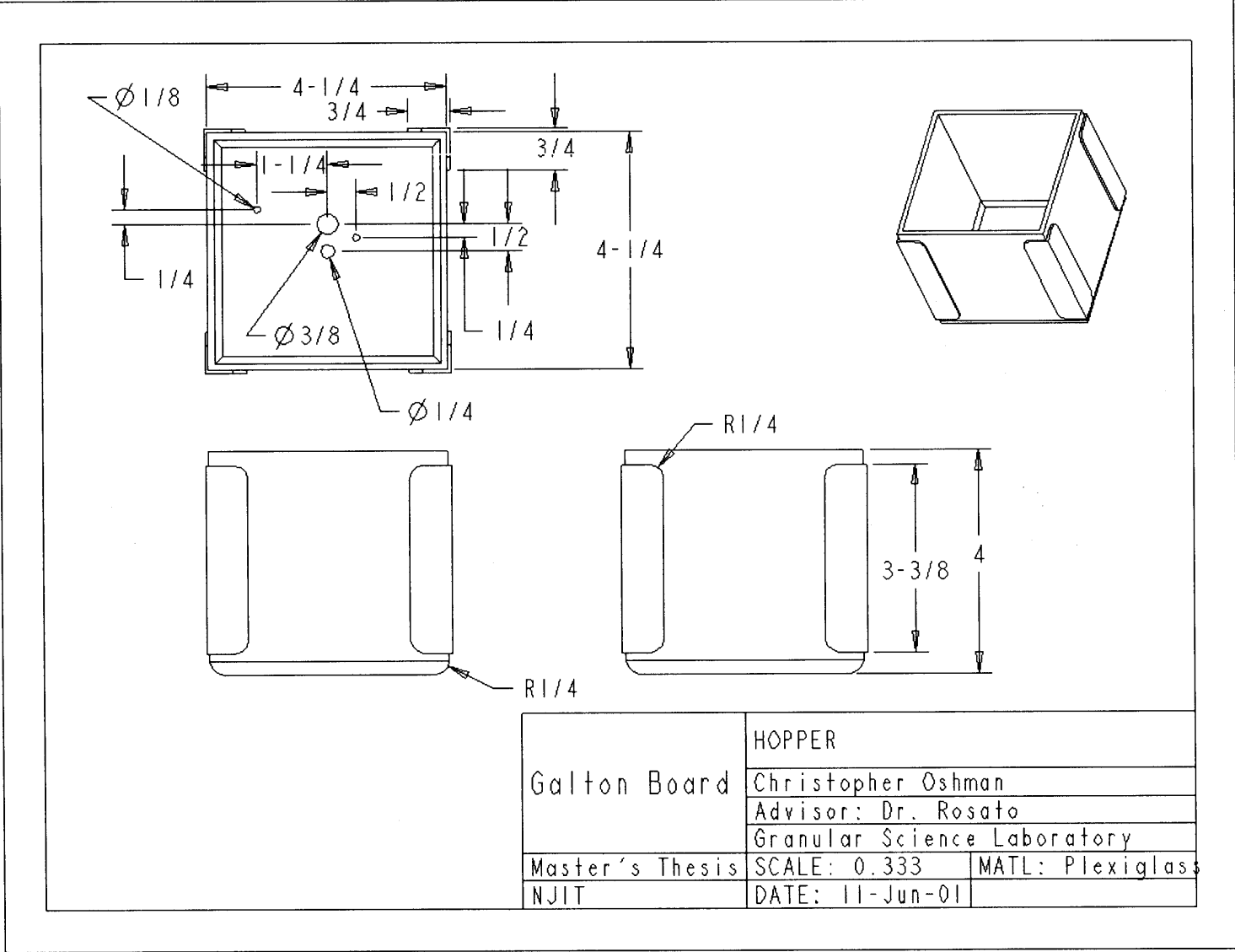
Drawing C.12 Galton board.



Drawing C.13 Glider.



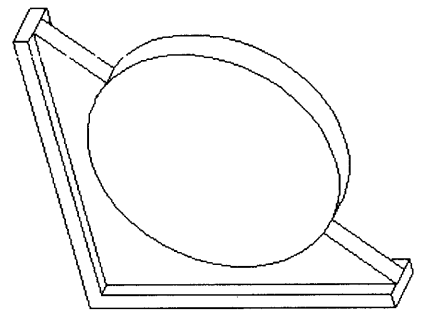
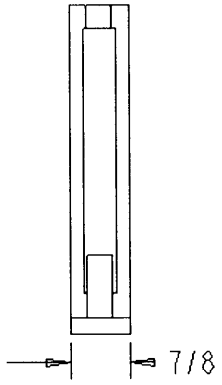
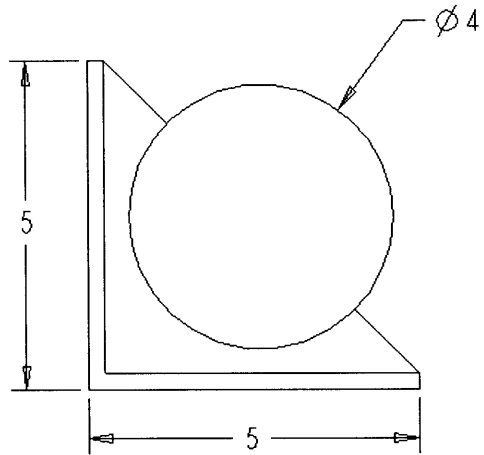
Drawing C.14 Hopper.



	HOPPER	
Galton Board	Christopher Oshman	
	Advisor: Dr. Rosato	
	Granular Science Laboratory	
Master's Thesis	SCALE: 0.333	MATL: Plexiglass
NJIT	DATE: 11-Jun-01	

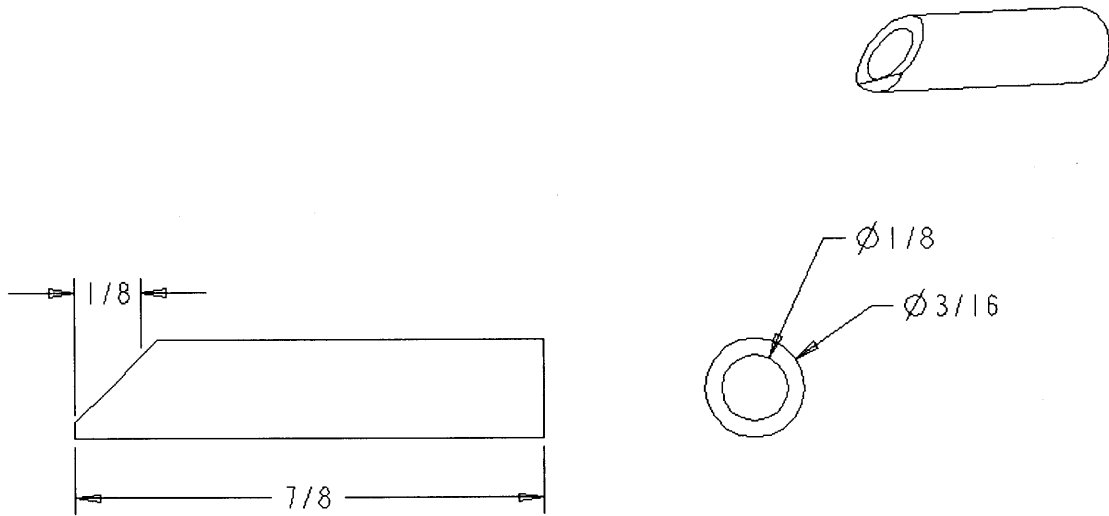
Drawing C.15 Level.

Angle Finder Plus Level
 Dasco Pro Inc.
 Rockford, IL



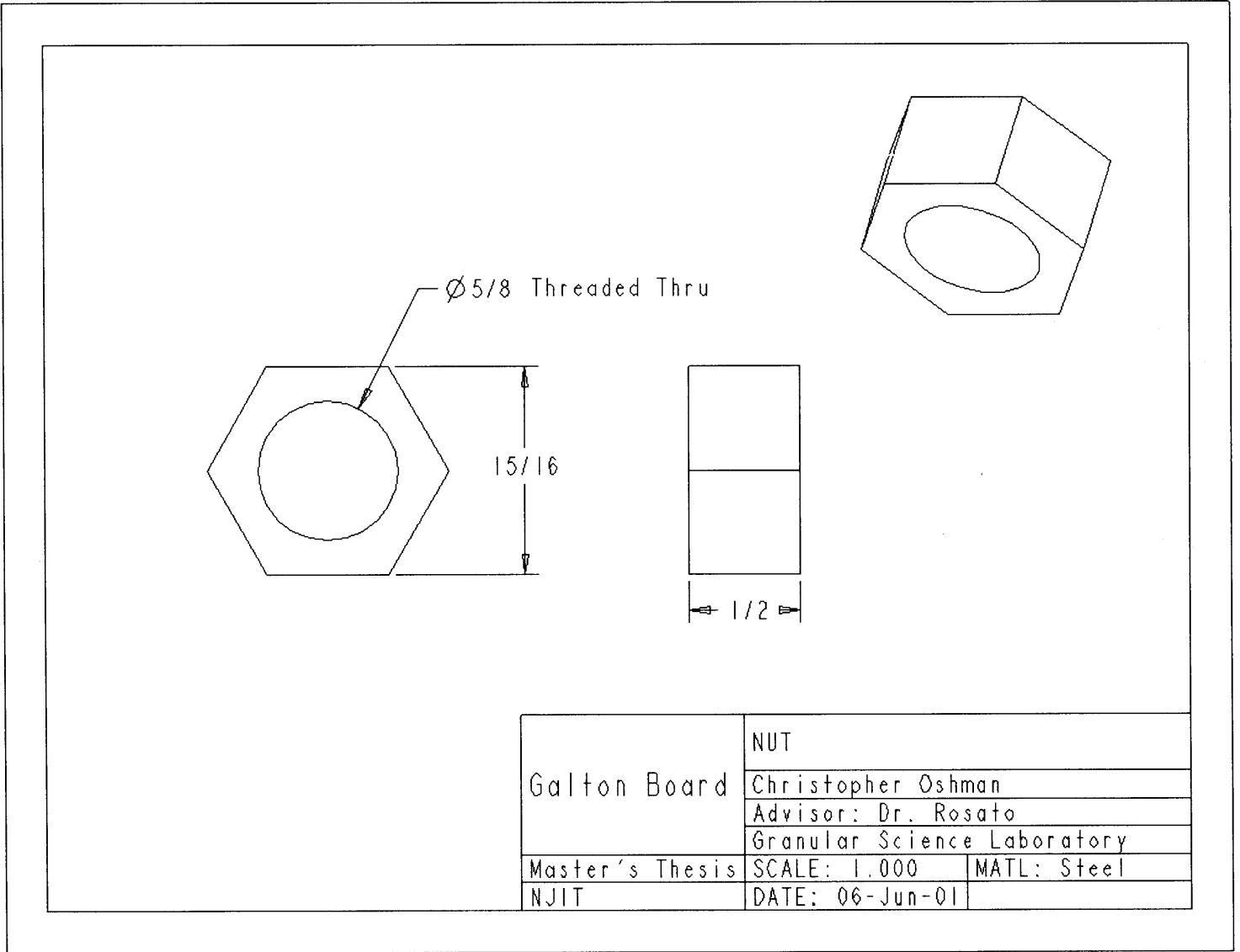
	LEVEL	
Galton Board	Christopher Oshman	
	Advisor: Dr. Rosato	
	Granular Science Laboratory	
Master's Thesis	SCALE: 0.500	MATL:
NJIT	DATE: 12-Jun-01	

Drawing C.16 Nozzle.

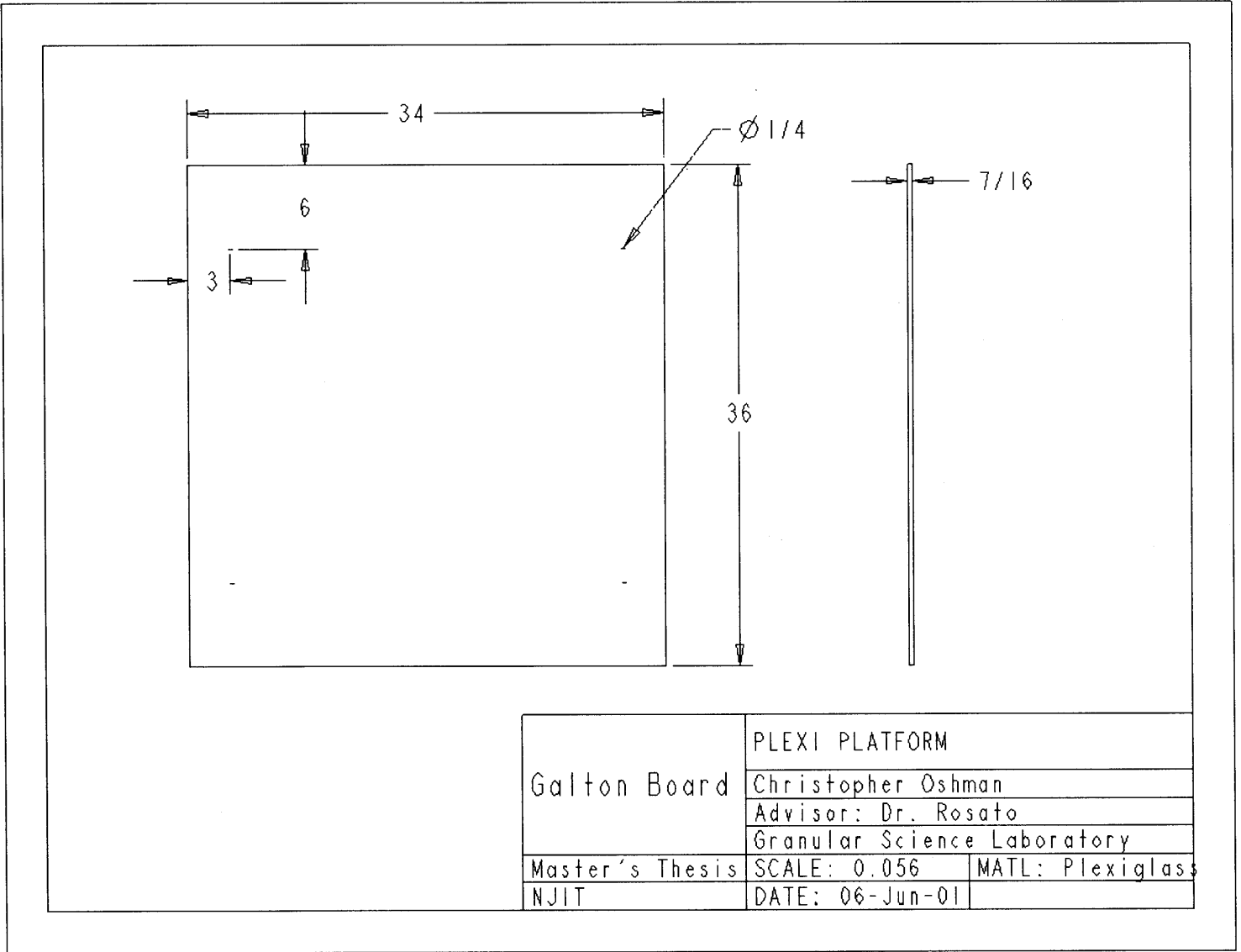


Galton Board	NOZZLE	
	Christopher Oshman	
	Advisor: Dr. Rosato Granular Science Laboratory	
Master's Thesis	SCALE: 2.000	MATL: Brass
NJIT	DATE: 06-Jun-01	

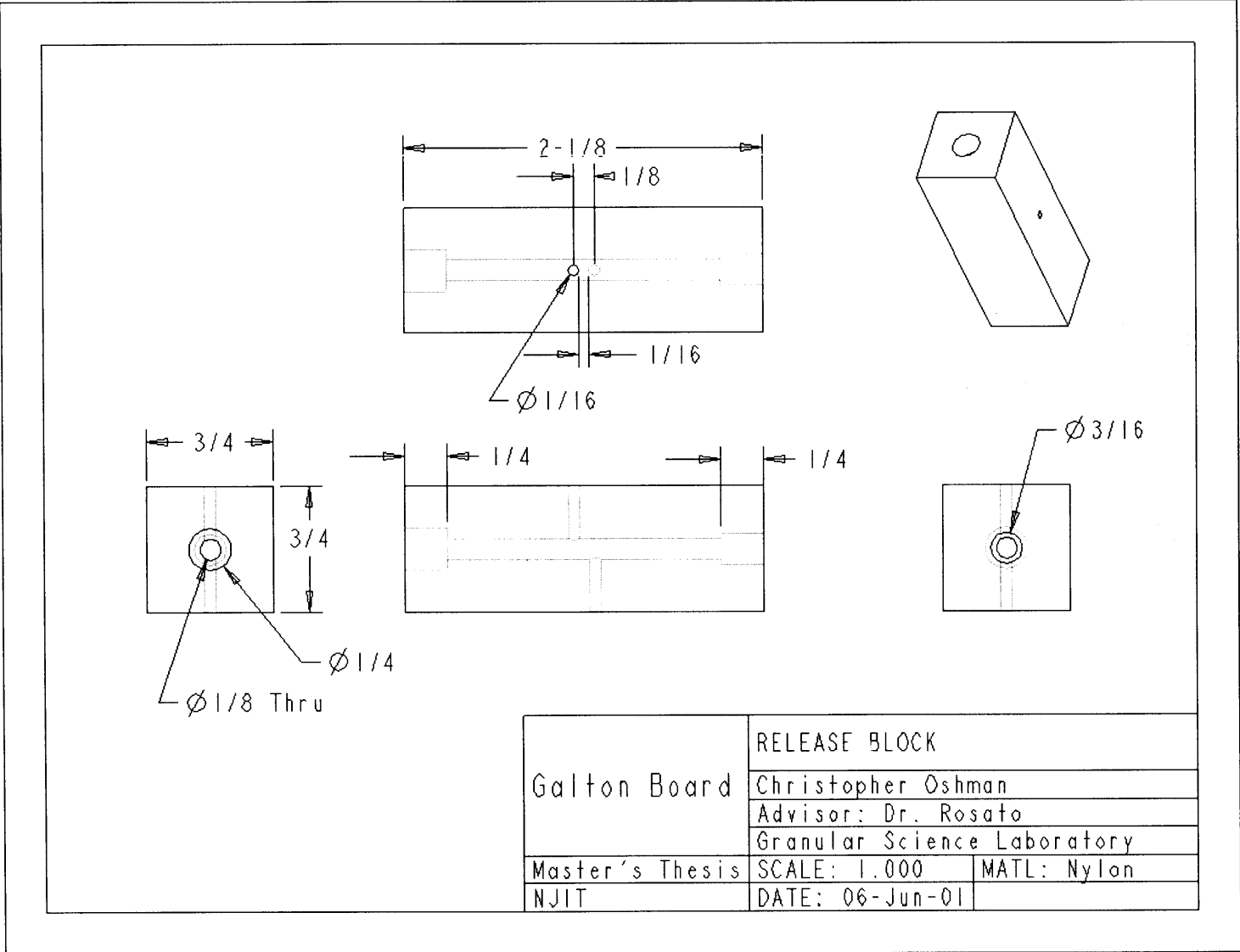
Drawing C.17 Nut.



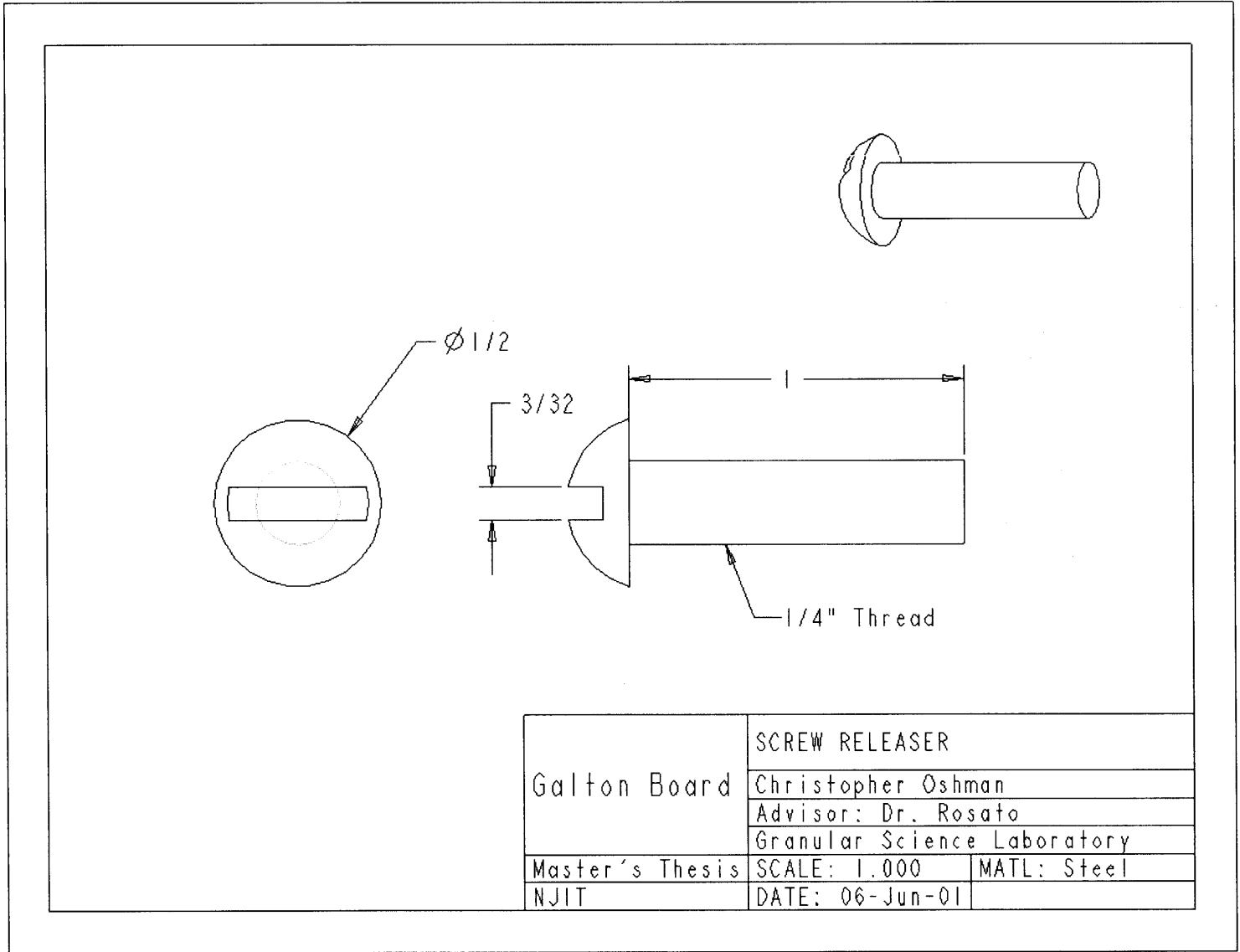
Drawing C.18 Plexiglass platform.



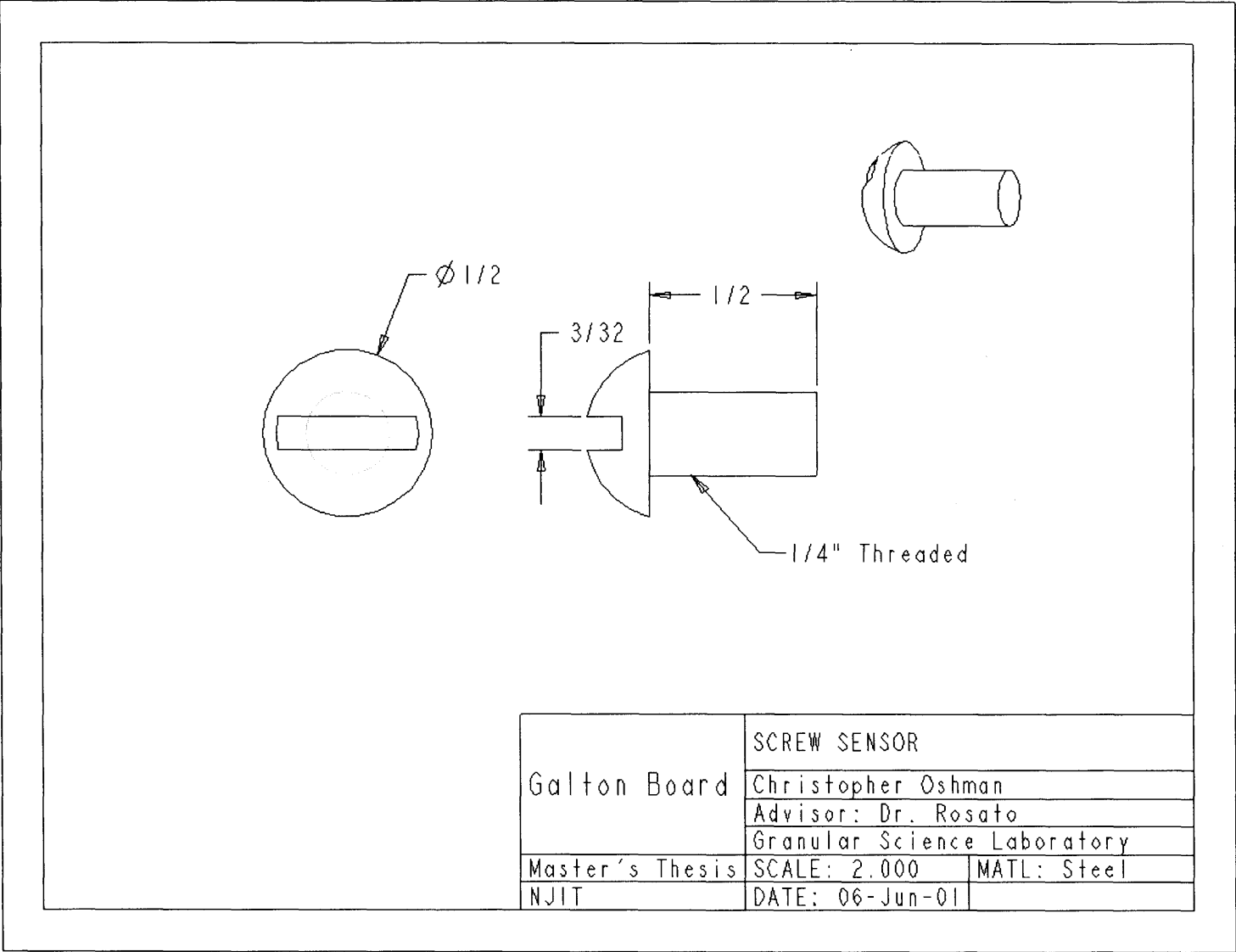
Drawing C.19 Release block.



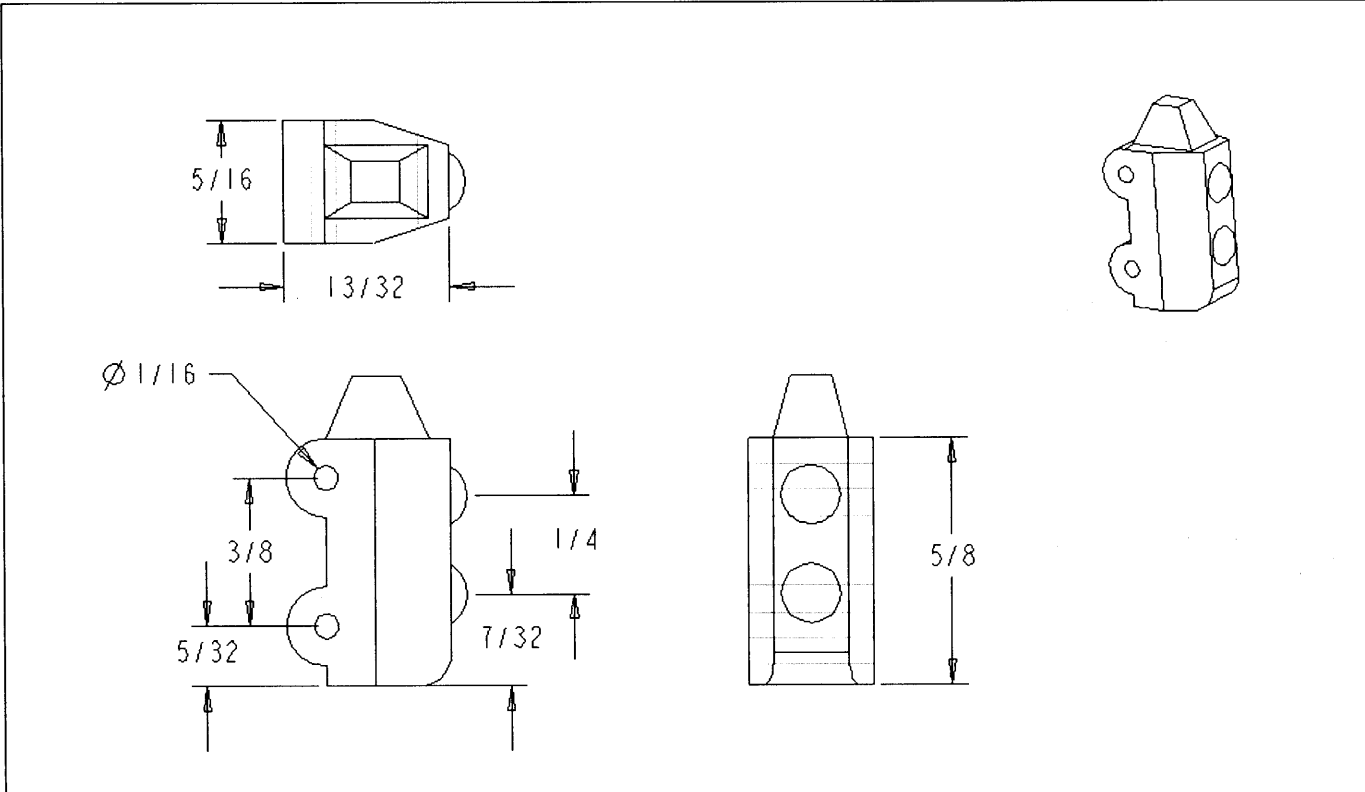
Drawing C.20 Screw for the releaser assembly.



Drawing C.21 Screw for the timing sensors.



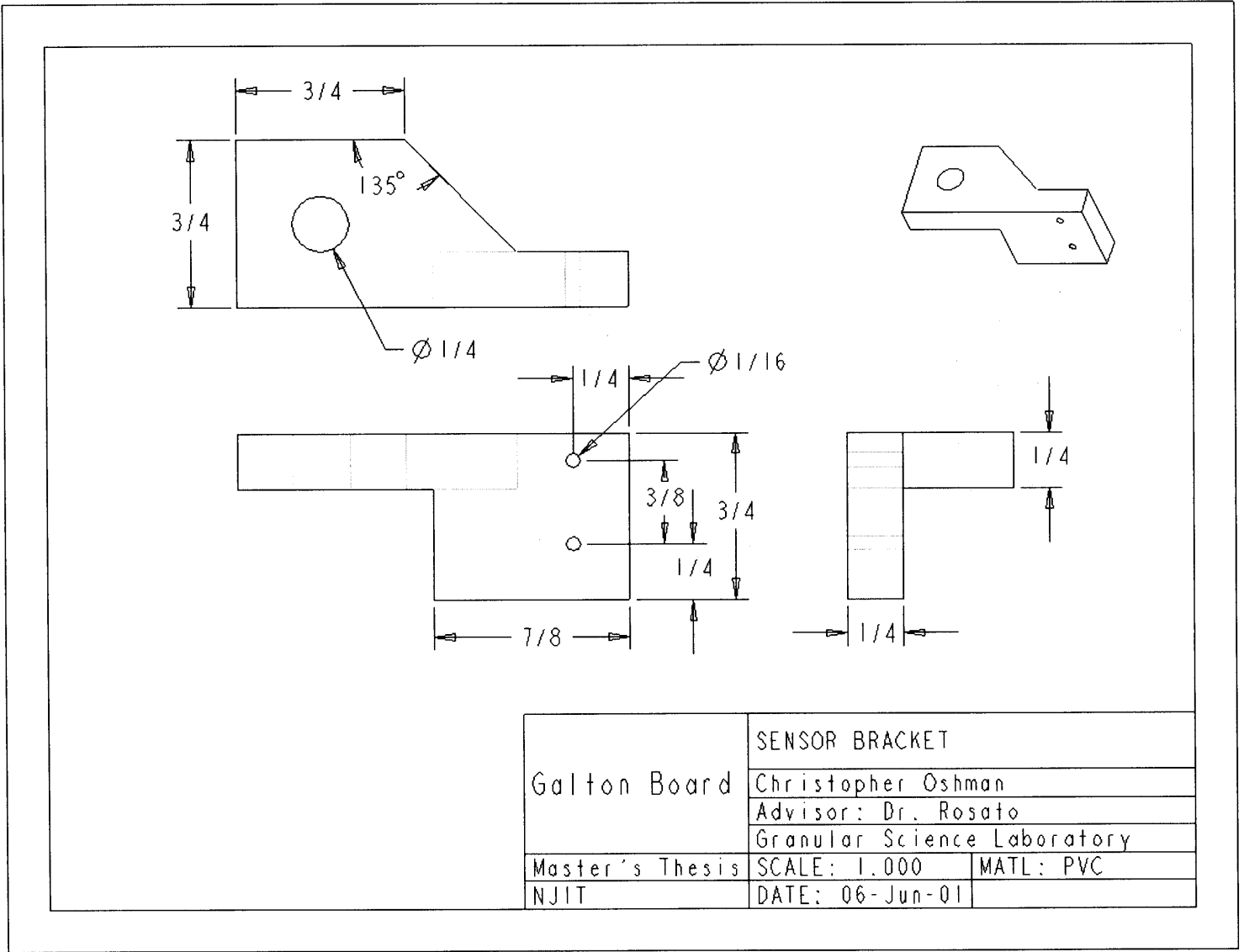
Drawing C.22 Timing sensor.



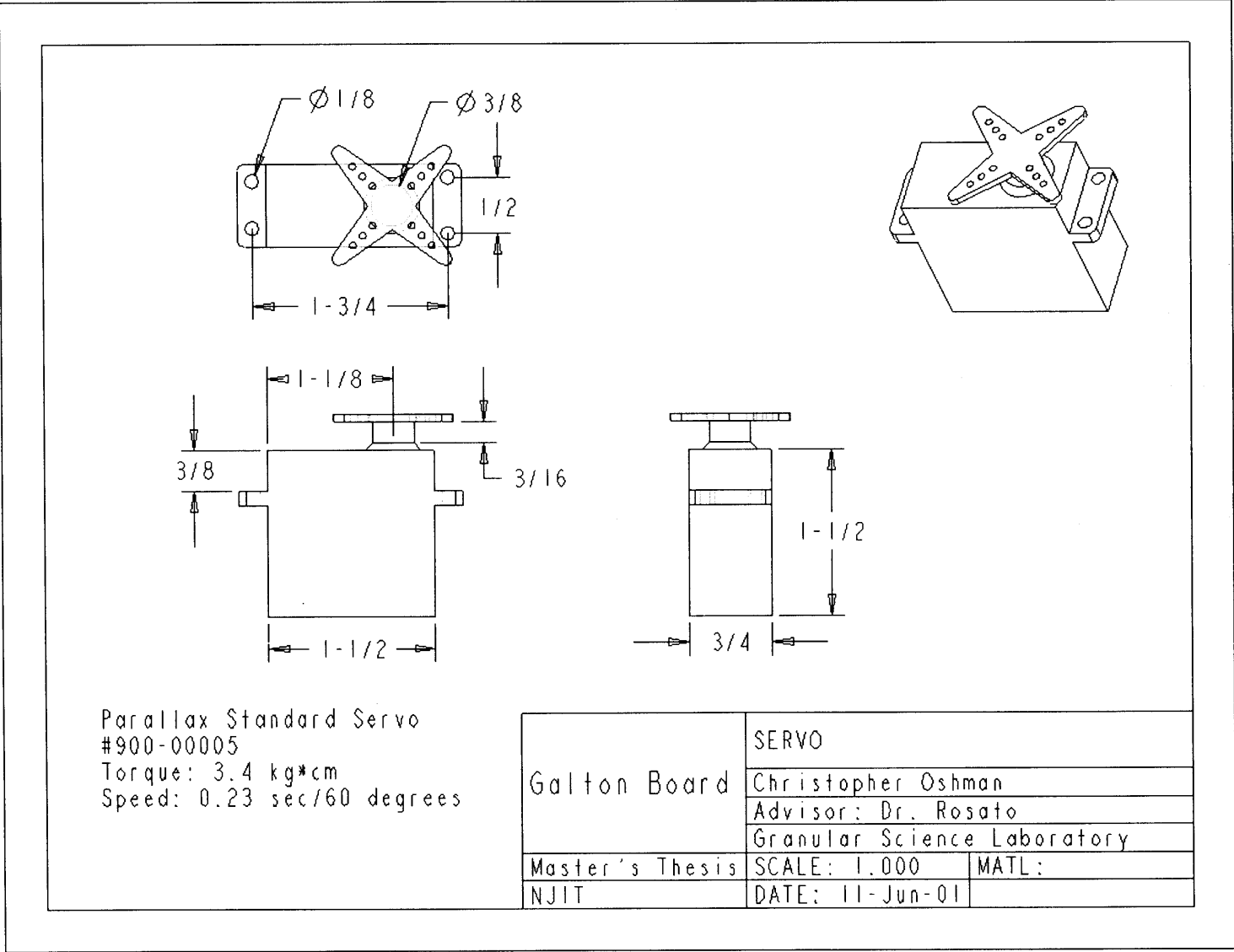
Amplified Mini Optical Sensor
 w/ Pin Point Beam
 Omron PN, E3T-ST12
 Digikey PN, OR592-ND

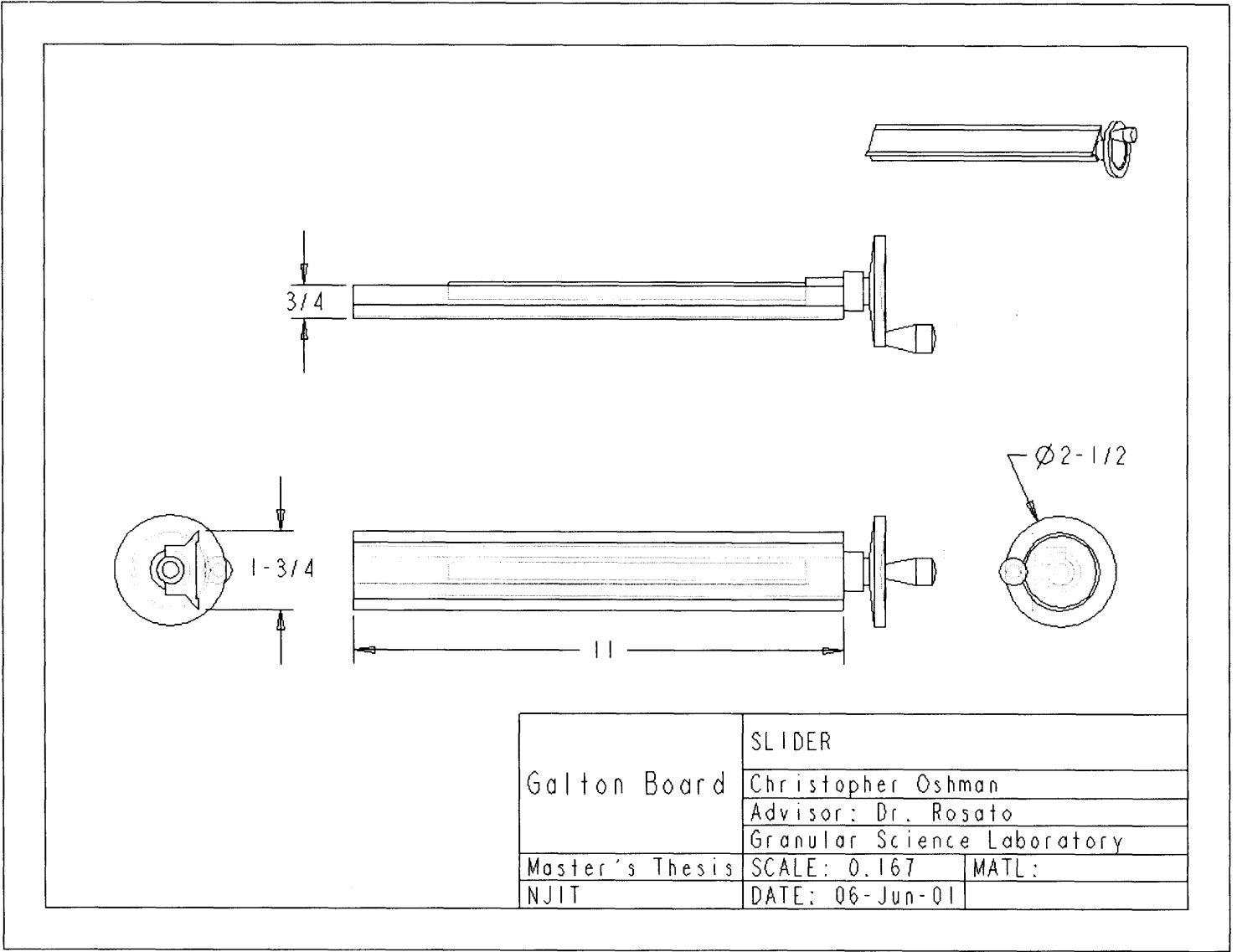
	SENSOR	
Galton Board	Christopher Oshman	
	Advisor: Dr. Rosato	
	Granular Science Laboratory	
Master's Thesis	SCALE: 2.000	MATL:
NJIT	DATE: 07-Jun-01	

Drawing C.23 Timing sensor bracket.



Drawing C.24 Agitation servo for the hopper.

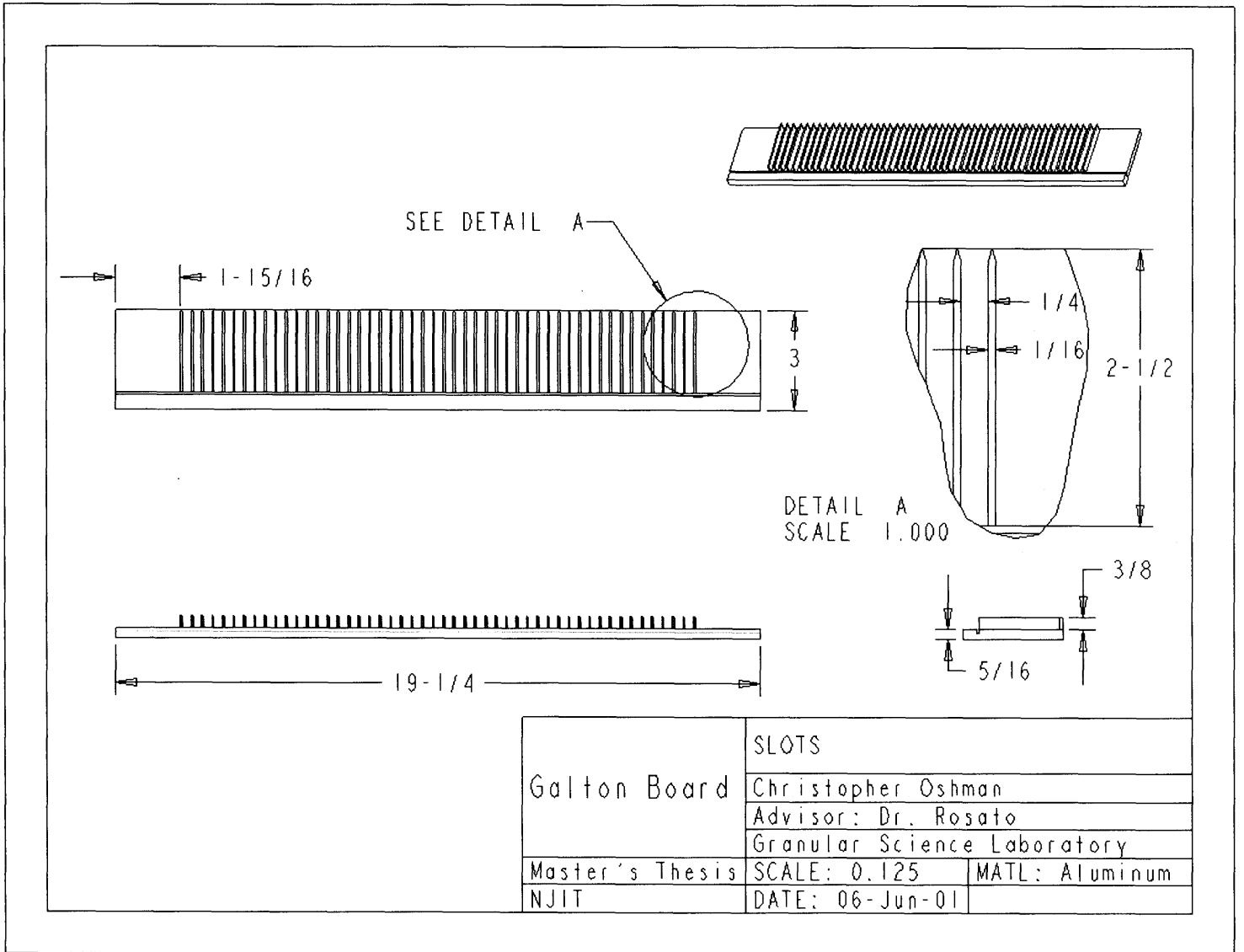




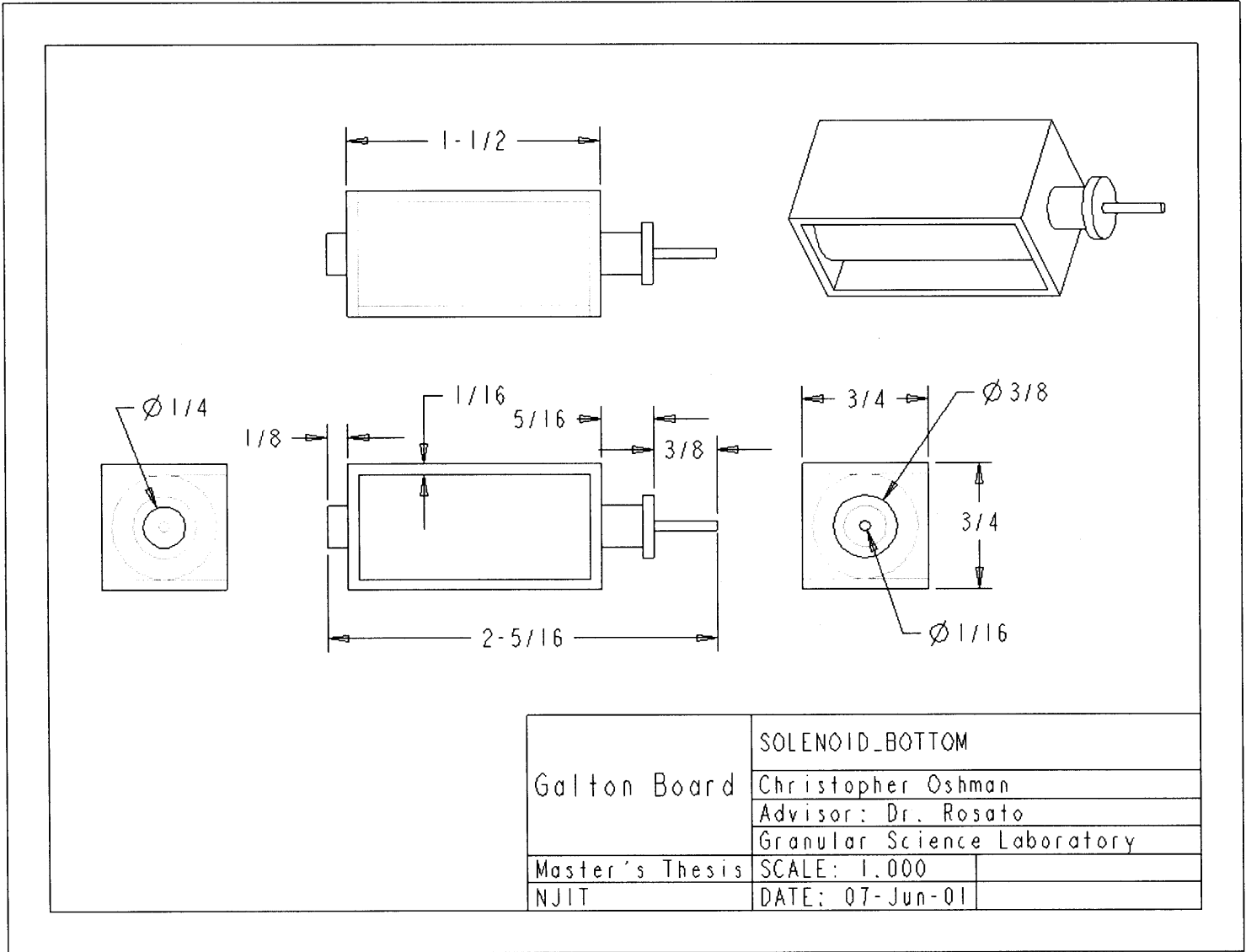
	SLIDER	
Galton Board	Christopher Oshman	
	Advisor: Dr. Rosato	
	Granular Science Laboratory	
Master's Thesis	SCALE: 0.167	MATL:
NJIT	DATE: 06-Jun-01	

Drawing C.25 Single axis movement slider.

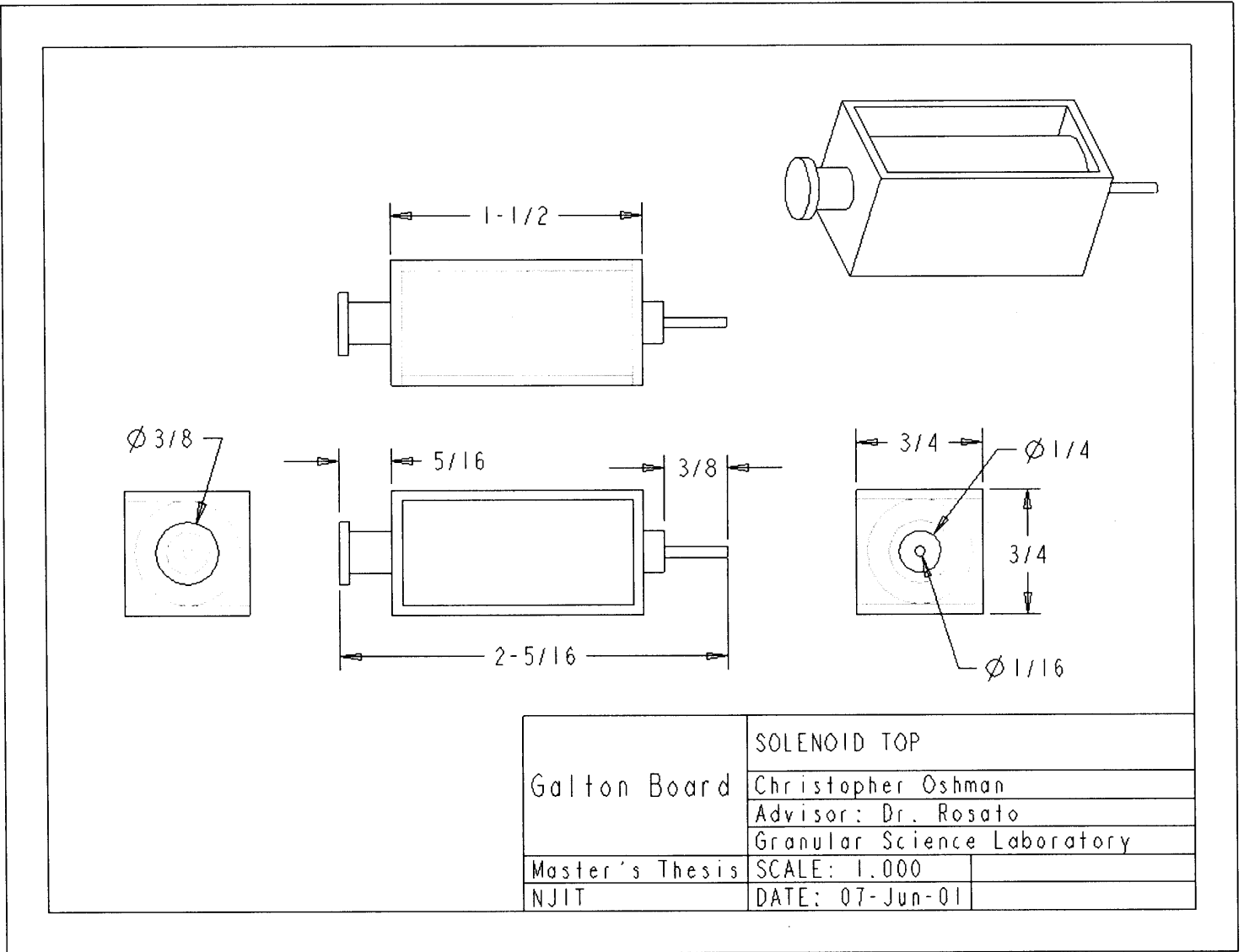
Drawing C.26 Slots assembly.



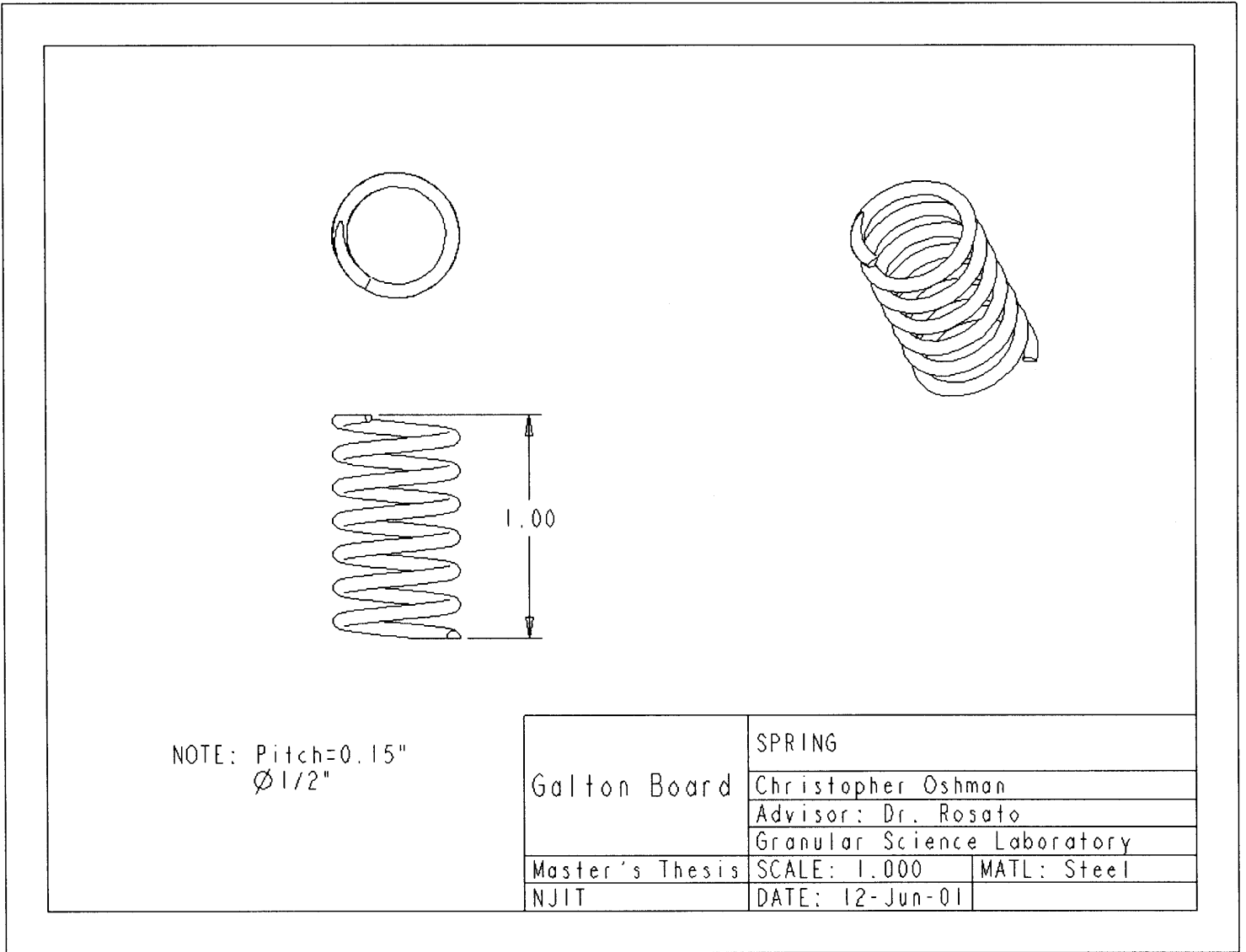
Drawing C.27 Bottom release solenoid valve.



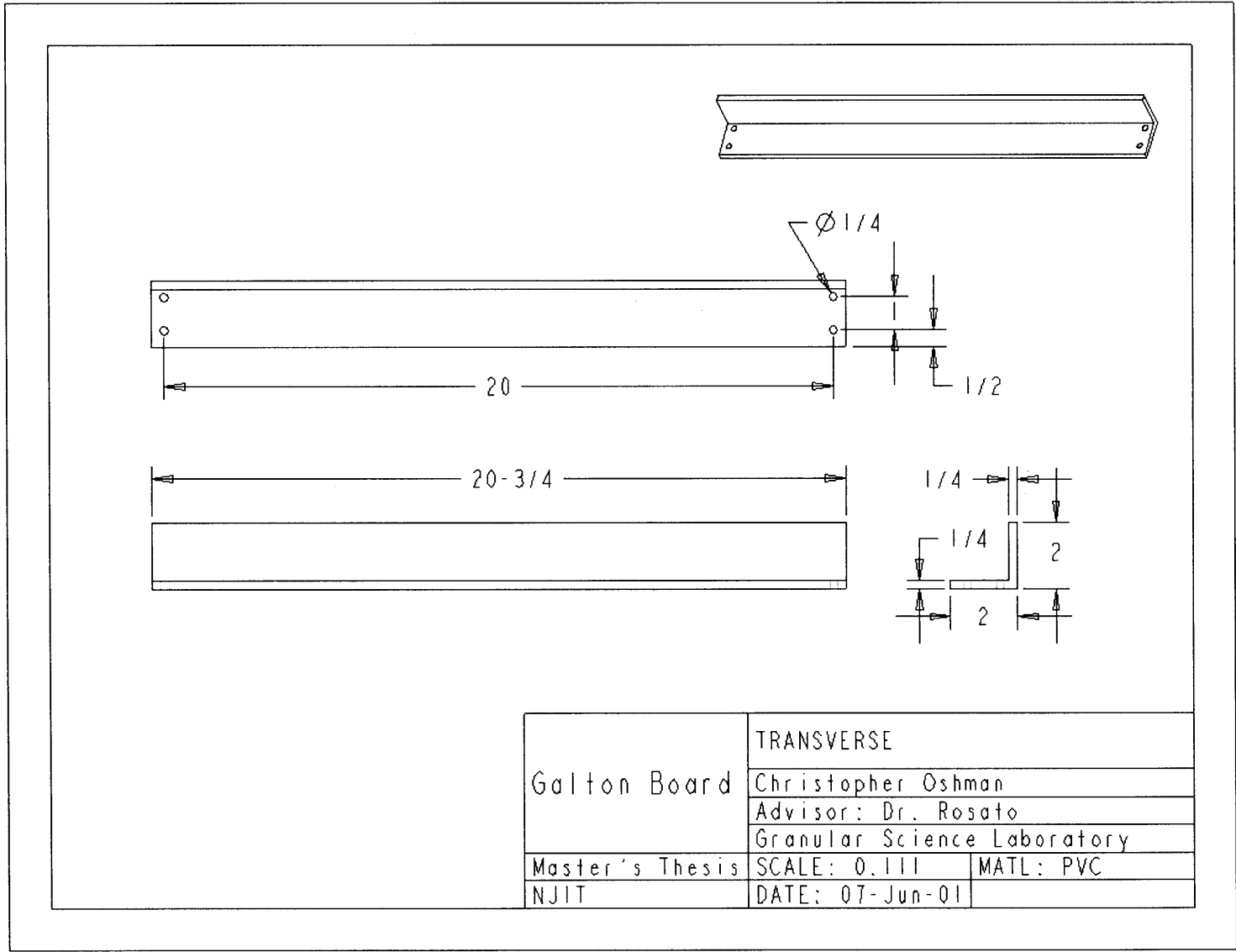
Drawing C.28 Top release solenoid valve.



Drawing C.29 Leveling spring.

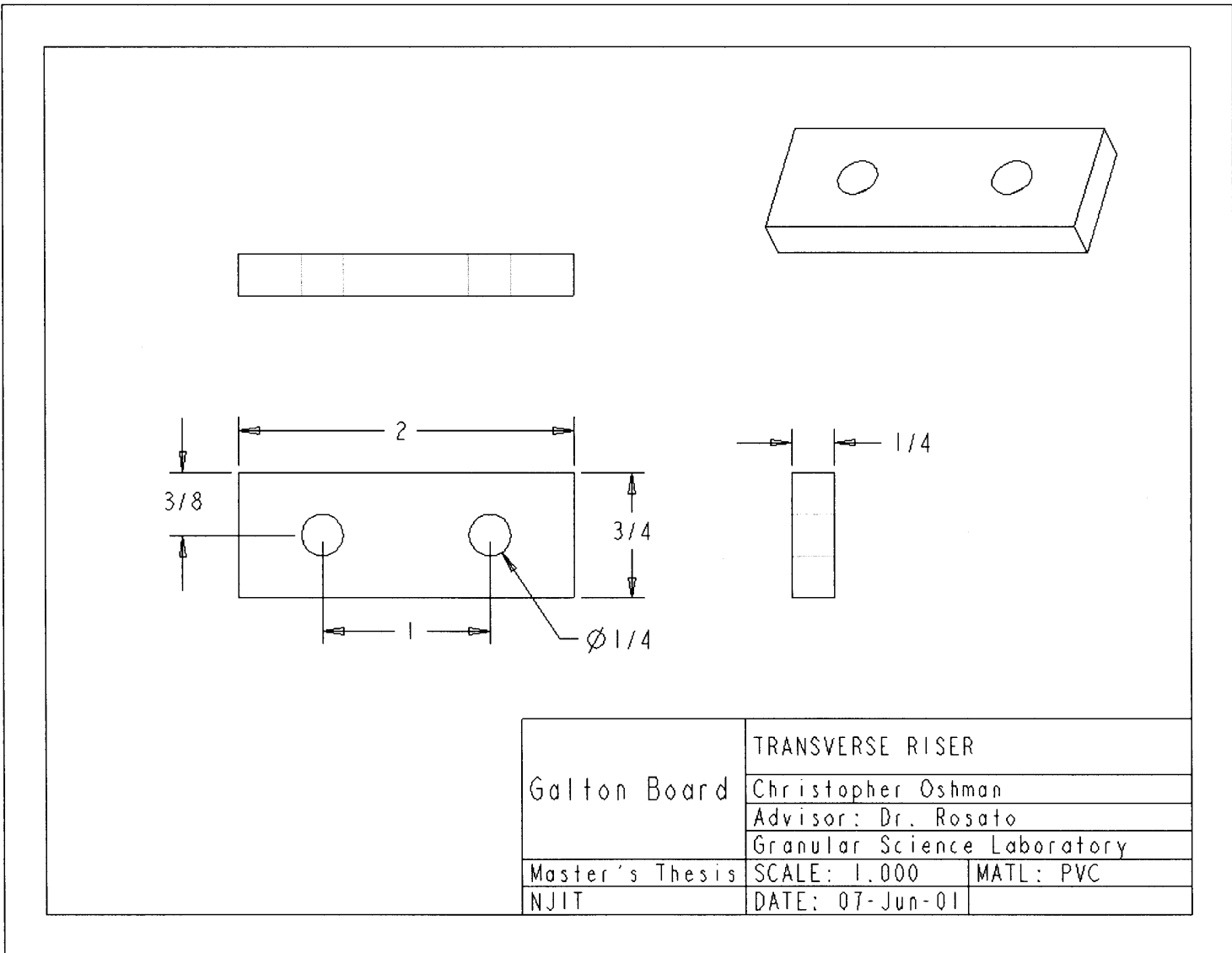


Drawing C.30 Transverse.

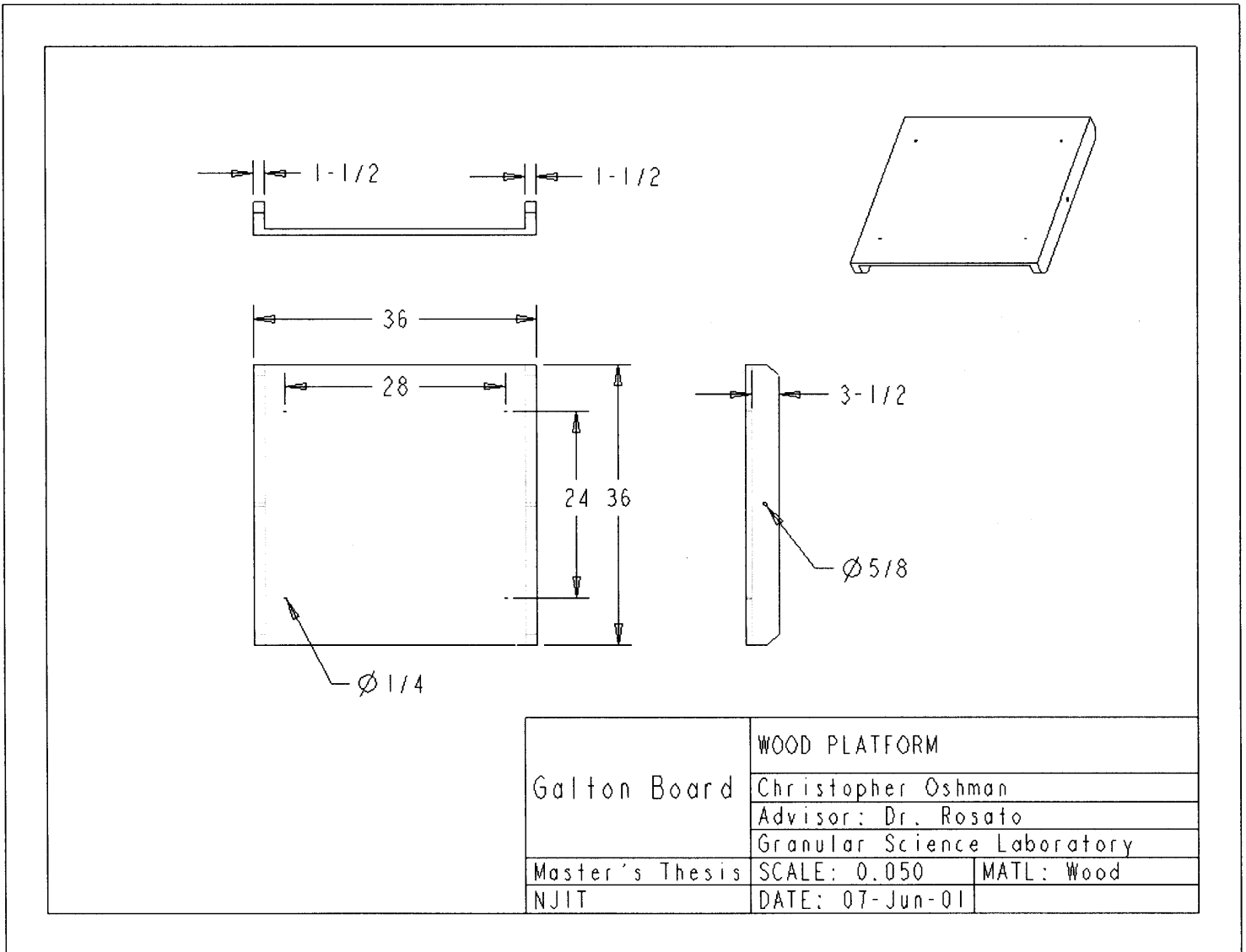


	TRANSVERSE	
Galton Board	Christopher Oshman	
	Advisor: Dr. Rosato	
	Granular Science Laboratory	
Master's Thesis	SCALE: 0.111	MATL: PVC
NJIT	DATE: 07-Jun-01	

Drawing C.31 Transverse riser.



Drawing C.32 Wooden platform.



REFERENCES

1. Kac, M. "Probability." *Scientific American*. 211 (1964): 92-108.
2. Bridgwater, J., N.W. Sharpe, and D.C. Stocker. "Particle Mixing by Percolation." *Trans. Institute of Chemical Engineers*. 47 (1969): 114-119.
3. Bridgwater, J., and N.D. Ingram. "Rate of Spontaneous Inter-Particle Percolation." *Trans. Institute of Chemical Engineers*. 49 (1971): 163-169.
4. Sergeev, S. P., T.V. Baronenkova, V.V. Dil'man, and I.Y. Kreindel. "Flow of Dispersed Medium in a Model of a Granular Bed." *Theoretical Foundations of Chemical Engineering (English Translation of Teoreticheskie Osnovy Khimicheskoi Tekhnologii)*. 22 (1988): 134-140.
5. Hoover, W. G., and B. Moran. "Viscous Attractor for the Galton Board." *Chaos*. 2 (1992): 599-602.
6. Lue, A., and H. Brenner. "Phase Flow and Statistical Structure of Galton-Board Systems." *Physical Review E*. 47 (1993): 3128-3144.
7. Ott, R.L., and W. Mendenhall. *Understanding Statistics*. Duxbury. Belmont, CA. 1994.
8. Ippolito, I., L. Sampson, S. Bourles, and D. Bideau. "Particle Diffusion in a Porous Medium." *Powders and Grains*. 97 (1997): 551-554.
9. Bruno, L., A. Calvo, I. Ippolito, S. Bourles, A. Valance, and D. Bideau. "Study on the Mixing of Discs in a Galton's Device." *IUTAM Symposium: Segregation in Granular Flows, USA (2000)*: 73-80.